IR 140-8 (I)

PROTOTYPE PRODUCTION PROCESS FOR FABRICATION OF WIRE AND TUBING BY HYDROSTATIC EXTRUSION-DRAWING

R. J. Fiorentino
J. C. Gerdeen
G. E. Meyer
B. D. Richardson
A. M. Sabroff

BATTELLE MEMORIAL INSTITUTE
COLUMBUS LABORATORIES

INTERIM ENGINEERING PROGRESS REPORT

February 1968

METALLURGICAL PROCESSING BRANCH
MANUFACTURING TECHNOLOGY DIVISION
AIR FORCE MATERIALS LABORATORY
DIRECTORATE OF LABORATORIES
AIR FORCE SYSTEMS COMMAND
WRIGHT-PATTERSON AIR FORCE BASE, OHIO

NOTICES

When U. S. Government drawings, specifications, or other data are used for any purpose other than in connection with a definitely related Government procurement operation, the United States Government thereby incurs no responsibility nor any obligation whatsoever; and the fact that the Government may have formulated, furnished, or in any way supplied the said drawings, specfications, or other data, is not to be regarded by implication or otherwise as in any manner licensing the holder or any other person or corporation, or conveying any rights or permission to manufacture, use, or sell any patented invention that may in any way be related thereto.

DDC RELEASE TO OTS NOT AUTHORIZED.

Qualified requesters may obtain copies of this report from DDC, Defense Document Service Center, Cameron Station, Alexandria, Virginia, 22134. Orders will be expedited if placed through the librarian or other person designated to request documents from DDC.

Copies of this report should not be returned to the Air Force Materials Laboratory unless return is required by security considerations, contractual obligations, or notice on a specific document.

This document is subject to special export controls and each transmittal to foreign governments or foreign nationals may be made only with prior approval to the Manufacturing Technology Division.

DEVELOPMENT OF THE MANUFACTURING CAPABILITIES OF THE HYDROSTATIC EXTRUSION PROCESS

R. J. Fiorentino
J. C. Gerdeen
W. R. Hansen
A. M. Sabroff
F. W. Boulger

FOREWORD

This Interim Engineering Progress Report covers the work performed under Contract No. AF 33(615)-1390 from 1 December 1965 to 28 February 1966. It is published for technical information only and does not necessarily represent the recommendations, conclusions, or approval of the Air Force.

This contract with Battelle Memorial Institute of Columbus, Ohio, was initiated under Manufacturing Methods Project No. 8-198, "Development of the Manufacturing Capabilities of the Hydrostatic Extrusion Process". It is being administered under the direction of Mr. Gerald A. Gegel of the Metallurgical Processing Branch (MATB), Manufacturing Technology Division, Air Force Materials Laboratory, Wright-Patterson Air Force Base, Ohio.

The program is being conducted at Battelle by the Metalworking Research Division with Mr. R. J. Fiorentino, Associate Chief, as project engineer. Other contributing to the program are Mr. W. R. Hansen, Research Metallurgist, Mr. A. M. Sabroff, Associate Chief, and Mr. F. W. Boulger, Division Chief. Mr. R. L. Jentgen, Project Leader in the Experimental Physics Division, is assisting in the fluid and lubrication studies of the program. Dr. J. C. Gerdeen, Research Mechanical Engineer, Mr. E. C. Rodabaugh, Senior Mechanical Engineer, and Mr. T. J. Atterbury, Chief of the Applied Solid Mechanics Division are contributing to the high-pressure container design study. Data from which this report has been prepared are contained in Battelle Laboratory Record Book Nos. 21799, 21990, 23055, and 23287.

ABSTRACT

Development of the Manufacturing
Capabilities of the
Hydrostatic Extrusion Process

R. J. Fiorentino
et al.
Battelle Memorial Institute

The purpose of the present program is to develop the manufacturing capabilities of the hydrostatic extrusion process. Among the specific applications to be studied are fabrication of wire, tubing, and shapes from relatively difficult-to-work materials such as refractory metal alloys, high-strength steels and aluminum alloys, titanium alloys, beryllium, and other selected materials.

During the interim period, a study of the critical process variables (lubricants, fluids, stem speed, billet surface finish, die design, extrusion ratio, extrusion shape, etc) was continued for cold hydrostatic extrusion of AISI 4340 steel, 7075-0 Al, and Ti-6Al-4V. Some of the important results include: (1) extrusion of 7075-0 Al rounds at exit speeds up to 3000 ipm without surface cracking, (2) extrusion of AISI 4340 rounds at exit speeds up to 740 ipm, (3) extrusion of 7075-Al tubing, 3/4-inch ID x 0.063 inch wall, at exit speeds up to 450 ipm, and (4) extrusion of AISI 4340 tubing, 3/4-inch ID x 3/16-inchwall, and (5) extrusion of a 7075 Al T-section at exit speeds up to 1080 ipm.

Another objective of the program was to conduct an analytical study to evaluate several high-pressure container design concepts. This was done in anticipation of the need for large containers capable of withstanding very high pressures up to about 450,000 psi if possible. Designs were compared on the basis of maximum pressure capability, probable fatigue life, size efficiency, fabricability, and other characteristics.

PUBLICATION REVIEW

Approved by: F. W. Boulger

F. W. Boulger, Chief
Metalworking Research Division

Approved by: P. J. Rieppel

P. J. Rieppel, Manager
Department of Process and Physical Metallurgy

DEVELOPMENT OF THE MANUFACTURING CAPABILITIES OF THE HYDROSTATIC EXTRUSION PROCESS

SUMMARY

HYDROSTATIC EXTRUSION STUDIES

Hydrostatic extrusion trials were continued to evaluate the critical process variables and specific process application studies were begun. The billet materials extruded were AISI 4340 steel, 7075-0 aluminum, and Ti-6Al-4V titanium alloy.

In extrusion of AISI 4340 rounds, the extrusion pressures were decreased 8 per cent by raising the stem speed from 1 to 6 ipm and then remained essentially constant up to 80 ipm, the maximum speed of the press. At 80 ipm, the "effective stem speed" was actually 148 ipm, which is well within the range used in commercial extrusion operations. In a study of hydrostatic fluid media, water was found to be very effective up to 185,000 psi, the maximum pressure reached thus far. Use of water in a commercial production operation would offer the advantages of low cost and ease of handling. In a study of die angles from 30 to 90 degrees, 45 degrees was found to be nearly optimum from the standpoint of minimizing pressure requirements.

The 7075-0 aluminum alloy was extruded into rounds at ratios up to 60:1 at room temperature. At a ratio of 20:1, the alloy was extruded at exit speeds up to 3000 ipm without surface cracking, a condition that is usually encountered in conventional hot extrusion unless the exit speeds are kept down to around 10 to 50 ipm. The problem of billet lubrication of 7075 Al during hydrostatic extrusion is alleviated by operating at stem speeds of 80 ipm. In a study of billet surface finish, grit-blasted finishes were effective in minimizing extruded-surface cracking and improving surface finish but were not able to prevent stick-slip.

In extrusion of Ti-6Al-4V rounds, several new billet lubrication systems were evaluated. Some appear promising and modifications of them are underway to obtain additional improvements.

A new die design for extrusion of a T-section was evaluated. The die entry consisted of a 45-degree conical surface leading into a 160-degree conical surface, the latter circumscribing the T-opening. T-sections of excellent surface quality were extruded from 7075 Al at a ratio of 7.3:1 and stem speeds up to 80 ipm from the die.

One of the strong potential applications of the hydrostatic extrusion process is for the production of tubing. A tooling arrangement for tube extrusion was designed and evaluated. Sound tubing, 0.750 inch ID x 0.063 inch wall, was produced from 7075 Al at a ratio of 12.2:1 and exit speeds of 450 ipm, the maximum ratio and speed attempted thus far. AISI 4340 tubing of high surface quality was produced at a ratio of 3.77:1. A problem of frictional drag between the tubing and mandrel was encountered, but it appears that this can be overcome by a slight modification of the mandrel.

ANALYSIS OF SEVERAL HIGH-PRESSURE CONTAINER DESIGN CONCEPTS

Four types of pressure vessel designs were analyzed in detail: a multi-ring container, a ring-segment container, a ring-fluid-segment container, and a pin-segment container (These are illustrated in Figure 7 of the text.). The multi-ring container is made up of cylindrical ring components. The ring-segment container is like the multi-ring container except that the second ring, adjacent to the liner, is a segmented ring. The ring-fluid-segment container is a combination of a ring-segment container on the inside with a multi-ring container on the outside, and with a fluid support pressure in between. The pin-segment container has a cylindrical inner liner supported by a pinned segment-plate arrangement. A wire-wrapped (strip-wound) vessel and a controlled fluid-fill vessel were also considered but in less detail.

The operating cycle of high-pressure containers for hydrostatic extrusion and forming consists of application of the pressure needed, followed by a decrease in the pressure to zero. Such highly cyclic conditions coupled with extreme operating pressures can be expected to cause fatigue failures of the containers. A fatigue strength criterion was selected as the basis of the study, because a high-pressure container for commercial application should, of course, be capable of repeated use without frequent failure.

To achieve the high pressure desired it was found necessary to use high-strength liner materials. For the high-strength steels (ultimate tensile strengths of 250,000 psi and greater) a maximum tensile stress criterion of fatigue was assumed and available uniaxial fatigue data from the literature were used in design evaluations. However, the fatigue behavior was left arbitrary in the analysis by formulating the analysis in terms of α_r and α_m, semirange and mean tensile stress parameters. The outer rings of the containers were assumed to be of more ductile materials in order to avoid catastrophic failures. A maximum shear criterion of fatigue was used for the ductile outer rings and the Goodman relation was used to relate the semirange and mean shear stresses.

For the analysis, equations were derived that relate the interface and the radial deformations between components. Elasticity solutions for stress and deformations were used together with fatigue relations to determine formulas for maximum bore pressures. Stresses due to the bore pressure and shrink-fit assembly were analyzed. The effect of temperature change (from operating temperature to room temperature) upon the prestresses (residual stresses) was included. The analyses for maximum pressure capability, residual stresses, and required shrink-fit interferences were programmed for calculation on Battelle's CDC 3400 computer.

Theoretically, large pressures (up to 1,000,000 psi in the ring-fluid-segment design) were found to be possible in the containers. However, designs based on the theoretical pressures were not always considered practicable because of manufacturing and assembly limitations. For example, a ring-fluid-segment container designed to its theoretical maximum pressure capability requires outside diameters of 229.5 inches and 573.5 inches for 6- and 15-inch-diameter bore designs, respectively. Such large-diameter cylinders would present problems in producibility, heat-treating, and transportation. This container design also requires a shrink-fit interference of 0.016 in./in., which is difficult, if not impossible, to achieve in assembly. This large interference

requirement is necessary to overcome excessive deformation of segments. Also relatively larger outside diameters are required for segmented containers because segments offer no hoop support to the liner. These are distinct disadvantages of containers using segments.

Because of the practicable design limitations, the designs were evaluated for outside diameters limited to 72 inches and interferences limited to 0.007 in./in. maximum. High-strength liner materials of 300,000 psi ultimate tensile strength were assumed for which some fatigue data were available. A fatigue life of 10^4-10^5 cycles was selected for ideal conditions, i.e., no stress concentrations or material flaws in the liner. On this basis, the predictions of maximum pressure capability for 6-inch-diameter bore designs, for example, are as follows:

Container	Outside Diameter, inches	Maximum Pressure, p, psi
Multi-ring	51.0	300,000
Ring-segment	60.0	290,000
Ring-fluid-segment	72.0	286,000
Pin-segment	72.0	195,000

These pressure capabilities apply at room or elevated temperatures, provided the ultimate strength of the liner is 300,000 psi at temperature. Higher maximum pressures are theoretically possible with higher strength materials. For example, a maximum pressure of 450,000 psi would be predicted for a container with a 450,000 psi ultimate strength liner material, if such a material could be found that had the same proportionate increase in its fatigue strength.

Residual stress limitations were also found for containers designed for high-temperature use. If the coefficient of thermal expansion of the liner is smaller than that of the outer components, then a decrease in temperature from operating temperature to room temperature may cause excessive residual stresses in the liner. Therefore, a higher coefficient of thermal expansion would be recommended for the liner.

There are other possible material limitations. The design evaluations conducted herein were based necessarily on the uniaxial fatigue data available for the liner materials, although a biaxial or triaxial state of stress exists in a pressure container. Also, a compressive mean stress on the liner was assumed beneficial. However, fatigue behavior of high-strength steels under combined stresses and compressive mean stress is unknown. In addition to fabrication and transportation difficulties, heat treatment of large cylindrical forgings may also present problems. In this respect a pin-segment-plate arrangement or a strip-wound layer offers advantages as a replacement of cylindrical rings for outer support members.

A materials study is proposed to determine data on the important properties of high-strength materials for high-pressure container applications. Based upon the design study just completed, a new high-pressure container design is suggested. This design is a combination of two multi-ring containers with a fluid-supporting pressure between the rings. It makes use of the benefits of fluid-support pressure and prestress from shrink-fit. It avoids some of the difficulties associated with the segmented containers. A pressure capability of 450,000 psi can be practicably achieved with this design, with a liner of only 300,000 psi ultimate tensile strength.

Additional details of analysis are included in the appendices of this report. Bending deformations and stresses within segments, and derivations of shrink-fit interferences are some of the items included. Computer programs used for calculations are also briefly described.

LIST OF SYMBOLS

N = the total number of components in a container; N also denotes the outermost component

n = a specific component when numbered from inside out; i.e., n = 1, 2, ..., N

r_n = outside radius of component n, inches

r_{n-1} = inside radius of component n, inches

r_o = bore radius of container, inches

r_N = outer radius of container, inches

k_n = wall ratio of component n, $k_n = r_n/r_{n-1}$

K = over-all wall ratio of container, $K = r_N/r_o$

K' = wall ratio of inner part of ring-fluid-segment container, $K' = r_3/r_o$

E_n = modulus of elasticity of component n, psi

p_n = pressure acting on component n at r_n when $p \neq 0$, psi

p_{n-1} = pressure acting on component n at r_{n-1} when $p \neq 0$, psi

p = bore pressure, psi, $p_o = p$

q_n = residual interface pressure acting on component n at r_n when p = 0, psi

q_{n-1} = residual interface pressure acting on component n at r_{n-1} when p = 0, psi

S = shear stress, psi

S_r = semi-range in shear stress for a cycle of bore pressure, psi

S_m = mean shear stress for a cycle of bore pressure, psi

S_{min} = minimum shear stress during a cycle of bore pressure, psi

S_{max} = maximum shear stress during a cycle of bore pressure, psi

σ = design tensile stress of ductile steel, psi ($\sigma \leqq$ ultimate tensile strength)

σ_1 = design tensile stress of high-strength steel, psi ($\sigma_1 \leqq$ ultimate tensile strength)

$(\sigma)_r$ = semirange in tensile stress for a cycle of bore pressure, psi

$(\sigma)_m$ = mean tensile stress for a cycle of bore pressure, psi

LIST OF SYMBOLS
(Continued)

$(\sigma)_{min}$ = minimum tensile stress during a cycle of bore pressure, psi

$(\sigma)_{max}$ = maximum tensile stress during a cycle of bore pressure, psi

σ_r = radial stress, psi

σ_θ = circumferential stress, psi

σ_z = axial (longitudinal) stress, psi

α_r = semirange stress parameter for high-strength steel, $\alpha_r = (\sigma)_r/\sigma_1$

α_m = mean stress parameter for a high-strength steel, $\alpha_m = (\sigma)_m/\sigma_1$

M_1 = bending moment on ring segment

M_2 = bending moment on pin segment

u = radial displacement, inches

v = circumferential displacement, inches

ν = Poisson's ratio

r, θ, z = cylindrical coordinates for radial, circumferential, and axial directions, respectively

Δ_n = interference required (as manufactured) between cylinder, n, and cylinder, n + 1, inches

Δ_{12} = interference required (as manufactured) between the liner, segments, and cylinder, 3, of the ring-segment and ring-fluid-segment containers, inches

TABLE OF CONTENTS

Page

HYDROSTATIC EXTRUSION STUDIES

INTRODUCTION 1

EQUIPMENT AND EXPERIMENTAL PROCEDURE 2

COLD HYDROSTATIC EXTRUSION OF AISI 4340 ROUNDS 5

- Stem Speed 5
- Lubrication System 5
- Die Angle 9
- Billet Surface Finish 9

COLD HYDROSTATIC EXTRUSION OF 7075-0 ALUMINUM ROUNDS 9

COLD HYDROSTATIC EXTRUSION OF Ti-6Al-4V ROUNDS 14

COLD HYDROSTATIC EXTRUSION OF T-SECTIONS 14

COLD HYDROSTATIC EXTRUSION OF TUBING. 19

FUTURE WORK 19

ANALYSIS OF SEVERAL HIGH-PRESSURE CONTAINER DESIGN CONCEPTS

INTRODUCTION 21

SCOPE OF ANALYSIS 21

BASIS AND METHOD OF ANALYSIS 25

METHOD OF PARAMETER NOTATION 25

FATIGUE CRITERIA 26

- Fatigue Criterion for Ductile Outer Cylinders 27
- Fatigue Criterion for High-Strength Liner 29

ELASTICITY SOLUTIONS 33

- Elasticity Solutions for a Cylinder 33
- Elasticity Solutions for Segmented Components 34
  - Ring Segment 34
  - Pin Segment 35

TABLE OF CONTENTS
(Continued)

	Page
NONDIMENSIONAL PARAMETER ANALYSIS	36
Multi-Ring Container	36
Static Shear Strength Analysis	36
Fatigue Shear Strength Analysis	38
High-Strength Liner Analysis	40
Ring-Segment Container	49
Ring-Fluid-Segment Container	53
Pin-Segment Container	62
Strip-Wound Container	63
Controlled Fluid-Fill Multi-Ring Container	66
DESIGN REQUIREMENTS AND LIMITATIONS FOR HIGH-PRESSURE CONTAINERS	67
Possible Manufacturing and Assembling Limitations	68
Residual Stress Limitations	71
Other Possible Material Limitations	72
RECOMMENDATIONS	75
Proposed Materials Study	75
Suggested High-Pressure Container	75
REFERENCES	78
APPENDIX A	
ELASTICITY SOLUTION FOR A RING SEGMENT	81
ELASTICITY SOLUTION FOR A PIN SEGMENT	83
SOLUTION FOR SHEAR STRESSES IN PINS	90
APPENDIX B	
DERIVATIONS OF FORMULAS FOR ASSEMBLY INTERFERENCES	95
APPENDIX C	
COMPUTER PROGRAMS AND EXAMPLE CALCULATIONS OF OPERATING AND RESIDUAL STRESSES	97

LIST OF TABLES

		Page
Table 1.	Billet Lubricants Evaluated in Current Hydrostatic Extrusion Program	4
Table 2.	Experimental Data for Cold Hydrostatic Extrusion of AISI 4340 Rounds	6
Table 3.	Experimental Data for Cold Hydrostatic Extrusion of 7075 Aluminum Rounds	11
Table 4.	Experimental Data for Cold Hydrostatic Extrusion of Ti-6Al-4V Alloy Rounds	15
Table 5.	Experimental Data for Cold Hydrostatic Extrusion of AISI 4340 Steel and 7075 Aluminum T-Sections	17
Table 6.	Experimental Data for Cold Hydrostatic Extrusion of AISI 4304 Steel and 7075 Aluminum Tubing	17
Table 7.	Torsional and Triaxial Fatigue Data of Vibrac Steel	28
Table 8.	Fatigue Strengths of High-Strength Steels from Room-Temperature Rotating-Beam Tests, $\alpha_m = 0$	30
Table 9.	Fatigue Strengths of High-Strength Steels from Room-Temperature Push-Pull Tests, $\alpha_m = \alpha_r$	30
Table 10.	Fatigue Strengths of High-Strength Steels from Push-Pull Tests at Elevated Temperatures	31
Table 11.	Elevated-Temperature Data for 18% Ni Maraging Steel and H-11 Steel	71
Table 12.	Liner-Bore Stress and Interferences for a 6-Inch Bore Multi-Ring Container with $K = 8.5$, $N = 5$, $K_1 = 2.0$, $K_n = 1.44$, $N \geq 2$, $\alpha_1 = 0.5$, $\alpha_m = -0.5$	73
Table 13.	Liner-Bore Stresses and Interferences for a 6-Inch Bore Multi-Ring Container with $K = 8.5$, $N = 5$, $K_1 = 2.0$, $K_n = 1.44$, $n \geq 2$, $\alpha_r = 0.5$, $\alpha_m = -0.3$	74
Table 14.	Stresses and Deflections in a Ring Segment, $K_2 = 2.0$, $\alpha = 60°$, $\nu = 0.3$	83
Table 15.	Deflections in Ring Segments, $\nu = 0.3$	84
Table 16.	Stresses and Deflections in a Pin Segment, $k_2 = 4.0$, $\alpha = 60°$, $\nu = 0.3$	91
Table 17.	Displacements and Maximum Hoop Stresses in Pin Segments, $\nu = 0.3$	93

LIST OF FIGURES

		Page
Figure 1.	Assembly Drawing of Tooling for Hydrostatic Extrusion . . .	3
Figure 2.	Effects of Stem and Billet Speed on Stem Pressure for Cold Hydrostatic Extrusion of AISI 4340 at an Extrusion Ratio of 5:1 .	8
Figure 3.	Effect of Extrusion Ratio on Pressure for Cold Hydrostatic Extrusion of 7075-0 Aluminum	13
Figure 4.	Die Configurations Used for Extruding T-Sections	16
Figure 5.	Hydrostatic Extrusions of Tubing and T-Section Produced From 7075 Aluminum at Room Temperature	18
Figure 6.	Mandrel Tooling Arrangement for Hydrostatic Extrusion of Tubing	20
Figure 7.	Schematic of High-Pressure-Container Design Concepts Analyzed in the Present Study	23
Figure 8.	Notations Used for Analysis of Container Design Concepts. . .	24
Figure 9.	Fatigue Diagram for 10^4-10^5 Cycles Life for High-Strength Steels at Temperatures of 75 F - 1000 F	32
Figure 10.	Maximum Pressure-to-Strength Ratio, p/2S, in Multi-Ring Container Designed on Basis of Static Shear Strength	39
Figure 11.	Maximum Pressure-to-Strength Ratio, p/σ, in Multi-Ring Container Designed on Basis of Fatigue Shear Strength. . . .	41
Figure 12.	Maximum Pressure-to-Strength Ratio, p/σ_1, in Multi-Ring Container With High-Strength Liner Based on the Fatigue Tensile of Liner.	43
Figure 13.	Limit to Maximum Pressure-to-Strength Ratio, p/σ, in Multi-Ring Container With High-Strength Liner Based on Shear Fatigue Strength of the Outer Rings	45
Figure 14.	Influence of Number of Rings on Maximum Pressure-to-Strength Ratio, p/σ, in Multi-Ring Container With High-Strength Liner .	46
Figure 15.	Influence of Liner Size on Maximum Pressure-to-Strength Ratio, p/σ, in Multi-Ring Container With High-Strength Liner .	47
Figure 16.	Comparison of Multi-Ring Container With Ring-Segment Container for Various k_1	51

LIST OF FIGURES
(Continued)

		Page
Figure 17.	Comparison of Multi-Ring Container With Ring-Segment Container for Various Segment Wall Ratios.	52
Figure 18.	Effect of Elastic Modulus of Segments on Pressure-to-Strength Ratio, p/σ_1, for the Ring-Segment Container	54
Figure 19.	Effect of Liner Size on Pressure-to-Strength Ratio, p/σ, for Ring-Segment Container	55
Figure 20.	Effect of Segment Size on the Pressure-to-Strength Ratio, p/σ_1, for the Ring-Fluid-Segment Container	57
Figure 21.	Effect of Segment Size on the Pressure-to-Strength Ratio, p/σ_3, for the Ring-Fluid-Segment Container	58
Figure 22.	Effect of Segment Size on the Pressure-to-Strength Ratio p/σ_1, for the Ring-Fluid-Segment Container.	59
Figure 23.	Effect of Segment Size on the Pressure-to-Strength Ratio, p/σ_3, for the Ring-Fluid-Segment Container	60
Figure 24.	Effect of Support Pressure p_3 on Bore Pressure Capability for the Ring-Fluid-Segment Container	61
Figure 25.	Maximum Pressure-to-Strength Ratio, p/σ_1, for the Pin-Segment Container	64
Figure 26.	Ratio of Interface Pressure Between Segments and Liner to Bore Pressure for the Pin-Segment Container.	65
Figure 27.	Controlled Fluid-Fill Cylindrical-Layered Container	66
Figure 28.	Suggested Fluid-Support Multi-Ring Container for High Pressure	76
Figure 29.	Geometry of Ring Segment	81
Figure 30.	Bending Deformation of Ring Segments	85
Figure 31.	Geometry of Pin Segment.	86
Figure 32.	Loading of Pin Segment	86
Figure 33.	Loading of Pins	87

DEVELOPMENT OF THE MANUFACTURING CAPABILITIES OF THE HYDROSTATIC EXTRUSION PROCESS

by

R. J. Fiorentino, J. C. Gerdeen, W. R. Hansen,
A. M. Sabroff, and F. W. Boulger

HYDROSTATIC EXTRUSION STUDIES

INTRODUCTION

The purpose of the present research program is to develop the manufacturing capabilities of the hydrostatic extrusion process with the aim of extruding high-quality shapes from materials of interest to the Air Force. It is a continuation of the recently completed program on Contract No. AF 33(600)-43328. The current program is divided into two phases with the following general objectives:

Phase I. Process-Development Studies

Part 1. (a) To study the effect of critical process variables on pressure requirements and surface quality in hydrostatic extrusion of AISI 4340 steel, Ti-6Al-4V titanium alloy, and 7075 aluminum alloy.

(b) To correlate all available hydrostatic-extrusion-pressure data with material properties wherever possible in order to assist direction of the experimental effort and maximize the information developed in the present program.

Part 2. To explore the hydrostatic extrudability of TZM molybdenum alloy (cast and wrought), beryllium, Cb-752 columbium alloy, powder compacts, and other materials to be selected later in the program.

Part 3. To conduct a design study for high-temperature, high-pressure hydrostatic extrusion tooling based on
(1) estimated pressure requirements for high-ratio extrusion of materials of interest to the Air Force,
(2) latest high-pressure-vessel technology, and
(3) latest tooling materials available.

Part 4. To conduct a process economic study on the construction, installation, and operation of equipment with the same operational and size requirements as the tooling developed in the previous program on Contract No. AF 33(600)-43328.

Phase II. Process-Application Studies

Part 1. To evaluate the application of the hydrostatic extrusion process for sizing and finishing conventionally hot-extruded (or rolled) structural shapes by various combinations of drawing and extruding. Primary emphasis will be on AISI 4340 steel, although some effort will be devoted to Ti-6Al-4V, 7075 aluminum, and selected refractory metals.

Part 2. To determine the feasibility of producing wire and filaments from TZM molybdenum alloy and beryllium by combinations of hydrostatic extrusion and drawing.

Part 3. To develop tooling and define process parameters necessary for the reduction of tube blanks to finish tubing from AISI 4340 and a selected columbium alloy.

Experimental trials to study the critical variables (Part I of Phase I) of the hydrostatic extrusion process were resumed during this quarterly period. In addition, initial experimental trials to fabricate tubing (Part 3 of Phase II) were conducted. A total of 87 extrusion trials were made, including extrusion of AISI 4340, Ti-6Al-4V, and 7075 Al into rounds, and extrusion of AISI 4340 and 7075 Al into T-sections and tubing. Important variables investigated included lubrication, stem speed, extrusion ratio, die design, and billet surface finish. Most of the conclusions drawn thus far must be considered tentative, however, until necessary quantitative evaluation of the physical, mechanical, and metallurgical properties of the extrusions is completed.

In addition to this experimental work, the complete results of the analytical study made on several container design concepts for high pressure are included in this report.

EQUIPMENT AND EXPERIMENTAL PROCEDURE

The hydrostatical extrusion tooling being used in the present program is that developed and fabricated in a previous Air Force program[1]. The general details of this tooling design are shown in a cross sectional view in Figure 1. Because a low-cycle-fatigue liner failure had been experienced after about 370 pressure cycles, the container design was revised such that the liner was replaced by two cylindrical rings which occupy the same volume as the liner. Details of the stress analysis for the design revision are contained in Interim Report No. 2[2]. The tooling is designed for use at fluid pressures up to 250,000 psi at room temperature and up to about 220,000 psi at 500 F. Specific details of the tooling and experimental procedure are given in Reference (1) and Interim Report No. 1[3].

A list of billet lubricants evaluated during the present report period is given in Table 1.

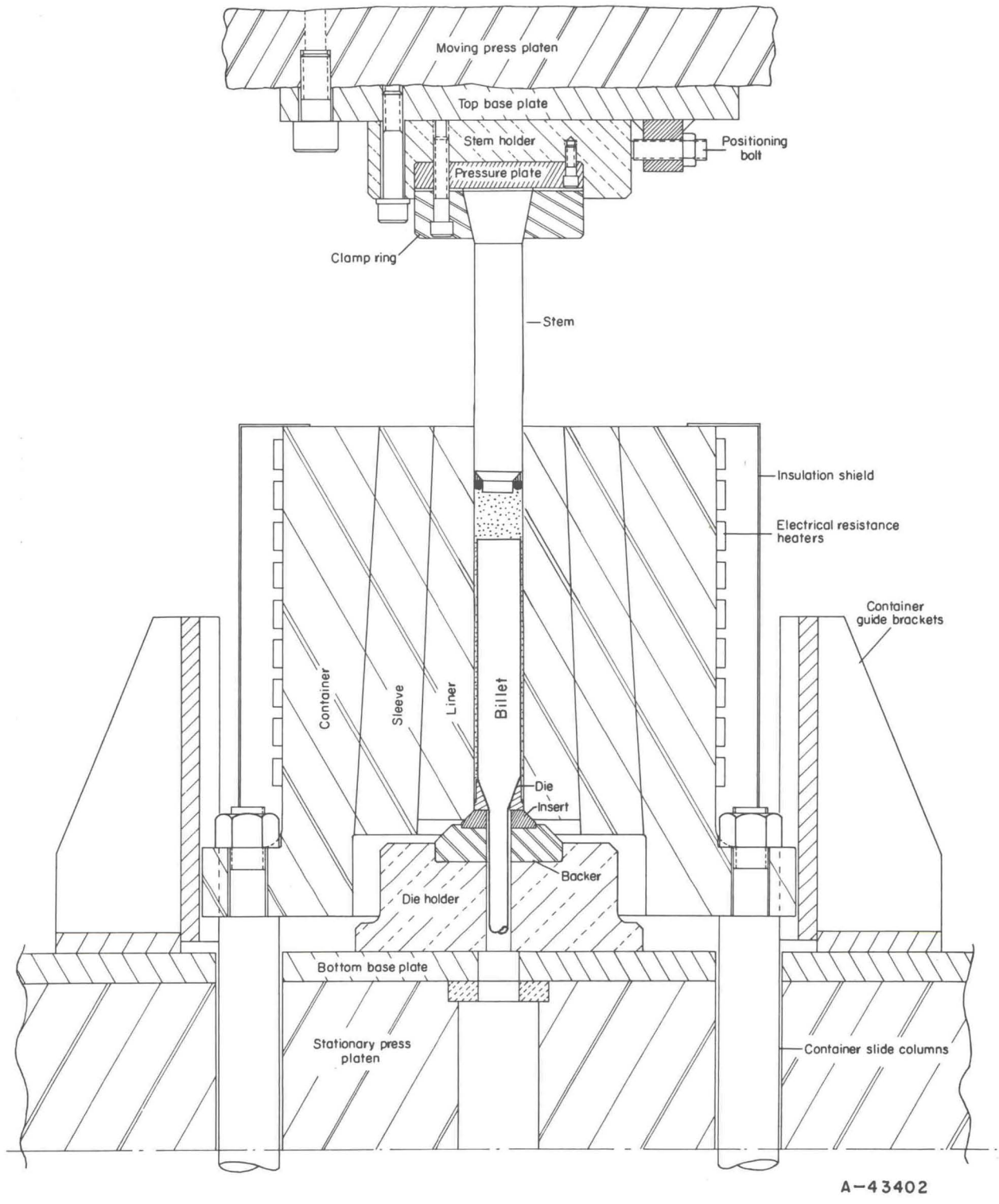

FIGURE 1. ASSEMBLY DRAWING OF TOOLING FOR HYDROSTATIC EXTRUSION

TABLE 1. BILLET LUBRICANTS EVALUATED IN CURRENT HYDROSTATIC EXTRUSION PROGRAM

Lubricant	Source	Description	Billet Materials Treated
L11	Commercial	"Castor wax" (hydrogenated castor oil; 158 F mp)	AISI 4340 and 7075 Al
L17	Battelle	20 w/o MoS_2 in castor wax	AISI 4340, Ti-6Al-4V, 7075 Al
L22	Battelle	20 w/o MoS_2 in polyethylene glycol, mw 1000	AISI 4340
L23	Battelle	20 w/o MoS_2 in low melting castor oil product	AISI 4340
L24	Battelle	20 w/o I_2 in naphthalene	Ti-6Al-4V
L25	Battelle	20 w/o I_2 and 10 w/o MoS_2 in naphthalene	Ti-6Al-4V
L26	Battelle	20 w/o I_2 in a chlorinated terphenyl (42% chlorine)	Ti-6Al-4V
L27	Battelle	50 w/o I_2 in oleic acid	Ti-6Al-4V
L28	Battelle	20 w/o MoS_2 in a chlorinated paraffin (70% chlorine)	Ti-6Al-4V
L29	Battelle	20 w/o MoS_2 in chloro-fluorocarbon wax, mp 200 F	Ti-6Al-4V
L30	Commercial	Cindol No. 4616	Ti-6Al-4V
L31	Commercial	Fluorocarbon telomer	Ti-6Al-4V
L32	Commercial	Polyethylene bag	Ti-6Al-4V

COLD HYDROSTATIC EXTRUSION OF AISI 4340 ROUNDS

Extrusion variables investigated for AISI 4340 steel included the following:

(1) Stem speed
(2) Lubrication system
(3) Die angle
(4) Billet surface finish

Experimental data obtained in each area are given in Table 2.

Stem Speed

The influence of stem speed on extrusion pressure and surface quality was evaluated for extrusion of AISI 4340 rounds at ratios of 3.33, 4, and 5:1. Stem speeds up to 80 ipm (the maximum speed of the hydraulic press) were investigated. Figure 2 shows the effect of stem speed on the stem breakthrough pressure in extrusion of AISI 4340 at a ratio of 5:1. Increasing the stem speed from 1 to 6 ipm decreased the stem breakthrough pressure by about 8 per cent. The stem pressures were essentially constant over the stem speed range from 6 to 80 ipm. The same general trend was reported previously[1] for hydrostatic extrusion of 1100-0 Al at stem speeds up to 20 ipm.

Although stem speeds above 6 ipm did not reduce extrusion pressure further, it is significant that hydrostatic extrusions of AISI 4340 of excellent surface quality can be produced at stem speeds of 80 ipm. Moreover, because the stem-to-billet cross sectional area ratio was 1.85:1, the "billet speed" on the "effective stem speed" was actually 148 ipm. This speed is well within the range used in production processes for conventional hot or cold extrusion. No problems in sealing were encountered. It appears likely that even faster stem speeds could be used without difficulty.

Lubrication System

Several billet lubricants and fluid media were evaluated at a stem speed of 20 ipm and extrusion ratios of 4 and 5:1. Some of the pertinent data obtained at a ratio of 4:1 are given below:

Trial	Hydrostatic Fluid	Billet Lubricant	Fluid Extrusion Pressure, 1000 psi	
			Breakthrough	Runout
289	Castor oil	L17	185.5	186.0
306	Castor oil	L17	186.0	186.0
294	Water	L17	175.0	183.5
295	Water	L17	187.0	186.0
301	Water	L17	186.5	186.0
302	Water	L17	186.0	185.0
303	Polyethylene glycol	L22	183.5	187.5
293	Polyethylene glycol	L23	185.5	179.0

TABLE 2. EXPERIMENTAL DATA FOR COLD HYDROSTATIC EXTRUSION OF AISI 4340 ROUNDS

Billet diameter - 1-3/4 inches Billet surface finish - 60 to 100 μ-inches, rms, except where noted.

Extrusion Ratio	Stem Speed, ipm	Die Angle, degrees	Hydrostatic Fluid	Billet Lubrication	Extrusion Pressure, 1000 psi				Length of Extrusion, inches	Comments
					Breakthrough		Runout			
					Stem	Fluid	Stem	Fluid		
5.0	20	30	Castor oil	L17	(273.0)[a]	(250.0)	--	--	0	Stopped at pressure indicated
5.0	20	45	Castor oil	L17	255.0	215.0	251.0	212.0	17-3/8	Slight P_b[b] peak; P_r[c] uniform
5.0	20	45	Castor oil	L17	(296.0)	(238.0)	--	--	1/16	Stopped at pressure indicated
5.0	20	45	Castor oil	L17	240.0	220.5	240.0	213.0	13-1/2	Slight P_b peak; P_r uniform
5.0	20	45	Castor oil	L17	248.0	222.0	248.0	216.0	13	Slight P_b peak; P_r uniform
5.0	20	60	Castor oil	L17	256.0	222.0	254.0	220.0	19-1/4	Slight P_b peak; P_r uniform
5.0	20	60	Castor oil	L17	259.0	232.0	257.0	230.0	14	No P_b peak; P_r uniform
5.0	20	90	Castor oil	L17	267.0	239.0	--	--	1-3/4	Stopped at P_b peak; no P_r
5.0	1	45	Castor oil	L17	266.0	242.0	263.0	233.0	6-1/4	Slight P_b peak followed by stick-
5.0	1	45	Castor oil	L17	260.0	229.0	256.5	222.0	11-1/2	No P_b peak; slight stick-slip
5.0	6	45	Castor oil	L17	255.0	231.0	256.0	227.0	12-7/8	Slight P_b peak; P_r uniform
5.0	20	45	Castor oil	L17	240.0	217.0	241.0	214.0	15	Slight P_b peak; P_r mostly uniform
5.0	80	45	Castor oil	L17	240.0	218.0	--	--	3-1/2	Very slight P_b peak; P_r not estim
5.0	80	45	Castor oil	L17	240.0	215.0	240.0	213.0	4-3/4	No P_b peak; P_r uniform
5.0	80	45	Castor oil	L17	237.0	216.0	243.0	216.0	14-1/4	No P_b peak; P_r very uniform
3.33	80	45	Castor oil	L17	--	160.5	--	--	8	Test data other than fluid P_b inv
3.33	80	45	Castor oil	L17	176.5	163.0	180.0	165.5	11-1/2	No P_b peak; P_r mostly uniform
3.33	80	45	Castor oil	L17	171.0	157.0	168.0	156.0	14	No P_b peak; P_r very uniform
4.0	20	45	Castor oil	L17	208.0	186.0	208.0	186.0	11	Very slight P_b peak; P_r uniform
4.0	20	45	Castor oil	L17	204.0	186.0	200.0	186.0	13	Very slight P_b peak; P_r uniform
4.0	80	45	Castor oil	L17	206.0	187.0	206.0	186.0	17	No P_b peak; P_r very uniform
4.0	20	45	Polyethylene glycol	L22	205.0	184.0	208.0	187.5	14	No P_b peak; P_r uniform
4.0	20	45	Polyethylene glycol	L23	204.0	186.0	201.0	179.0	14-3/4	Slight P_b peak; slight stick-slip
4.0	20	45	Water	L17	192.0	175.0	205.0	184.0	9	No P_b peak; P_r mostly uniform
4.0	20	45	Water	L17	204.0	187.0	212.0	186.0	13	No P_b peak; P_r very uniform
4.0	20	45	Water	L17	206.0	186.5	212.0	186.0	15	No P_b peak; P_r very uniform
4.0	20	45	Water	L17	202.0	186.0	204.0	185.0	13	Very slight P_b peak; P_r very unif
5.0	20	45	Polyethylene glycol	L22	249.0	229.0	249.0	226.0	15-1/2	No P_b peak; P_r uniform

TABLE 2. (Continued)

Item	Trial	Extrusion Ratio	Stem Speed, ipm	Die Angle, degrees	Hydrostatic Fluid	Billet Lubrication	Extrusion Pressure, 1000 psi				Length of Extrusion, inches	Comments
							Breakthrough		Runout			
							Stem	Fluid	Stem	Fluid		
4	276	5.0	20	45	Polyethylene glycol	L22	278.0	224.0	--	--	3/4	Stem seal broke just after breakthrough
	275	5.0	20	45	Polyethylene glycol	L23	247.0	230.0	245.0	228.0	13-1/4	Slight P_b peak; P_r uniform

(a) Parentheses indicate that true breakthrough pressure was not attained.

(b) P_b - breakthrough pressure.

(c) P_r - runout pressure.

(d) Billet surface finish was obtained by grit blasting followed by vapor blasting.

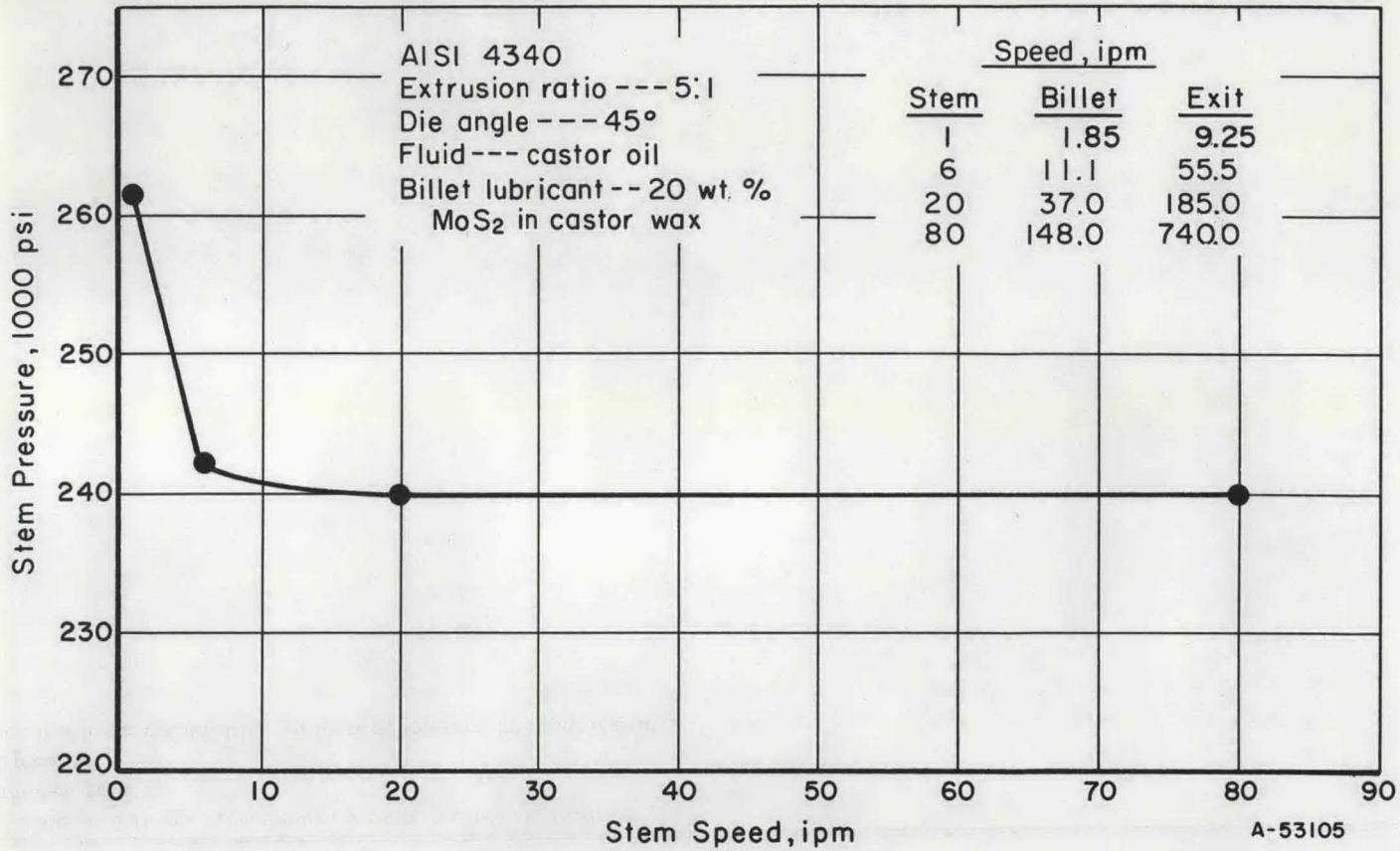

FIGURE 2. EFFECT OF STEM AND BILLET SPEED ON STEM PRESSURE FOR COLD HYDROSTATIC EXTRUSION OF AISI 4340 AT AN EXTRUSION RATIO OF 5:1

It is seen that no significant pressure differences were obtained under any of the above conditions. However, runout extrusion pressures and extrusion surface quality were generally better with either water or castor oil as the fluid medium than with polyethylene glycol. In addition, polyethylene glycol in combination with either L22 or L23 lubricant gave somewhat higher extrusion pressures than did castor oil at an extrusion ratio of 5:1.

A significant aspect of these results is the finding that water performs quite well as a fluid medium at the pressures reached thus far (185,000 psi). Water would certainly be advantageous in a commercial production operation from the standpoint of cost and handling.

Die Angle

Included die angles of 30, 45, 60, and 90 degrees were investigated at an extrusion ratio of 5:1 and a stem speed of 20 ipm with L17 lubricant, and castor oil for the hydrostatic fluid. The extrusion pressures were highest for die angles of 30 and 90 degrees. For a die angle of 60 degrees, the extrusion runout pressure was slightly higher (about 5 per cent) than that obtained for the 45-degree die. Based on available results, it is concluded that an included die angle of 45 degrees approaches the optimum under these extrusion conditions.

Billet Surface Finish

The effect of billet surface finish on extrusion pressure and surface quality was investigated for AISI 4340 at ratios of 4 and 5:1. A comparison was made between standard machined surface finishes (about 60 to 100 microinches, rms) and relatively rough surfaces obtained by grit blasting followed by vapor blasting. The latter step was used to remove superficial grit, and any sharp points and edges caused by the grit. Stem speeds of 20 and 80 ipm were used. Castor oil or water were used as the fluid media and L17 as the billet lubricant.

The extrusion pressures and extruded surface finishes (by visual examination) were found to be about the same for either the machined or grit billet finish. This is an indication that the billet lubricant used was quite effective by itself, and that a rough billet surface finish in this case does not cause any significant pressure reduction.

COLD HYDROSTATIC EXTRUSION OF 7075-0 ALUMINUM ROUNDS

Among the critical process variables investigated thus far with 7075 Al are:

(1) Extrusion ratio
(2) Stem speed
(3) Lubrication
(4) Billet surface finish

The experimental data are given in Table 3. With this material, the effects of these variables are particularly important because of the tendency of the alloy to stick-slip during extrusion. The stick-slip problem stems from momentary breakdown of the billet lubricant. In these extrusion trials, castor oil was used as the fluid, and the billets were lubricated with either L11 or L17.

In spite of the problem of stick-slip, good extrusions at ratios of 20:1, 40:1, and 60:1 were produced at room temperature. Lubricant L17 was found to be very effective in minimizing the tendency toward surface cracking compared to L11. Moreover, of particular significance is the fact that surface cracking was eliminated (based on preliminary inspection) in the 20:1 ratio extrusions by increasing the stem speed from 20 to 80 ipm. Elimination of surface cracks is believed to be associated with the fact that the stem speed of 80 ipm eliminated stick-slip during runout. Cracking tends to occur in the portions of the rod that are suddenly extruded during the "slip" part of stick-slip. These portions are extruded at extremely rapid rates, perhaps in the order of several thousand inches per minute. Exit surface temperatures may become excessive under these conditions and lead to cracking.

This aluminum alloy is known for its tendency to crack during conventional hot extrusion. To prevent cracking, the exit extrusion speeds are kept very low, sometimes as low as 6 to 12 ipm. It has been shown thus far that, with hydrostatic extrusion, sound extrusions can be produced at exit speeds of about 3000 ipm. (This was calculated based on a ratio of 20:1, and a billet speed of 148 ipm produced at the stem speed of 80 ipm.) Obviously, this would be a very significant potential advantage in a production operation.

At ratios of 40:1 and 60:1, the maximum stem speed attempted thus far was 20 ipm. Stick-slip still occurred under these conditions. The effect of extrusion ratio on hydrostatic extrusion pressure is shown in Figure 3. Plots are shown for both breakthrough and runout pressures. The runout pressures are based on the pressure minimums reached after breakthrough. Past experience has shown that such minimums are, in fact, the runout pressures when stick-slip is eliminated. Figure 3 shows the breakthrough pressures to be considerably higher than the runout pressures. An improvement in lubrication to prevent stick-slip would greatly reduce the extrusion pressure requirements, although the fluid breakthrough pressure for extrusion at a ratio of 60:1 with the present lubricant is only 200,000 psi, still substantially below the maximum pressure capability of the present tooling. Extrusion ratios in the order of 100:1 appear to be feasible at present, but even much larger ratios should be possible with better billet lubricants.

A study was made of the effect of billet surface finish on stick-slip and cracking. Machined surfaces varying in roughness from 50 to 500 microinches, rms were investigated in addition to finishes produced by grit blasting followed by vapor blasting. Although the results thus far may not be conclusive, definite trends are evident.

At an extrusion ratio of 20:1, surface finishes in the order of 50 microinches, rms, resulted in the highest stick-slip pressure peaks (beyond the breakthrough pressure point) regardless whether Lubricant L11 (Trial 251) or L17 (Trial 308) was used. Increasing the surface roughness to 300-500 microinch range lowered these stick-slip pressure peaks, but generally did not succeed in preventing them, except in one case (Trial 249). A macroscopic examination of the extrusion butt of Trial 249 is being made to determine whether any special surface finish characteristics may have helped to prevent stick-slip in this case.

TABLE 3. EXPERIMENTAL DATA FOR COLD HYDROSTATIC EXTRUSION OF 7075 ALUMINUM ROUNDS[a]

Die Angle ------- 45 degrees Fluid -------- Castor oil

Item	Trial	Extrusion Ratio	Stem Speed, ipm	Billet Surface Finish microinches, rms	Billet Lubrication	Extrusion Pressure, 1000 psi				Length of Extrusion, inches	Comments
						Breakthrough		Runout			
						Stem	Fluid	Stem	Fluid		
1	251	20.0	20	50	L11	199.0	174.0	--	--	--	Small P_b peak; severe stick-slip
	250	20.0	20	110-130	L11	180.0	160.0	--	--	30 1/2	Small P_b peak; severe stick-slip
	249	20.0	20	270	L11	149.0	136.0	142.0	130.0	87 5/8	Small P_b peak; P_r uniform
	297	20.0	20	300	L11	146.0	133.5	140.0	128.0	49 1/2	Small P_b peak; severe stick-slip
	298	20.0	20	350	L11	142.0	130.0	141.5	129.5	40	Small P_b peak; severe stick-slip
	299	20.0	20	400	L11	146.5	134.0	137.0	125.0	44	Small P_b peak: severe stick-slip
	256	20.0	20	Grit[b]	L11	173.0	157.0	--	--	22 3/8	Severe stick-slip
	273	20.0	20	Grit	L11	165.0	161.0	--	--	26 9/16	Severe stick-slip
	283	20.0	20	Grit	L11	155.0	142.0	147.0	134.5	30	Moderate P_b peak; severe stick-slip
	255[c]	20.0	20	300	L17	162.0	159.0	--	--	0	P_b not reached
	271[c]	20.0	20	350	L17	239.0	225.0	--	--	0	P_b not reached
	272[c]	20.0	20	400	L17	274.0	248.0	--	--	0	P_b not reached
2	308	20.0	20	35-50	L17	199.0	186.5	--	--	17	Severe stick slip
	309	20.0	20	100-250	L17	167.0	153.0	139.0	124.5	50	Severe stick slip
	329	20.0	20	350	L17	148.0	135.0	143.0	131.0	41	Severe stick slip
	330	20.0	20	500	L17	149.0	136.0	147.0	134.5	51	Severe stick slip
	281	20.0	20	Grit	L17	(d)	149.0	(d)	130.0	43	Severe stick-slip
	282	20.0	20	Grit	L17	(d)	149.0	(d)	131.5	46	Severe stick-slip
3	310	20.0	80	100-120	L17	167.0	153.0	139.0	127.0	79	High P_b peak; P_r uniform
	317	20.0	80	60 on taper 260 on rest	L17	160.0	146.5	144.0	127.5	64	High P_b peak; P_r uniform
	311	20.0	20	Grit	L17	167.0	150.0	141.5	125.0	80	High P_b peak; P_r uniform
4	318	40.0	20	45-65	L17	197.0	180.0	157.0	142.5	90	High P_b peak; severe stick-slip
	319	40.0	20	Grit	L17	195.0	180.0	161.0	142.5	88	High P_b peak; severe stick-slip
5	327	60.0	6	Grit	L17	239.0	216.5	173.0	156.0	60	High P_b peak; severe stick-slip
	322	60.0	20	Grit	L17	217.0	202.0	171.0	153.0	81	High P_b peak; severe stick-slip
	324	60.0	20	60-100	L17	222.0	201.5	167.0	147.0	90	High P_b peak; severe stick-slip

Footnotes on following page.

Footnotes for Table 3

(a) The 7075 Al billets were in the annealed condition, except where noted.
(b) "Grit" refers to a billet surface obtained by grit blasting followed by vapor blasting.
(c) Trials 255, 271, and 272 were attempted with 7075 Al billets in the T6 condition.
(d) Stem load cell recorder did not function.

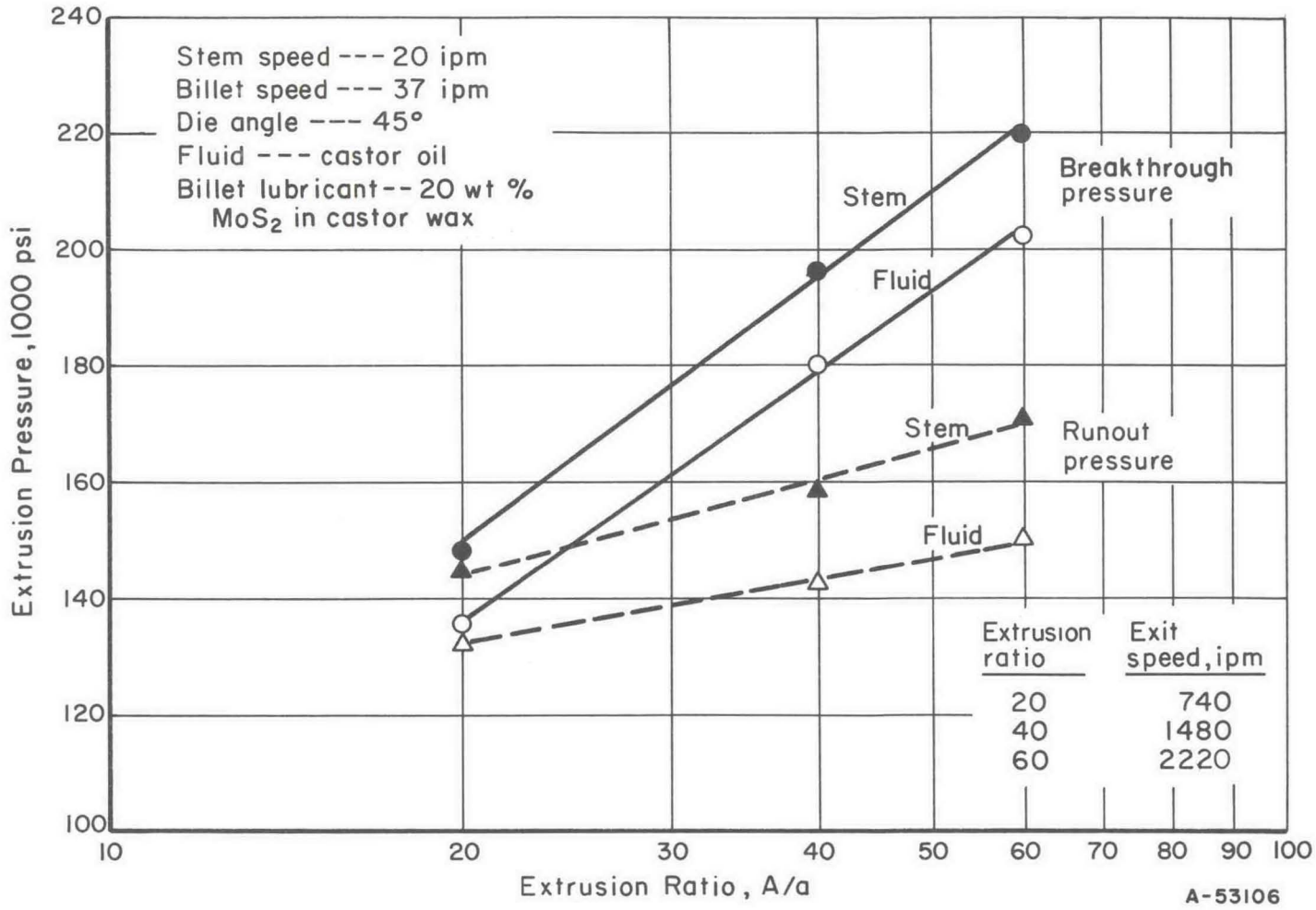

FIGURE 3. EFFECT OF EXTRUSION RATIO ON PRESSURE FOR COLD HYDROSTATIC EXTRUSION OF 7075-0 ALUMINUM

The grit billet finishes did not succeed in preventing stick-slip but were effective in improving the finish of the extruded product and minimizing cracking. Grit blasting produces a matte finish which smoothens out fairly well on the extruded surface. The machined finish, however, results in a slight helical groove pattern which becomes more pronounced with increasing initial surface roughness and extrusion ratio. In fact, the helical groove pattern has been observed on grit-blasted billets that were extruded at ratios of 40 and 60:1. This is evidence of the machined surface that had been covered over by grit blasting. It appears also that, in the case of relatively rough machined billets (300-500 μ-in.) and high ratios, the helical grooves become sites for initiating surface cracks.

COLD HYDROSTATIC EXTRUSION OF Ti-6Al-4V ALLOY ROUNDS

Ti-6Al-4V alloy has the same tendency for stick-slip during extrusion as 7075 aluminum. Moreover, when the billet lubricant breaks down to a point where metal-to-metal contact occurs, the alloy tends to gall or adhere severely to the die. Efforts to extrude Ti-6Al-4V alloy were concentrated on determining a better lubrication system than those investigated previously[1]. Data are given in Table 4 for extrusions made with various lubricants at stem speeds of 6 inches per minute and an extrusion ratio of approximately 3.33:1.

The combination of L17 with a fluoride-phosphate coating (C2) appeared promising (Trial 286). The breakthrough fluid pressure (186,000 psi) was about 6 per cent lower than that obtained (202,000 psi) with L11 and L8 lubricants (castor wax over a 10 wt % graphite-gum resin mixture) in the previous program[1]. Moreover, no stick-slip nor severe pressure buildup occurred during runout.

Lubricants L24 through L27 contained substantial quantities of iodine. The purpose of the iodine was to react chemically with the billet surface to form a product that would offer less frictional resistance than the titanium alloy itself. Except for L27, these lubricants appeared to reduce the tendency toward stick-slip. However, the improvements did not appear to be significant.

Some modifications of the present lubricants and new lubricants are being planned for evaluation in the next series of extrusion trials.

COLD HYDROSTATIC EXTRUSION OF T-SECTIONS

A series of extrusion trials was conducted to investigate the effect of die design for extrusion of a T-section. A photograph of the two dies evaluated is given in Figure 4. One die design, used in the previous program[1], consists of a conical entry defined by a single angle of 45 degrees. The other die design differs in that the conical entry is defined by a compound angle: a 45-degree conical surface leading into a 160-degree conical surface, the latter circumscribing the T-opening. The latter design offers the potential advantage of reducing die machining costs. Also, the latter design permits the die bearing surface to be less irregular, which may be an advantage during extrusion. However, it was recognized that the relatively flat area near the T-opening would raise the extrusion pressure over that obtained with the "single-angle" die but the extent of this pressure rise had to be determined by experiment.

TABLE 4. EXPERIMENTAL DATA FOR COLD HYDROSTATIC EXTRUSION OF Ti-6Al-4V ALLOY ROUNDS

Die Angle ----- 45 degrees
Fluid --------- Castor oil
Stem Speed ---------- 6 ipm
Billet Surface Finish ------ 60-100 microinches, rms

Item	Trial	Extrusion Ratio[a]	Billet Lubrication		Extrusion Pressure, 1000 psi				Length of Extrusion, inches	Comments
					Breakthrough		Runout			
			Coating	Lubricant	Stem	Fluid	Stem	Fluid		
1	264	3.33	C2[c]	L17	214.0	200.0	(b)	(b)	5/8	Slight P_b peak; severe stick-slip
	286	3.23	C2[c]	L17	202.0	186.0	209.0	192.0	6-1/2	Slight P_b peak; P_r increased toward end of stroke
	278	3.31	None	L17	244.0	222.0	(b)	(b)	5/8	Slight P_b peak; severe stick-slip
	279	3.23	None	L17	240.0	219.0	(b)	(b)	5/8	Same as above
	291	3.31	None	L17	202.0	188.0	--	--	6-1/2	Slight P_b peak; moderate stick-slip followed by severe stick-slip
2	300	3.19	None	L24	202.0	187.0	216.0	196.0	11	Slight P_b peak; moderate stick-slip followed by uniform P_r
3	296	3.31	None	L25	224.0	210.0	212.0	196.0	11-1/2	High P_b peak; moderate stick-slip followed by uniform P_r
4	290	3.21	None	L26	223.0	203.0	210.0	186.5	11-3/4	High P_b peak; moderate stick-slip followed by moderate stick-slip
5	292	3.21	None	L27	217.0	194.0	219.0	188.5	5-1/2	Slight P_b peak followed by severe stick-slip
6	267	3.33	None	L28	245.0	226.0	(b)	(b)	5/8	Stopped at indicated pressure
	314	3.19	None	L28	249.0	225.5	--	--	0	Billet cocked; die broke
	337	3.33	None	L28	240.0	221.5	--	--	1/8	Stopped at indicated pressure
7	266	3.33	None	L29	240.0	224.0	(b)	(b)	5/8	Slight P_b peak; severe stick-slip
	313	3.19	None	L29	262.0	235.0	--	--	1/8	Stopped at indicated pressure
	338	3.33	None	L29	246.0	222.0	--	--	0	Billet cocked; die broke
8	268	3.33	None	L30	214.0	200.0	(b)	(b)	7/16	Slight P_b peak; severe stick-slip
	304	3.28	None	L30	250.0	223.0	--	--	0	Billet cocked; die broke
	307	3.19	None	L30	228.0	205.0	240.0	204.0	9-1/2	Slight P_b peak; severe stick-slip followed by moderate stick-slip
9	269	3.33	None	L31	240.0	222.0	(b)	(b)	5/8	Slight P_b peak; severe stick-slip
	305	3.19	None	L31	264.0	237.0	--	--	1/8	Stopped at indicated pressure
10	270	3.33	None	L32	226.0	208.0	(b)	(b)	5/8	Slight P_b peak; severe stick-slip

(a) Extrusion ratio initially at 3.33:1 (70 per cent area reduction) but was decreased slightly later when extrusion die orifices were remachined to remove score marks.
(b) Stopped after breakthrough but before runout pressures were obtained.
(c) C2 - Fluoride-phosphate coating.

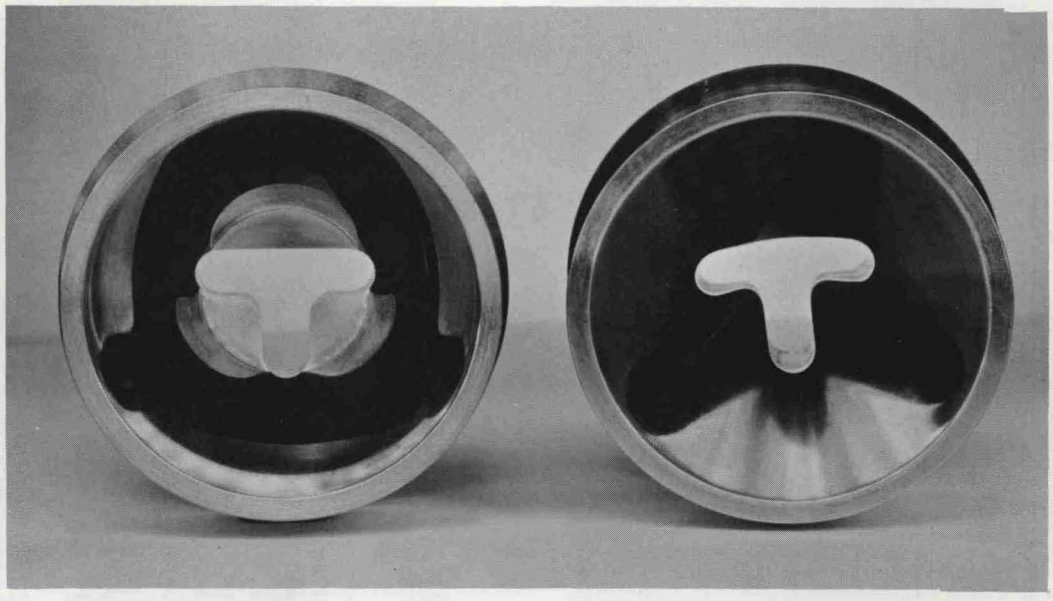

FIGURE 4. DIE CONFIGURATIONS USED FOR EXTRUDING T-SECTIONS

Left: Compound-angle die, 45-degree entry angle leading into a 160-degree angle
Right: Single-angle die with 45-degree entry

The extrusion trials were conducted with AISI 4340 and 7075 Al billets. The experimental data are contained in Table 5. The first trial was made with AISI 4340 at an extrusion ratio of 3:1 with the single-angle T-die. Unfortunately, the billet cocked some time after breakthrough. During the attempt to remove the billet and partial extrusion from the die, the die split into three pieces at the T-corners. At first glance, it appears that the failure was probably due to the high stresses imposed at T-corners by cocking of the billet.

Some worthwhile information was obtained, however, with both die designs. The breakthrough fluid pressure was 210,000 psi (Trial 316) for the single-angle die. However, breakthrough was not reached at 236,000 to 245,000 psi (Trails 341 and 342) for the compound-angle die. Thus, it appears that the pressure penalty for extrusion of AISI 4340 is quite high with the latter die design.

T-sections of excellent surface quality were extruded from 7075 aluminum at a ratio of 7.3:1 with the compound-angle die. (Single-angle die trials will be made in the future for comparison purposes.) Stem speeds of 6, 20, and 80 ipm were investigated. Although this stem speed range did not influence the extrusion pressure requirements, it had a pronounced effect on stick-slip and extruded surface quality. With stem speeds of 6 ipm, extrusion was accompanied by severe stick-slip. At a stem speed of 20 ipm, stick-slip was less severe. Increasing the stem speed to 80 ipm completely eliminated stick-slip and resulted in an extruded surface of very high quality. The T-section extruded at 80 ipm is shown in Figure 5.

TABLE 5. EXPERIMENTAL DATA FOR COLD HYDROSTATIC EXTRUSION OF AISI 4340 STEEL AND 7075 ALUMINUM T-SECTIONS

Billet lubricant---L17 Fluid--- Castor oil

Item	Trial	Material	Die Design	Die Angle, degrees	Extrusion Ratio	Stem Speed	Billet Surface Finish, microinches, rms	Extrusion Pressure, 1000 psi: Breakthrough Stem	Breakthrough Fluid	Runout Stem	Runout Fluid	Length of Extrusion, inches	Comments
1	316	4340	Single angle	45	3.0	6	50-100	232.0	210.0	--	--	2-1/4	Slight P_b peak; severe stick-slip. Die broken on extrusion removal.
2	341	4340	Compound angle	45, 160	3.0	6	Grit[a]	256.0	236.0	--	--	1/8	Stopped at indicated pressure.
	342	4340	Compound angle	45, 160	3.0	6	Grit	274.0	245.5	--	--	1/8	Stopped at indicated pressure.
3	321	7075	Compound angle	45, 160	7.3	6	Grit	133.0	122.0	120.0	110.0	17	High P_b peak; severe stick-slip.
	320	7075	Compound angle	45, 160	7.3	6	30-200	133.0	118.0	119.0	106.0	12-1/2	High P_b peak; severe stick-slip.
	325	7075	Compound angle	45, 160	7.3	20	Grit	123.0	115.0	118.5	109.0	15	Moderate P_b peak; moderate stick-slip.
	326	7075	Compound angle		7.3	80	40-130	130.0	119.0	112.0	103.5	22-1/2	High P_b peak; Pr uniform.

(a) Grit billet surface finish obtained by grit blasting followed by vapor blasting.

TABLE 6. EXPERIMENTAL DATA FOR COLD HYDROSTATIC EXTRUSION OF AISI 4340 STEEL AND 7075 ALUMINUM TUBING[a]

Die angle --------45 degrees
Fluid ----------Castor oil
Billet lubricant --- L17

Billet size ------1.750 OD x 0.750 ID
Mandrel --------0.7485 dia at top
0.7460 dia at bottom
Billet surface ---25 to 100 microinches, rms

Item	Trial	Material	Die Orifice, inches	Extrusion Ratio	Stem Speed, ipm	Extrusion Pressure, 1000 psi: Breakthrough Stem	Breakthrough Fluid	Runout Stem	Runout Fluid	Length of Extrusion, inches	Comments
1	336	4340	1.107	3.77	6	174.0	158.5	179.0	154.5	9-1/2	No P_b peak; uniform P_r followed by pressure rise.
2	331	7075	1.107	3.77	6	49.6	47.0	48.0	47.0	9-1/2	No P_b peak; very slight stick-slip.
	333	7075	1.107		20	48.0	48.0	48.0	48.0	14-1/4	No P_b peak; P_r uniform.
3	335	7075	0.875	12.2	1	135.0	126.0	98.7	92.0	48	High P_b peak; severe stick-slip.
	332	7075	0.875	12.2	6	121.0	110.5	98.0	86.8	42	High P_b peak; severe stick-slip.
	334	7075	0.875	12.2	20	118.0	106.0	100.0	89.2	36	Moderate P_b peak; severe stick-slip.

(a) P_b = breakthrough pressure; P_r = runout pressure.

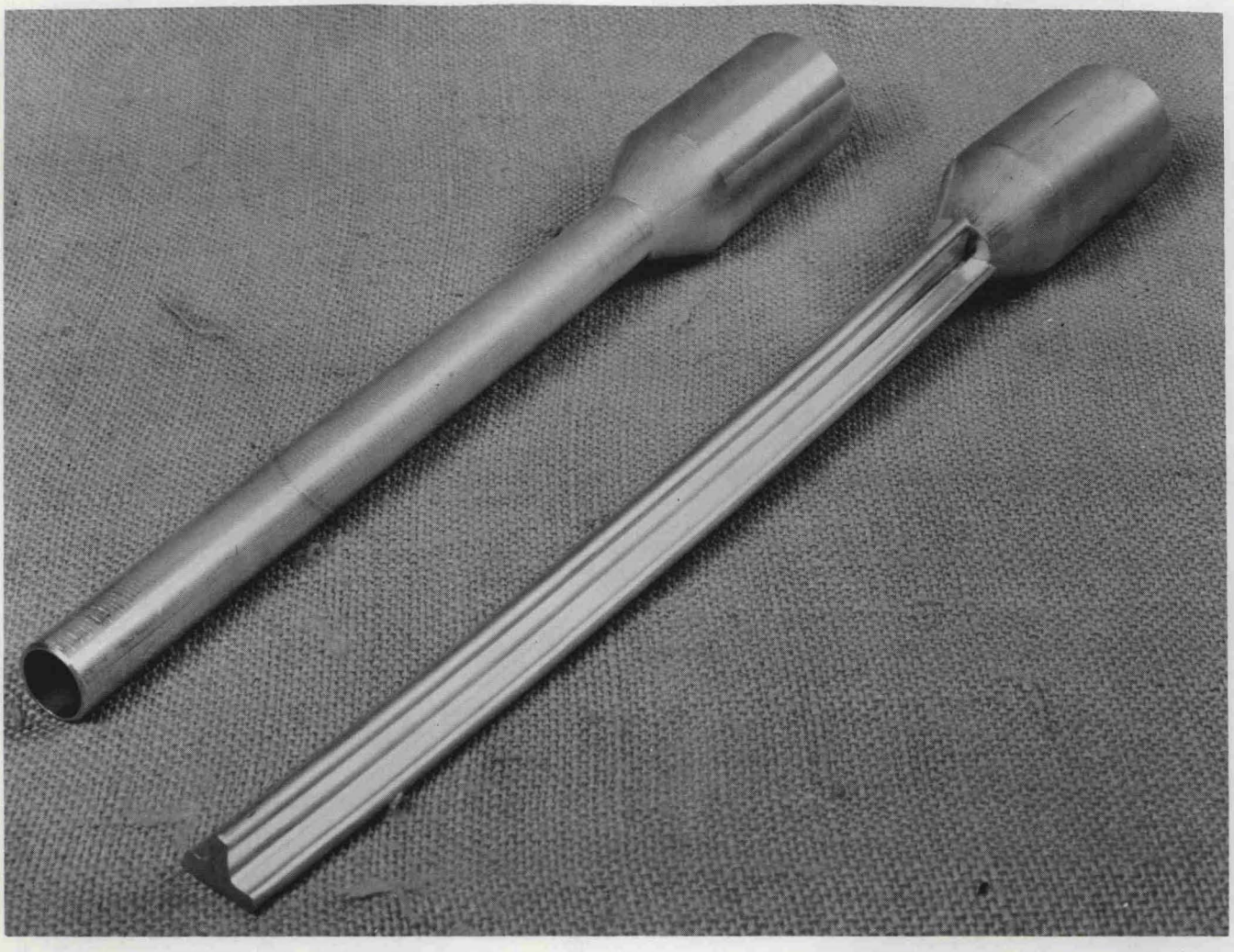

FIGURE 5. HYDROSTATIC EXTRUSIONS OF TUBING AND T-SECTION PRODUCED FROM 7075 ALUMINUM AT ROOM TEMPERATURE.

	Extrusion Ratio	Section Size, inch
Tubing	12. 2:1	0. 875 OD x 0. 750 ID x 0. 063 wall
T-Section	7. 3:1	0. 938 x 0. 688 x 1/4-inch thick

COLD HYDROSTATIC EXTRUSION OF TUBING

The mandrel tooling arrangement designed for the initial trials of hydrostatic extrusion of tubing is shown schematically in Figure 6. The mandrel is a floating rather than fixed type. It anchored at its top end by a guide which rests directly on the billet top and fits the liner bore closely. Although not shown in Figure 6, the guide contains flats on its OD surface to permit free flow of the hydrostatic fluid medium. As the billet extrudes, the mandrel and guide move with it. The tubing is extruded over a moving mandrel, and the latter is tapered slightly to reduce frictional drag on the tubing. The mandrel can be made a fixed type by placing a tube spacer between the guide and the top flat surface of the die. This arrangement may be investigated later if necessary.

Tubing was produced from both 7075 Al and AISI 4340. The experimental data are given in Table 6. 7075 Al tubing was extruded to the following sizes at ratios of 3.77 and 12.2:1 at stem speeds up to 20 ipm:

	Tube Size, inches		
Ratio	OD	ID	Wall
3.77:1	1.107	0.750	0.178
12.2:1	0.875	0.750	0.063

At a stem speed of 20 ipm, stick-slip was prevented at the lower ratio only. Tubing of excellent surface quality was produced under these conditions. At a ratio of 12.2:1, stick-slip persisted at the stem speed of 20 ipm but tubing of fair surface quality was still produced as seen in Figure 5. The lathe machine marks orginally on the billet are evident on the tube surface, indicating that lubrication during the "slip" portion of stick-slip was sufficiently good to preserve the pattern. If undesirable, such patterns can probably be prevented or minimized by changing the original billet surface finish or modifying the die design.

About 10 inches of AISI 4340 tubing of high surface quality was produced at an extrusion ratio of 3.77:1. The runout pressure was uniform at first, indicating that lubrication was good. Toward the end of the stroke, the runout pressure began to rise continuously without any evidence of stick-slip. Examination of the extrusion afterward revealed that the pressure rise was due to excessive frictional drag of the tubing over the bottom portion of mandrel. Part of the frictional drag may have been due to the simultaneous thermal contraction of the tubing and thermal expansion of the mandrel. To prevent or minimize this problem, the taper on the mandrel will be increased to provide greater clearance between it and the extruded tubing.

FUTURE WORK

During the next interim report period evaluation of extrusion trials made during this report period will be continued. These efforts will include quantitative measurement of extruded surface quality as well as determination of mechanical properties where appropriate. Also, it is expected that hot extrusion trials will be started, and efforts will continue in preparing for experimental work with other extrusion shapes and materials.

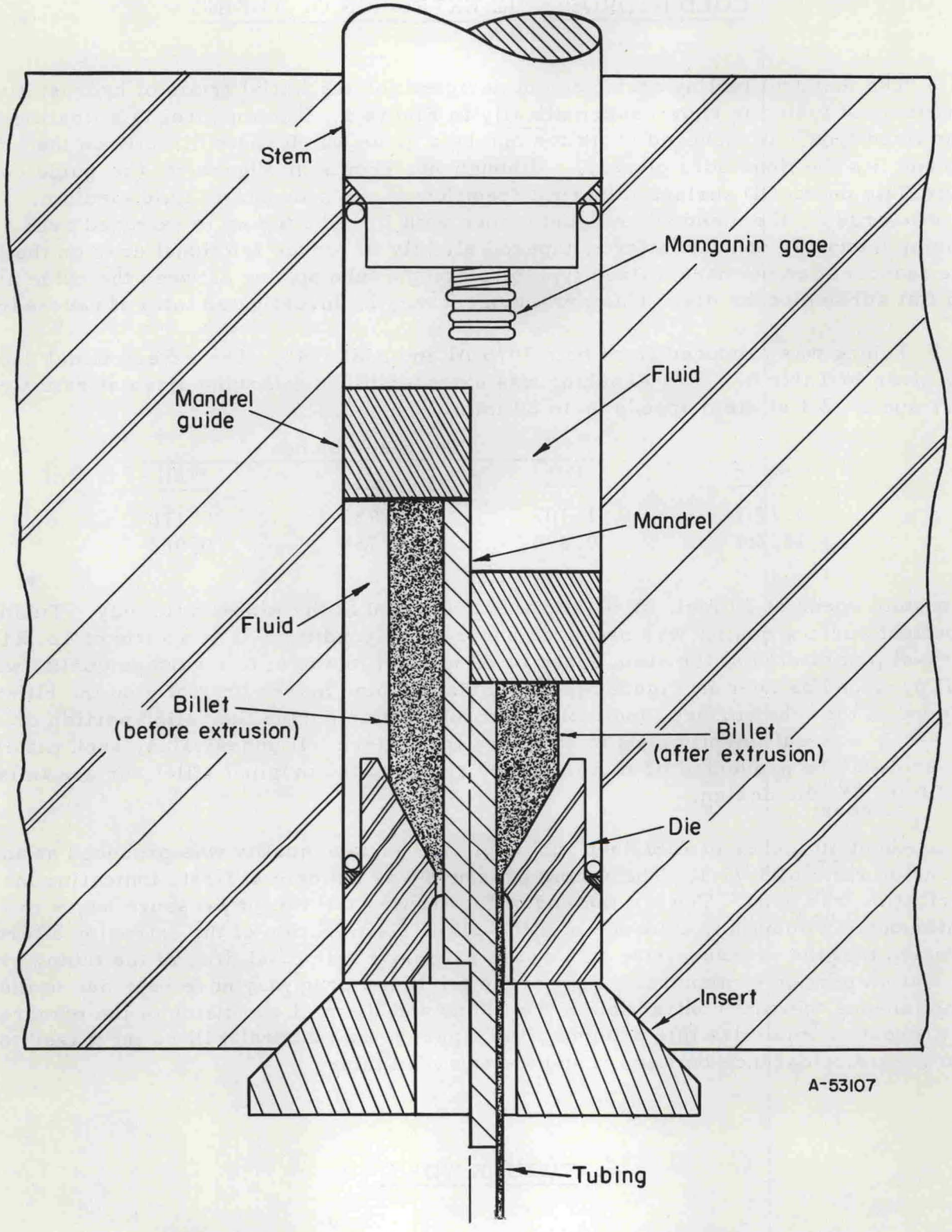

FIGURE 6. MANDREL TOOLING ARRANGEMENT FOR HYDROSTATIC EXTRUSION OF TUBING

ANALYSIS OF SEVERAL HIGH-PRESSURE CONTAINER DESIGN CONCEPTS

INTRODUCTION

This design analysis is part of a research program to develop the manufacturing capabilities of the hydrostatic extrusion process. An important component of the extrusion equipment is the pressure container. The purpose of this design study was to determine the maximum pressure capability of several containers at the fluid pressures expected in advanced hydrostatic forming processes. Containment of bore fluid pressures up to 450,000 psi at room temperature and at temperatures of 500 F and 1000 F was considered. The results of the study also pertain to other applications, besides hydrostatic extrusion, where such pressures are encountered.

A summary report of the important results of this study has already been given as part of the last interim progress report (Report IV for 1 September 1964-30 November 1965). The present report gives a complete and detailed description of the analysis including a comprehensive presentation of results.

SCOPE OF ANALYSIS

The purpose of this study is to determine the maximum pressure capability of several designs of vessels for containing fluids at the pressures encountered in hydrostatic extrusion and other hydrostatic forming processes. Containment of bore fluid pressures up to 450,000 psi at room temperature and at temperatures of 500 F and 1000 F is considered.

The operating cycle of these high-pressure containers consists of application of the pressure needed for extrusion or forming, followed by a decrease in the pressure to zero. To be useful in production, the high-pressure containers must withstand a large number of such operating cycles. Therefore, fatigue strength of component materials must be an important design consideration. However, consideration of fatigue strength appears to be lacking in design analyses heretofore. The general method of design analysis has been to use a safety factor on the yield pressure. As the design pressures have been steadily increased, material limitations have necessitated lower factors of safety, sometimes less than 1.1. Consequently, fatigue failures are being experienced. Because of the extreme operating pressures being considered for hydrostatic extrusion and other forming operations (up to about 450,000 psi), it was essential that the various container design concepts be analyzed and compared on the basis of a fatigue criterion.

In order to estimate the pressure capability of each container, stress analyses are conducted. Only stresses due to the bore pressure and shrink-fit assembly are analyzed; no thermal gradients are assumed present. However, the effect of temperature change (from operating temperature to room temperature) upon the prestress (residual stresses) is included in the analyses. Excessive residual stresses may result because of differences in thermal expansion of the component parts of each container.

Four types of pressure vessel designs were analyzed in detail. These are:

(1) Multi-ring container,
(2) Ring-segment container,
(3) Ring-fluid-segment container, and
(4) Pin-segment container.

The four cylindrical containers are shown in Figure 7. A wire-wrapped (strip-wound) vessel and a controlled fluid-fill, cylindrical-layered container were also considered, but only briefly.

The multi-ring container was one of the first design modifications of the monoblock thick-walled cylinder*. An initial compressive stress at the bore is achieved by shrink-fit assembly of successive cylinders each manufactured to provide an interference fit with its mating cylinder. The multi-ring container has been analyzed on the basis of static shear strength by Manning[4, 5, 6].

The ring-segment container with one outer ring was patented by Poulter[7] in 1951. One intent of this design is to reduce the pressure acting upon the outer ring by using a segmented cylinder to redistribute the pressure at a larger diameter. However, the inner cylinder is always subject to the bore pressure. The external diameter of the vessel necessarily increases with increasing segment size.

The ring-fluid-segment container makes use of the fluid-pressure support principle. This container is essentially constructed of two parts. The inner part is a ring-segment-type container with one outer ring, but with a fluid support pressure, p_3, as shown in Figure 8(c). The outer part is a multi-ring container subject to an internal pressure, p_3, the support pressure for the inner part. The advantage of this design is that the fluid pressure (p_3) provides a compressive hoop stress at the bore which counteracts the tensile hoop stress resulting from the bore pressure, p. Theoretically, p_3 can be changed in proportion to the change in bore pressure in order to reduce the bore stress over an entire cycle of bore pressure. This variation of p_3 with the bore pressure is assumed in the analysis.

The origin of the ring-fluid-segment concept is not clear. Ballhausen[8] patented an approach of this sort in 1963. Another application of the same principle was patented by G. Gerard and J. Brayman[9], also in 1963. A similar design, but with additional features, was reported by F. J. Fuchs[10] in 1965.

The pin-segment design is an approach proposed by Zeitlin, Brayman, and Boggio[11]. Like the ring-segment container this vessel also uses segments to reduce the pressure that must be carried by the external support. Unlike the ring-segment container, the pin-segment container has segmented disks (thin plates) rather than segmented cylinders. Also, the external supporting members in this case are pins rather than an external ring. The pins carry the reaction to the bore pressure predominantly in shear.

All four containers have one thing in common: the liner is subject to the full bore pressure. The four containers differ in the manner and in the amount they constrain the liner.

*The monoblock thick-wall cylinder is the simplest type of pressure container. However, for the very high pressure levels considered in this study it is a relatively inefficient design.

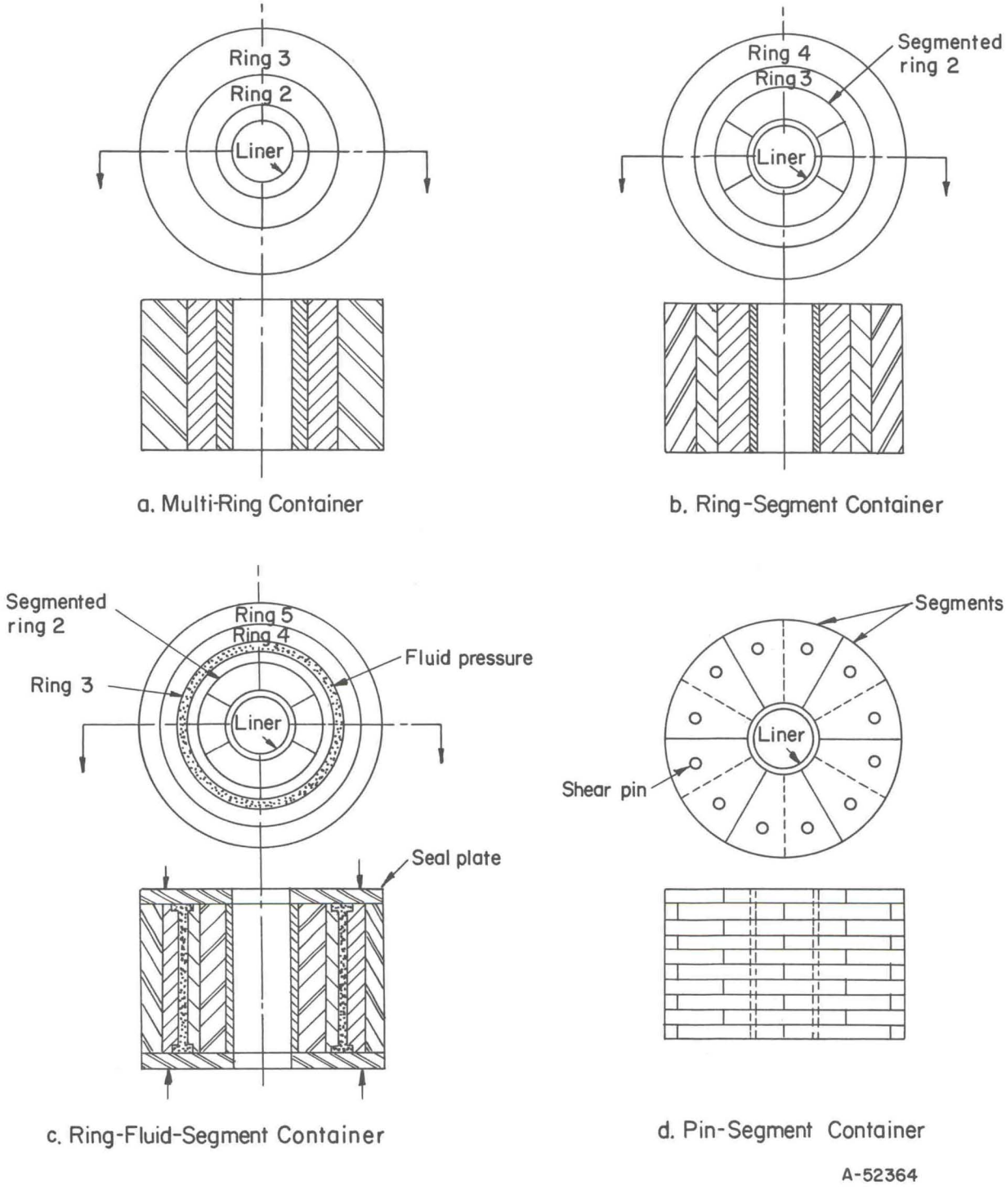

FIGURE 7. SCHEMATIC OF HIGH-PRESSURE-CONTAINER DESIGN CONCEPTS ANALYZED IN THE PRESENT STUDY

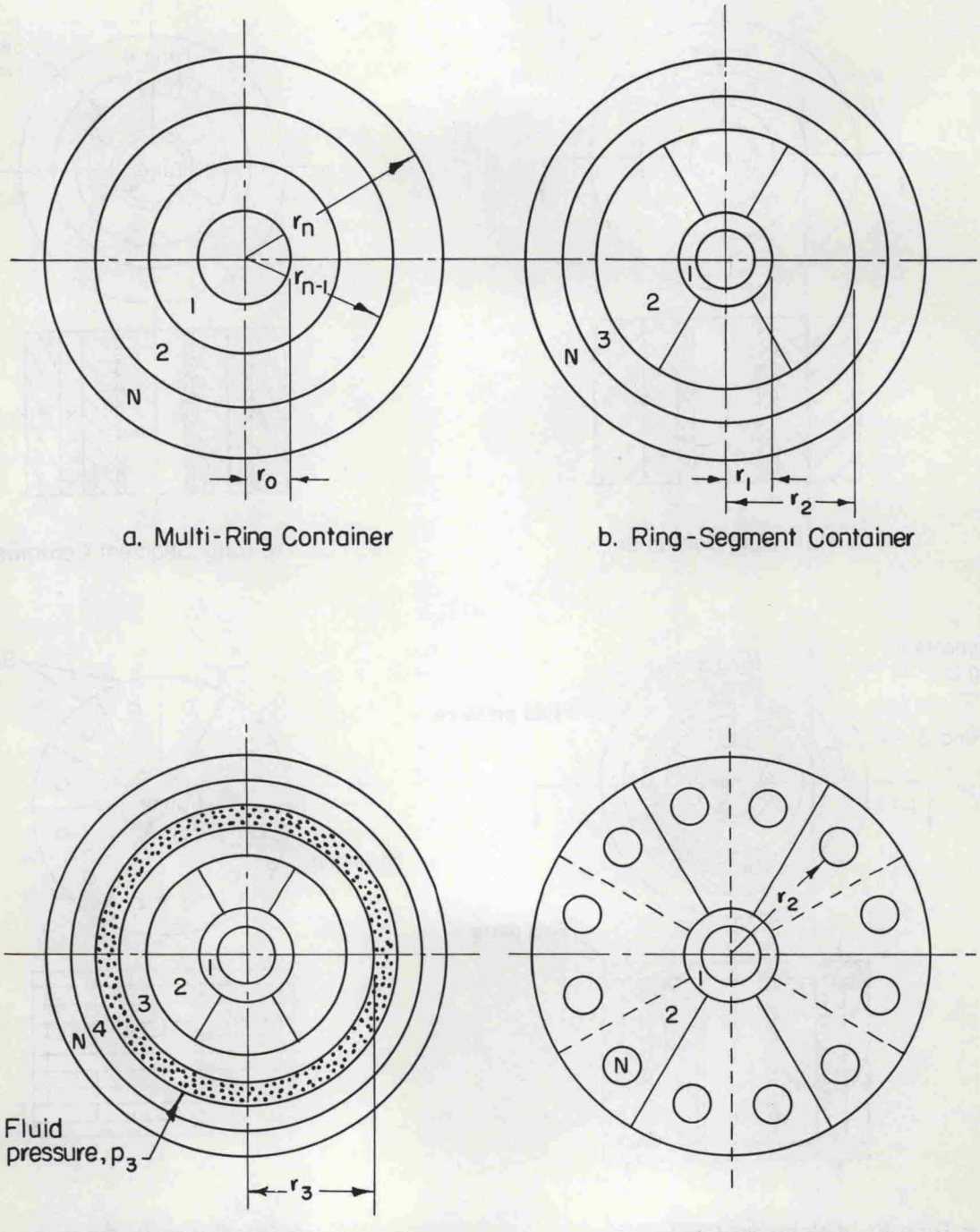

FIGURE 8. NOTATIONS USED FOR ANALYSIS OF CONTAINER DESIGN CONCEPTS

BASIS AND METHOD OF ANALYSIS

In this study the four design concepts for high-pressure containers are evaluated on the basis of a selected strength criterion for the component materials. Different strength criteria could be chosen, each of which could lead to different predictions of maximum pressure capability. If rupture under static load is the strength criterion then a burst pressure can be predicted. This pressure would be higher than the yield pressure predicted on the basis of static yield strength. However, a vessel subject to a great number of cycles of pressure less than the yield pressure could fail by fatigue. A high-pressure container for commercial hydrostatic extrusion should, of course, be capable of repeated use without frequent failure. Therefore, it was considered essential that a fatigue strength criterion be used as the basis of evaluation in this study.

It also has to be ascertained what kind of stress and strain analysis is needed – elastic, plastic, or elastic-plastic. This is determined from the fatigue life desired. Manson and Hirschberg[12] have shown that for most materials, failure by low-cycle fatigue (life less than about 1000 cycles) involves almost entirely plastic strain. Above about 1000 cycles life the amount of plastic strain is appreciably smaller, and above 100,000 cycles life the plastic strain is negligible. For the relatively high-strength materials, however, the strain at fracture is predominantly elastic for lifetimes as low as 100 cycles. Because lifetimes greater than 1000 cycles are desirable in commercial applications, and since high pressures require use of high-strength materials, elasticity theory rather than plastic or elastic-plastic analysis is used. Use of elastic theory rather than elastic-plastic theory also aids the study because elasticity solutions are easier to formulate and can be superimposed.

For the analysis, equations are derived that relate the interface pressures and the radial deformations between components. Elasticity solutions for stresses and deformations are used together with fatigue relations to determine formulas for maximum bore pressures.

METHOD OF PARAMETER NOTATION

The components of each design are identified from the inside out by the numbers 1, 2, 3, ..., N. N refers to the outermost component. As indicated in Figure 8, the components have the following radii:

$$\begin{aligned} r_0,\ r_1 &= \text{inner and outer radii, respectively, of component 1, the liner} \\ r_{n-1},\ r_n &= \text{inner and outer radii, respectively, of component n, } n = 1, 2, \ldots, N. \end{aligned} \qquad (1)$$

For the multi-ring container all the components are circular hollow cylinders. For the ring-segment and ring-fluid-segment containers, component 2 refers to the segments. The only exception to the notation on the radii occurs in the pin-segment design where the segment is divided for analysis into two parts and where r_2 is the radius to the inside of the pins as shown in Figure 8(d).

The bore pressure and interface pressures are identified as follows:

$p_0 = p$ = internal, bore pressure on liner

p_{n-1}, p_n = operating interface pressures acting on component n at r_{n-1} and r_n, respectively, when $p \neq 0$

q_{n-1}, q_n = residual interface pressures acting on component n at r_{n-1} and r_n, respectively, when $p = 0$.

Because the outer radius of each container refers to a free surface, the pressure there is zero,

$$p_N = 0, \qquad q_N = 0 \tag{3a, b}$$

The definition of the q_n gives

$$q_0 = 0 \tag{4}$$

Wall ratios for each component are defined as follows:

$$k_n = \frac{r_n}{r_{n-1}} \tag{5}$$

where k_n is the wall ratio for component n. The over-all diameter ratio of the container is defined as

$$K = \frac{r_N}{r_o} \tag{6}$$

From Definitions (5) and (6) we find that the following relation exists between K and the k_n:

$$K = k_1 k_2 k_3 \ldots k_N \quad . \tag{7}$$

FATIGUE CRITERIA

Two fatigue criteria are formulated here in order that both relatively low-strength ductile materials and high-strength, more brittle materials may be used in one design. The intention is to use high-strength steels as liner materials and lower strength ductile steels for the outer cylinders in order to prevent catastrophic brittle failure.

Fatigue Criterion for Ductile Outer Cylinders

From both torsion and triaxial fatigue tests on low-strength (120 to 150 ksi ultimate strength) steels conducted by Morrison, Crossland, and Parry[13] it is concluded that a shear criterion applies. Therefore, a shear theory of failure is assumed for outer rings made of ductile steel.

In order to formulate a fatigue relation, the semirange in shear stress and the mean shear stress are needed. These stresses are defined as

$$S_r = \frac{S_{max} - S_{min}}{2}$$

$$S_m = \frac{S_{max} + S_{min}}{2} \qquad (8a, b)$$

respectively.

The Goodman fatigue relation in terms of shear stresses is assumed. This relation is

$$\frac{S_r}{S_e} + \frac{S_m}{S_u} = 1, \text{ for } S_m \geqq 0 \quad ,$$

where S_e is the endurance limit in shear and S_u is the ultimate shear stress. For $S_u = 1/2\ \sigma_u$, where σ_u is the ultimate tensile stress, this relation can be rewritten as:

$$\frac{S_r}{S_e} \quad \frac{2S_m}{\sigma_u} = 1, \ S_m \geqq 0 \qquad (9)$$

The stresses S_r and S_m given by Equations (8a, b) can be calculated from elasticity solutions. In order to employ the fatigue relation (9) for general use, it is assumed that S_e can be related to S_u. This is a valid assumption as shown by Morrison, et al[13]. Referring to Reference (13), the ratio S_e/S_u can be established. Table 7 lists some fatigue data and results of calculation of S_e from Equation (9).

From Table 7 it is evident that fluid pressure contacting the material surface has a detrimental effect on fatigue strength; the endurance limit S_e for unprotected triaxial fatigue specimens is lower than that for torsional specimens. However, protection of the bore of triaxial specimens increases S_e under triaxial fatigue to a value equal that for torsional fatigue. Since in the high-pressure containers, outer cylinders are subject to interface contact pressures and not to fluid pressures, it is assumed that the latter data in Table 7 are applicable in the present analysis. Therefore, the following relation between S_e and σ_u is assumed:

$$S_e = \frac{1}{3}\sigma_u \qquad (10)$$

TABLE 7. TORSIONAL AND TRIAXIAL FATIGUE DATA ON VIBRAC STEEL[a]

Test	Stresses, psi				
	σ_u	S_r	S_m	S_e	S_e/σ_u
Torsion	126,000	43,700	0	43,700	0.347
	149,000	52,900	0	52,900	0.354
Triaxial (unprotected bore)	126,000	20,900	20,900	31,300[c]	0.248
	149,000	26,300	26,300	40,600	0.273
Triaxial[b] (protected bore)	126,000	26,500	26,500	45,900	0.363

(a) From Reference (13). Composition of this steel is 0.29 to 0.3 C, 0.14 to 0.17 Si, 0.64 to 0.69 Mn, 0.015 S, 0.013 P, 2.53 to 2.58 Ni, 0.57 to 0.60 Cr, 0.57 to 0.60 Mo.

(b) The bore of the cylindrical specimens was protected with a neoprene covering.

(c) S_e for the triaxial tests is calculated from Equation (9).

Substitution of Relation (10) into (9) gives

$$3S_r + 2S_m = \sigma_u \tag{11}$$

For design purposes this equation can be made conservative by rewriting it as

$$3S_r + 2S_m = \sigma, \text{ where } \sigma \leqq \sigma_u \tag{12}$$

Equation (12) now has a factor of safety, σ_u/σ and can be expected to predict lifetimes of 10^6 cycles and greater for ductile steels based upon the Goodman relation and available fatigue data. (Of course, stress concentration factors due to geometrical discontinuities or material flaws would reduce the expected lifetime.)

Fatigue Criterion for High-Strength Liner

Triaxial fatigue data on high-strength steels ($\sigma_u \geqq 250$ ksi) are not available. Fatigue data in general are very limited. Therefore, a fatigue criterion for high-strength steels under triaxial fatigue cannot be as well established as it was for the lower strength steels. The high-strength steels are expected to fail in a brittle manner. Accordingly, a maximum tensile stress criterion of fatigue failure is postulated.

Because fatigue data are limited while tensile data are available the tensile stresses $(\sigma)_r$ and $(\sigma)_m$ are related to the ultimate tensile strength by introduction of two parameters α_r and α_m. These are defined as follows:

$$\alpha_r = \frac{(\sigma)_r}{\sigma_1}, \qquad \alpha_m = \frac{(\sigma)_m}{\sigma_1} \tag{13a, b}$$

where $(\sigma)_r$ is the semirange in stress, $(\sigma)_m$ is the mean stress*, and σ_1 is less than or equal to the ultimate tensile strength depending upon the factor of safety desired. In order to get some estimations of what values α_r and α_m may be, some data from the literature are tabulated in Tables 8, 9, and 10. These data are for rotating-beam and push-pull tests.

The fatigue life again is found to depend on the range in stress and the mean stress, and upon the temperature. This dependence is illustrated in Figure 9 for 10^4 to 10^5 cycles life in terms of the parameters α_r and α_m. (Points (α_r, α_m) above the curves in Figure 9 would correspond to $<10^4$-10^5 cycles life and points below the curves would correspond to $>10^4$-10^5 cycles life.) The 1000 F temperature data are for Vascojet 1000. Although α_r increases with temperature for this steel, the ultimate tensile strength decreases and the fatigue strength at 10^4 to 10^5 cycles for $\alpha_m = 0$ remains nearly constant over the temperature range of 75 F to 1000 F.

*$(\sigma)_r$ and $(\sigma)_m$ are defined by expressions similar to Equations (8a, b) for S_r and S_m.

TABLE 8. FATIGUE STRENGTHS OF HIGH-STRENGTH STEELS FROM ROOM-TEMPERATURE ROTATING-BEAM TESTS, $\alpha_m = 0$

Material	Reference	Ultimate Tensile Strength, ksi	Yield Tensile Strength, ksi	α_r, Stress Range Parameter[a], for Cycles 10^4	10^5	10^6	10^7
18% Ni maraging steel	(14)	300	280		0.49	0.43	0.41
	(15)	300	285		0.33	0.31	0.30[b]
	(16)	295	285	0.68	0.44	0.38	0.36
		270	265	0.74	0.43	0.37	0.37
H-11 (CEVM)	(16)	250-280	210-230	0.75	0.57	0.54	0.54
D6AC	(17)[c]	270	237	0.66	0.41	0.37	0.37
Vascojet 1000	(17)[c]	309	251		0.45	0.29	0.29

(a) $\alpha_r \equiv (\sigma)_r/\sigma_u$, $\alpha_m \equiv (\sigma)_m/\sigma_u$, where $(\sigma)_r$, $(\sigma)_m$, σ_u are the semi range, mean, and ultimate tensile stresses, respectively.
(b) These are stated to be 90 per cent probability data.
(c) Tests in Reference (17) were push-pull tests with, $\alpha_m = 0$.

TABLE 9. FATIGUE STRENGTHS OF HIGH-STRENGTH STEELS FROM ROOM-TEMPERATURE PUSH-PULL TESTS, $\alpha_m = \alpha_r$

Material	Reference	Ultimate Tensile Strength, ksi	Yield Tensile Strength, ksi	α_r, Stress Range Parameter[a], for Cycles 10^4	10^5	10^6	10^7
18% Ni maraging steel	(16)	295	285	0.40	0.25	0.22	0.22
		270	265	0.43	0.28	0.25	0.24
H-11 (CEVM)	(16)	280-300		0.38	0.31	0.29	0.29
D6AC	(17)	270	237	0.44	0.33	0.28	0.28
Vascojet 1000	(17)	309	251		0.33	0.27	0.19

(a) $\alpha_r \equiv (\sigma)_r/\sigma_u$, $\sigma_m \equiv (\sigma)_m/\sigma_u$, where $(\sigma)_r$, $(\sigma)_m$, σ_u are the semi range, mean, and ultimate tensile stresses, respectively.

TABLE 10. FATIGUE STRENGTHS OF HIGH-STRENGTH STEELS FROM PUSH-PULL TESTS AT ELEVATED TEMPERATURES[a]

Material	Test Temp., F	Ultimate Tensile Strength, ksi	Yield Tensile Strength, ksi	Test Conditions[c]	α_r, Stress Range Parameter[b], for Cycles 10^4	10^5	10^6	10^7
D6AC	450	260	175	$\alpha_m = 0$	0.56[d]	0.48	0.40	0.31
				$\alpha_m = \alpha_r$	0.41	0.35	0.31	0.26
	550	230	160	$\alpha_m = 0$	0.65	0.52	0.41	0.33
				$\alpha_m = \alpha_r$	0.44	0.38	0.34	0.29
Vascojet 1000	800	260	200	$\alpha_m = 0$	0.69	0.56	0.42	0.31
				$\alpha_m = \alpha_r$		0.40	0.32	0.23
	1000	230	176	$\alpha_m = 0$	0.75[d]	0.61	0.43	0.26
				$\alpha_m = \alpha_r$		0.39	0.27	0.21

(a) Data are taken from Reference (17).

(b) $\alpha_r \equiv (\sigma)_r/\sigma_u$, $\sigma_m \equiv (\sigma)_m/\sigma_u$, where $(\sigma)_r$, $(\sigma)_m$, σ_u are the semi range, mean, and ultimate tensile stresses, respectively, at temperature.

(c) The cycle rate was 3100 cps.

(d) S-N curve extrapolated to 10^4 cycles.

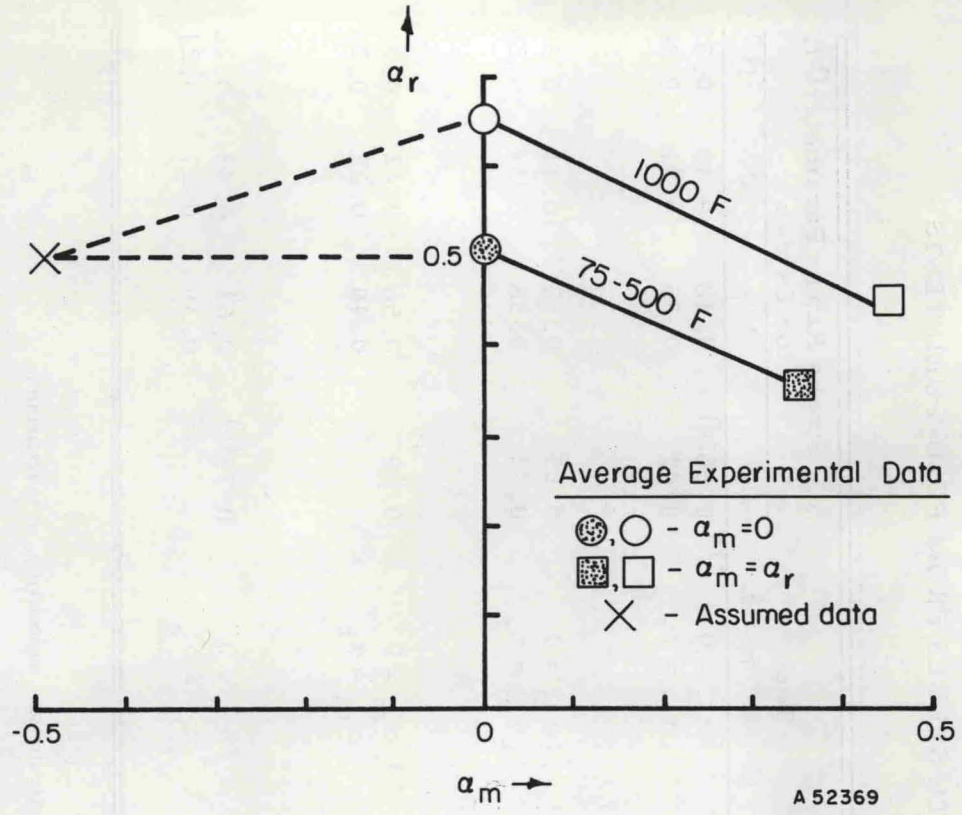

FIGURE 9. FATIGUE DIAGRAM FOR 10^4-10^5 CYCLES LIFE FOR HIGH-STRENGTH STEELS AT TEMPERATURES OF 75 F – 1000 F

α_r and α_m are defined by Equations (13a, b)

The fatigue data available are only for positive and zero mean stresses. However, there is evidence that compressive mean stress may significantly increase the fatigue strength[13, 18]. The reasons for this are thought to be that compression may reduce the detrimental effect of fluid pressure entering minute cracks or voids in the material and the compression may restrain such flaws from growing. Since the liner of a high-pressure container can be precompressed by shrink-fit assembly, an important factor in triaxial fatigue may be the prestress that can be initially provided. Therefore, for 10^4 to 10^5 cycles triaxial fatigue life, α_r and α_m are assumed to be

$$\alpha_r = 0.5, \ \alpha_m = -0.5 \qquad (14a, b)$$

as indicated in Figure 9. With $\alpha_m = -\alpha_r$ the maximum tensile stress at the bore would be zero.

In order to approximate a life of one cycle, it is assumed that

$$\alpha_r = 1.0, \ \alpha_m = 0, \text{ for one cycle} \qquad (15a, b)$$

which represents a cycle between $\pm\alpha_u$, the ultimate strength.

ELASTICITY SOLUTIONS

Cylindrical polar coordinates (r, θ, z) are used in the analysis. Axial symmetry is assumed; the stresses are independent of the angle θ. End effects are not considered*; the stresses found are independent of the axial coordinate z.

Elasticity Solutions for a Cylinder

The two-dimensional solutions for a cylinder loaded by uniform inner and outer pressures is given by Timoshenko and Goodier[19]. The expressions for stresses and displacement in cylinder n are

$$\sigma_r = \frac{1}{k_n^2 - 1}\left[p_{n-1} - p_n k_n^2 - (p_{n-1} - p_n)\left(\frac{r_n}{r}\right)^2 \right]$$

$$\sigma_\theta = \frac{1}{k_n^2 - 1}\left[p_{n-1} - p_n k_n^2 + (p_{n-1} - p_n)\left(\frac{r_n}{r}\right)^2 \right] \qquad (16a\text{-}c)$$

$$\tau_{r\theta} = 0$$

$$\frac{u}{r} = \frac{1}{E_n(k_n^2 - 1)}\left[(1 - \nu)(p_{n-1} - p_n k_n^2) + (1 + \nu)(p_{n-1} - p_n)\left(\frac{r_n}{r}\right)^2 \right] \qquad (17a, b)$$

$$v = 0$$

where σ_r, σ_θ, and $\tau_{r\theta}$ are the radial stress, hoop stress, and shear stress, respectively, and where u and v are the radial and circumferential displacements, respectively. The radii r_n, the pressures p_n, and the wall ratios k_n have been defined previously by Equations (1), (2), and (5). Equations (16a-c) also give the residual stresses if the operating pressures p_n are replaced by the residual pressures q_n.

For a fatigue analysis of a cylinder of ductile material the range and mean shear stresses are needed. The greatest range in the shear stress in a cylinder occurs at the bore on a plane oriented at 45 degrees to the r and θ axes. The shear stress there is given by

$$S = \frac{\sigma_\theta - \sigma_r}{2} \qquad (18)$$

*It may be important to consider end effects depending upon the method of end closure in the design. These effects and possible axial stresses resulting from large shrink fits may not be negligible.

Formulating the range in stress from the Definition (8a), we get

$$S_r = \frac{1}{2}\left[\frac{\sigma\ (p_n, p_{n-1}) - \sigma_r(p_n, p_{n-1})}{2} - \frac{\sigma_\theta(q_n, q_{n-1}) - \sigma_r(q_n, q_{n-1})}{2} \right] \text{ at } r = r_{n-1} \quad ,$$

hence,

$$S_r = \frac{k_n^{\,2}}{2(k_n^{\,2}-1)} \left[(p_{n-1} - p_n) - (q_{n-1} - q_n) \right], \text{ at } r = r_{n-1} \tag{19}$$

The mean shear stress at the same location on the same plane is

$$S_m = \frac{1}{2(k_n^{\,2}-1)} \left[(p_{n-1} - p_n k_n^{\,2}) + (q_{n-1} - q_n k_n^{\,2}) \right], \text{ at } r = r_{n-1} \tag{20}$$

Elasticity Solutions for Segmented Components

Elasticity solutions for the segments were derived. The derivations are outlined in Appendix A and only the results are given here. There are two types of segments. The ring segment is loaded by p_1 at r_1 and by p_2 at r_2. The pin segment is loaded by p_1 at r_1 but by more complex loading at r_2.

Ring Segment

The results for the ring segment are:

$$\sigma_r = (\sigma_r)_c + \frac{4M_1 p_1}{\beta_1} f_1(r)$$

$$\sigma_\theta = (\sigma_\theta)_c + \frac{4M_1 p_1}{\beta_1} f_2(r) \tag{21a-c}$$

$$\tau_{r\theta} = 0$$

$$\frac{u}{r} = (u)_c + \frac{M_1 p_1}{E_2 \beta_1} f_3(r) + \frac{G_1 p_1}{r} \cos\theta$$

$$\frac{v}{r} = \frac{8M_1 p_1}{E_2 \beta_1} (k_2^{\,2}-1)\,\theta - \frac{G_1 p_1}{r} \sin\theta \tag{22a, b}$$

where:

$$f_1(r) = \left(\frac{r_2}{r}\right)^2 \log k_2 + k_2^2 \log\left(\frac{r}{r_2}\right) + \log\left(\frac{r_1}{r}\right)$$

$$f_2(r) = -\left(\frac{r_2}{r}\right) \log k_2 + k_2^2 \log\left(\frac{r}{r_2}\right) + \log\left(\frac{r_1}{r}\right) + k_2^2 - 1$$

$$f_3(r) = -4(1+\nu)\left(\frac{r_2}{r}\right) \log k_2 + 4(1-\nu)\left[k_2^2 \log\left(\frac{r}{r_2}\right) - \log\left(\frac{r}{r_1}\right)\right] - 4(k_2^2 - 1) \qquad (23a\text{-}c)$$

and where $(\sigma_r)_c$, $(\sigma_\theta)_c$, and $(u)_c$ are given by Equations (16a-c) and (17a, b) for $k_n = k_2$, $p_{n-1} = p_1$, $p_n = p_2$, and $E_n = E_2$. For a ring segment p_1 and p_2 are related for equilibrium as follows:

$$p_2 = p_1/k_2 \qquad (24)$$

Formulas for the constants β_1, G_1, and M_1 (functions of k_2) are given in Appendix A. M_1 represents a bending moment that causes a bending displacement v as shown in Equation (22b).

Pin Segment

The solution for the pin segment is more complicated due to the pin loading at r_2. The resulting expressions are:

$$\sigma_r = (\sigma_r)_c + \frac{4M_2p_1}{\beta_1} f_1(r) + g_{m1}(r) \cos m\theta$$

$$\sigma_\theta = (\sigma_\theta)_c + \frac{4M_2p_1}{\beta_1} f_2(r) + g_{m2}(r) \cos m\theta \qquad (25a\text{-}c)$$

$$\tau_{r\theta} = g_{m3}(r) \sin m\theta$$

$$\frac{u}{r} = (u)_c + \frac{M_2p_1}{E_2\beta_1} f_3(r) + \frac{G_2p_1}{r} \cos\theta + \frac{1}{E_2} g_{m4}(r) \cos m\theta \qquad (26a, b)$$

$$\frac{v}{r} = \frac{8M_2p_1}{E_2\beta_1}(k_2^2 - 1)\theta - \frac{G_2p_1}{r} \sin\theta + \frac{1}{E_2} g_{m5}(r) \sin m\theta$$

where $(\sigma_r)_c$, $(\sigma_\theta)_c$, and $(u)_c$ are again given by Equations (16a-c) and (17a, b) for $k_n = k_2$, $p_{n-1} = p_1$, $p_n = p_2$, and $E_n = E_2$. For a pin segment p_2 is related to p_1 as follows:

$$p_2 = \frac{(m^2-1)(1 + 2\cos \pi/m)}{2(m^2-2)(1 + \cos \pi/m)} \left(\frac{p_1}{k_2}\right) \tag{27}$$

where m defined as

$$m = 2N_s \tag{28}$$

and where N_s is the number of segments per disc.

The functions $f_1(r)$, $f_2(r)$, and $f_3(r)$ are again given by Equations (23a-c) and β_1, G_2, M_2, g_{m1}, ..., $g_{m5}(r)$ are given in Appendix A.

The elasticity solutions now can be used to determine formulas for maximum pressure capability from the fatigue relations. This is done in the next section.

NONDIMENSIONAL PARAMETER ANALYSIS

The maximum pressure that is possible in any one container is a function of the material fatigue strength, the amount of prestress, the number of components N, and the wall ratios k_n. In order to determine the function dependence on these variables and to determine the best designs a nondimensional analysis is now presented. The calculations for the analysis of each design were programmed on Battelle's CDC 3400 computer.

Multi-Ring Container

Static Shear Strength Analysis

Although a fatigue criterion of failure has been chosen it is illustrative to review an analysis based upon static shear strength for ductile materials first conducted by Manning[4]. The method outlined here differs from that of Manning and is more straightforward. In this analysis the optimum design is found such that each component of the same material has the same value of maximum shear stress S under the pressure load p. The given information is $p_o = p$, $p_N = 0$, and K. The unknowns are the interface pressures p_n, (N-1) in number; the k_n, N in number and S. The total unknowns are 2N. There are N equations resulting from Equation (18) and having the form

$$S = (p_{n-1} - p_n)\frac{k_n^2}{k_n^2-1}, \quad n = 1, 2, \ldots, N \tag{29}$$

There is Equation (7) relating the k_n and K. Also N-1 equations can be formulated from the requirement that S be a minimum, i.e.,

$$\frac{\partial S}{\partial k_n} = 0, \quad n = 1, 2, \ldots, N-1 \tag{30}$$

(There are not N equations in the Form (30) because there is one Equation (7) relating the k_n.) Thus, there are also 2N equations which can be solved for the 2N unknowns. The solution gives

$$p_n = p_{n-1} - \frac{(k_n^2 - 1)}{k_n^2} S, \quad n = 1, 2, \ldots, N-1 \tag{31}$$

$$k_1 = k_2 = \ldots = k_N \tag{32}$$

$$S = \frac{p}{N} \frac{K^{2/N}}{(K^{2/N} - 1)} \tag{33}$$

The residual pressures q_n and the required interferences for the shrink-fit assembly have yet to be found. The radial stress σ_{rn} at the radius r_n resulting from the bore pressure p is given by Equation (16a) with K replacing k_n, p replacing p_{n-1}, r_N replacing r_n, r_n replacing r, and $p_n = p_N = 0$. σ_{rn} becomes:

$$\sigma_{rn} = \frac{p}{K^2 - 1} (1 - k_{n+1}^2 \, k_{n+1}^2 \ldots k_N^2) \tag{34}$$

The pressure p_n is the sum of q_n and $(-\sigma_{rn})$. Therefore,

$$q_n = p_n - (-\sigma_{rn}) \tag{35}$$

The interference as manufactured, Δ at r , is given by

$$\frac{\Delta_n}{r_n} = \frac{-u_n(r_n)}{r_n} \quad \frac{u_{n+1}(r_n)}{r_n} \tag{36}$$

where

$u_n(r_n)$ = radial deformation at r_n of cylinder N due to the residual pressure q_n at r_n and the residual pressure q_{n-1} at r_{n-1}.

and

$u_{n+1}(r_n)$ = radial deformation at r_n of cylinder n+1 due to the residual pressure q_n at r_n and the residual pressure q_{n+1} at r_{n+1}.

Substituting the Expressions (35) for q_n into Expressions (17a) for the u_n and substituting the results into Equation (36), we find that Δ_n/r_n reduces to:

$$\frac{\Delta_n}{r_n} = \frac{2p}{NE} \tag{37}$$

The result p/2S given by Equation (33) is plotted in Figure 10 for various N. The limit curve is given by

$$\left(\frac{p}{2S}\right)_{limit} = \frac{K^2-1}{K^2} \tag{38}$$

at which limit the minimum shear stress becomes equal to -S at the bore in the inner cylinder.

Figure 10 has been obtained under the assumption that $\frac{\sigma_\theta - \sigma_r}{2}$ always gives the maximum shear stress. As pointed out by Berman[20], the maximum shear stress in a closed-end container* is given by $\frac{\sigma_z - \sigma_r}{2}$ when $\sigma_z > \sigma_\theta$. Therefore, it is important to know the limit to $\frac{p}{2S}$ for which σ_z becomes equal to σ_θ. σ_z is given by

$$\sigma_z = \frac{p}{K^2-1}$$

σ_θ is given by Equation (16b). Equating σ_θ at r_o to σ_z, we get the surprising result that the limit to $\frac{p}{2S}$ in this case is also given by Equation (38). Thus, the limit curve in Figure 4 has two meanings: it is the limit at which the minimum of the shear stress $\frac{\sigma_\theta - \sigma_r}{2}$ from residual pressures becomes equal to -S at the bore, and it is also the limit at which the bore shear stresses $\frac{\sigma_\theta - \sigma_r}{2}$ and $\frac{\sigma_z - \sigma_r}{2}$ become equal under the bore pressure p.

From the limit curve in Figure 10 and from Equation (38) it is found that

$$\lim_{K \to \infty} \left(\frac{p}{2S}\right) = 1 \tag{39}$$

Thus, the maximum pressure possible in a multi-ring container designed on the basis of static shear strength using ductile materials is p = 2S. For a ductile material with a tensile yield strength of 2S = 180,000 psi, this means that the maximum pressure is limited to 180,000 psi.

Fatigue Shear Strength Analysis

The optimum design of a multi-ring container having all rings of the same material and based on fatigue shear strength is found by an analysis similar to that conducted on the basis of static shear strength. Instead of minimizing S in Equation (30), σ given by the fatigue relation, Equation (12) is minimized, i.e.,

$$\frac{\partial \sigma}{\partial k_n} = 0, \quad n = 1, 2, \ldots, N-1 \tag{40}$$

*Containers for hydrostatic extrusion generally are not closed-end containers. The effect of axial stress is included here for completeness.

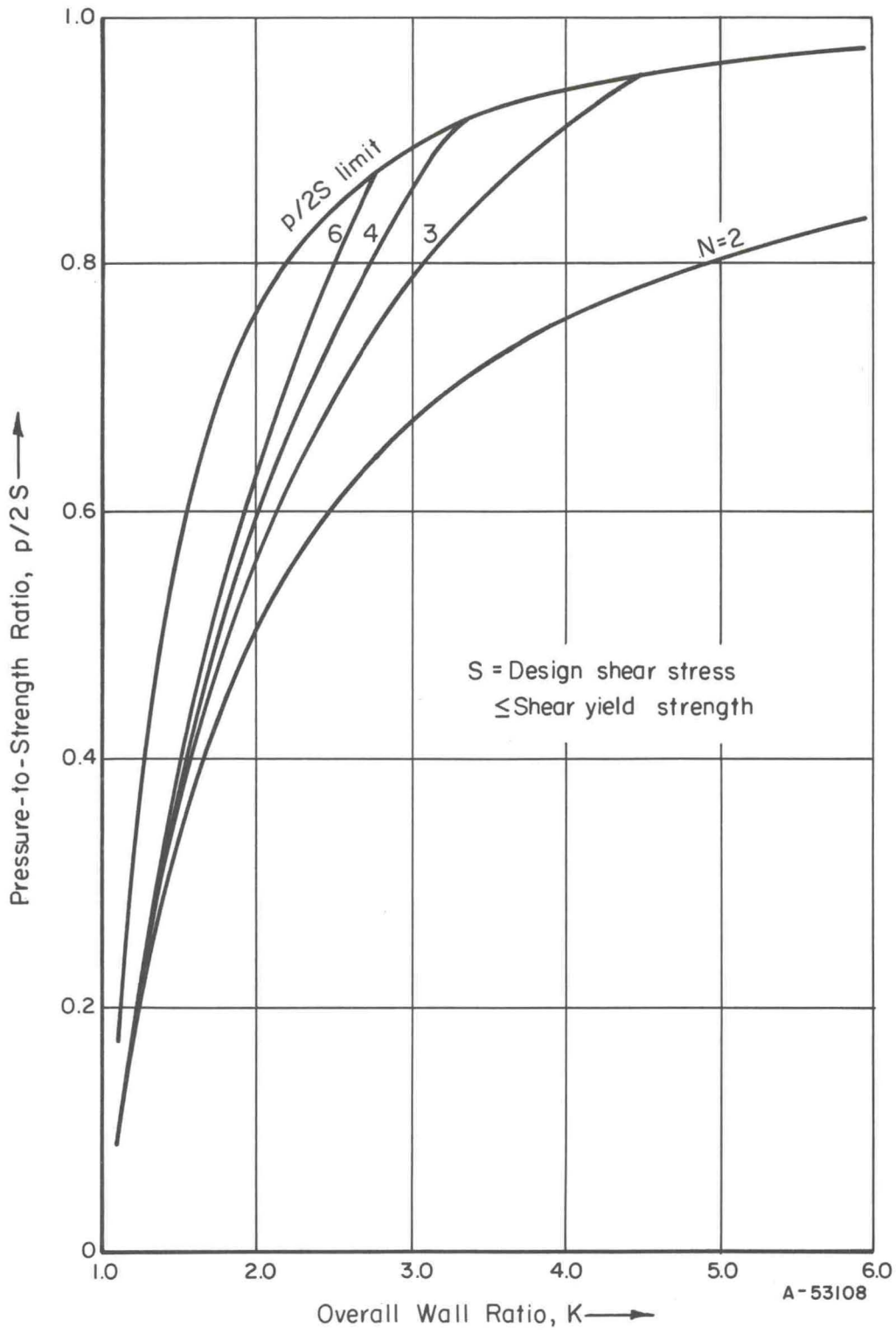

FIGURE 10. MAXIMUM PRESSURE-TO-STRENGTH RATIO, p/2S, IN MULTI-RING CONTAINER DESIGNED ON BASIS OF STATIC SHEAR STRENGTH

Each ring is assumed to be of the same ductile material.

The stresses S_r and S_m needed in expressing σ in Equation (12) are given by Equations (19) and (20).

The results of carrying out the analysis are:

$$p_n = p_{n-1} + \frac{p(k_n^2-1)}{4(K^2-1)}\, k_{n+1}^2\, k_{n+2}^2 \cdots k_N^2 - \frac{\sigma(k_n^2-1)}{2k_n^2},\ m = 1, 2, \ldots, N-1 \qquad (41)$$

$$k_1 = k_2 \cdots = k_N \qquad (42)$$

$$\sigma = \frac{5}{2N}\, p\, \frac{K^{2/N}}{K^{2/N}-1} \qquad (43)$$

The q_n are again given by Equation (35) and the resulting interference required is

$$\frac{\Delta_n}{r_n} = \frac{5p}{2NE} \qquad (44)$$

The result p/σ is plotted in Figure 11. The limit curve is for $S_m = 0$ in the inner cylinder and is given by

$$\lim_{K \to \infty} \left(\frac{p}{\sigma}\right) = \lim_{K \to \infty} \left(\frac{2}{3}\frac{K^2-1}{K^2}\right) = \frac{2}{3} \qquad (45)$$

If a ductile material has an ultimate tensile strength of 210,000 psi, then Equation (45) gives a maximum pressure of 140,000 psi based upon the shear fatigue criterion.

These results on ductile materials show that higher strength materials will have to be used in order to reach the high pressures desired. Accordingly, an analysis of a multi-ring container with a high-strength liner is now described.

High-Strength Liner Analysis

The hoop stress σ_θ at the bore of the liner undergoes the greatest range in stress during a cycle of pressure. Therefore, the tensile fatigue criterion is applied to the σ_θ stress. The range in the σ_θ stress at the bore of a multi-ring container depends only upon the over-all ratio K and the bore pressure p and is independent of the number of rings, i.e.,

$$(\sigma_\theta)_r = \frac{p}{2}\frac{K^2+1}{K^2-1} \qquad (46)$$

(Equation (46) is found from Equation (16b) for $r = r_o$, $r_n = r_N$, and $k_n = K$.)

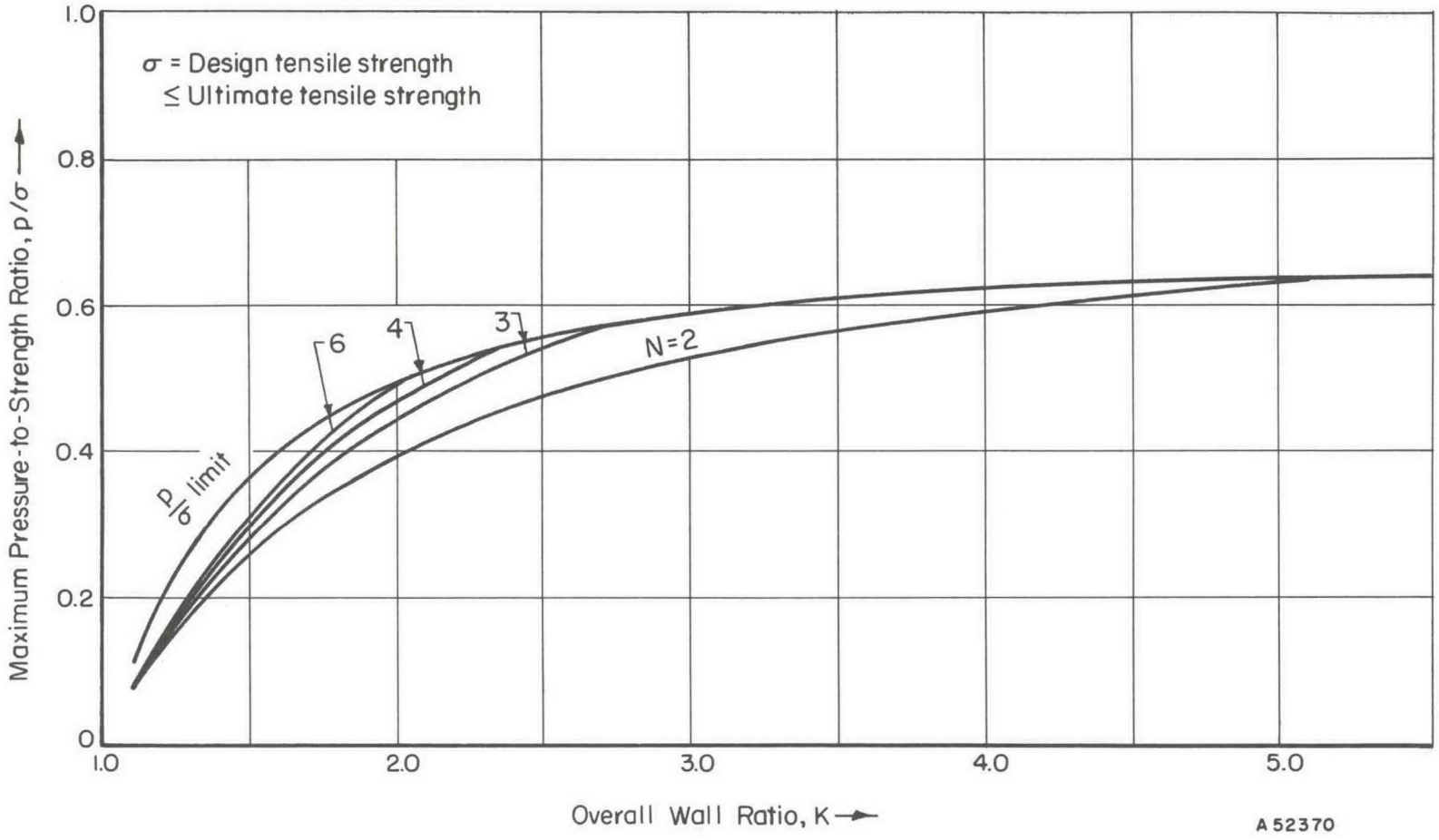

FIGURE 11. MAXIMUM PRESSURE-TO-STRENGTH RATIO, p/σ, IN MULTI-RING CONTAINER DESIGNED ON BASIS OF FATIGUE SHEAR STRENGTH

Each ring is assumed to be of the same ductile material.

In the formulation of the tensile fatigue criterion the parameter α has been defined by Equation (13a). Thus, from Equations (13a) and (46) it is found that

$$\frac{p}{\sigma_1} = 2\alpha_r \frac{K^2 - 1}{K^2 + 1}, \quad \sigma_1 \leqq \sigma_u \tag{47}$$

where σ_u is the ultimate tensile stress of the liner. The ratio p/σ_1 is plotted in Figure 12 for various K and α_r.

The fatigue data at room temperature of high-strength steels ($\sigma_u \leqq 300,000$ psi) listed previously in Tables 8, 9, and 10 are generally for $\alpha_r \leqq 0.5$ for lifetimes of 10^4 and greater. Hence, it is concluded that the maximum repeated pressure possible in a multi-ring container with a liner of $\sigma_u = 300,000$ psi is approximately 300,000 psi if appreciable fatigue life is required. This conclusion presupposes that the outer components can also be designed to withstand the required interface pressure and that sufficient precompression can be provided in the liner so that $\alpha_r = 0.5$ can be expected to give up to 10^4 cycles life. This is investigated next.

The stress range parameter α_r depends on the mean stress parameter α_m. The mean stress depends not only on the bore pressure p but on the interface pressures p_1 and q_1 between the liner and the second cylinder. The magnitudes of p_1 and q_1 that are possible depend upon the geometry and strength of the outer cylinders.

The outer rings are assumed to be all made of the same ductile material. Conducting a fatigue shear strength analysis of a multi-ring container having a pressure fluctuating between q_1 and p_1, we find from a method similar to that used in arriving at Equation (42) (using Equation (40) for n = 2, 3, ..., N-1), that in this case also the optimum design has

$$k_2 = k_3 = \ldots = k_n \tag{48}$$

Calculating the mean stress σ_m at the bore of the liner, equating $\alpha_m \sigma_1$ to σ_m from Equation (13b), substituting for q_1 from Equation (35), eliminating σ_1 by use of Equation (47), and solving for p_1, one finds

$$p_1 = \frac{p}{K^2 - 1}\left[\frac{K^2 - k_1^2}{k_1^2} + \frac{(K^2 + 1)}{4}\,\frac{(k_1^2 - 1)}{k_1^2}\,\frac{(\alpha_r - \alpha_m)}{\alpha_r}\right] \tag{49}$$

The other interface pressures p_n, $n \geq 2$ are again given by Equation (41). Eliminating the pressures p_1 and p_n, $n \geq 2$ from Equations (49) and (41), and solving for the pressure-to-strength ratio p/σ, one gets

$$\frac{p}{\sigma} = \frac{2(K^2 - 1)(k_n^2 - 1)(N-1)\,k_1^2\,\alpha_r}{k_n^2\left[5(K^2 - k_1^2) + (\alpha_r - \alpha_m)(K^2 + 1)(k_1^2 - 1)\right]} \tag{50}$$

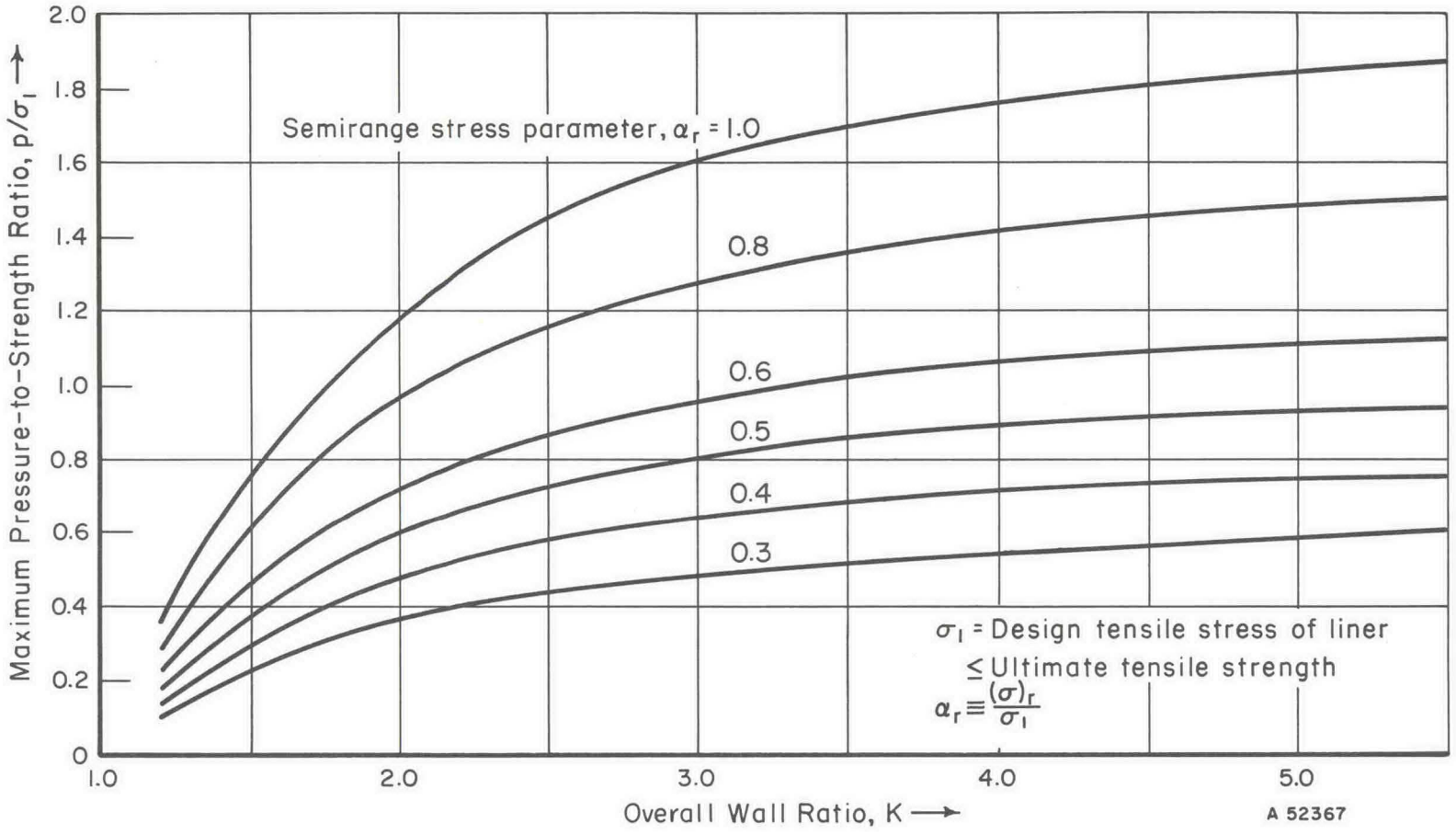

FIGURE 12. MAXIMUM PRESSURE-TO-STRENGTH RATIO, p/σ_l, IN MULTI-RING CONTAINER WITH HIGH-STRENGTH LINER BASED ON THE FATIGUE TENSILE STRENGTH OF LINER

The k_n, $n \geqq 2$ in Equation (50) are equal as shown by Equation (48). Whereas, p/σ_1 depended only upon α_r and K (Equation (47)), p/σ depends on N, k_n, and α_m in addition.

The ratio p/σ can also be limited by the requirement on Relations (9) and (12) that the mean shear stress S_m in cylinder No. 2 at r_1 obeys the relation $S_m \geqq 0$. $S_m = 0$ gives

$$(\frac{p}{\sigma})_{limit} = \frac{2}{3} \frac{(K^2 - 1)}{K^2} \quad k_1^2 \tag{51}$$

The limit curves are plotted in Figure 13. As evident from Figure 13, the pressure limit for the outer rings can be increased by increasing k_1. This means that the liner has a great effect on p. The strength of the liner, σ_1, influences p in Equation (47). The size of the liner, k_1, limits p in Equation (51).

Whether or not p/σ can be allowed as high as the limit, however, depends on the other factors N, α_r, K, etc., as shown by Equation (50). This dependence is rather complicated. Example curves of p/σ are plotted in Figures 14 and 15 for $\alpha_r = 0.5$ and $\alpha_m = -0.5$. As shown by these curves p/σ increases with N and also increases with k_1 for $N = 5$, $K \geqq 6.5$.

Suppose p = 300,000 psi as determined from Equation (47) for $\alpha_r = 0.5$ and $\sigma_1 = 300{,}000$ psi. Then from Figure 15, K must be 9.0 for $k_1 = 1.75$ and $N = 5$ if $\sigma = 210{,}000$. Thus, the multi-ring cylinder must be quite large in size to support maximum repeated pressures.

The interferences Δ_n and residual pressures q_n have yet to be determined for the multi-ring container. Since the liner and the outer rings are assumed to be made from two different materials, thermal expansions must be included in the interference calculations. It is assumed that no thermal gradients exist; all components reach the same temperatures uniformly. Therefore, the interference required between the liner and the second cylinder is expressed as

$$\frac{\Delta_1}{r_1} = - \frac{u_1(r_1)}{r_1} + \frac{u_2(r_1)}{r_1} - \alpha_1 \Delta T + \alpha_2 \Delta T \tag{52}$$

where

Δ_1 = manufactured interference

$u_1(r_1)$ = radial deformation of liner at r_1 due to residual pressure q_1 at r_1

$u_2(r_1)$ = radial deformation of cylinder No. 2 at r_1 due to residual pressures q_1 at r_1 and q_2 at r_2

α = coefficient of thermal expansion at temperature

ΔT = temperature change from room temperature.

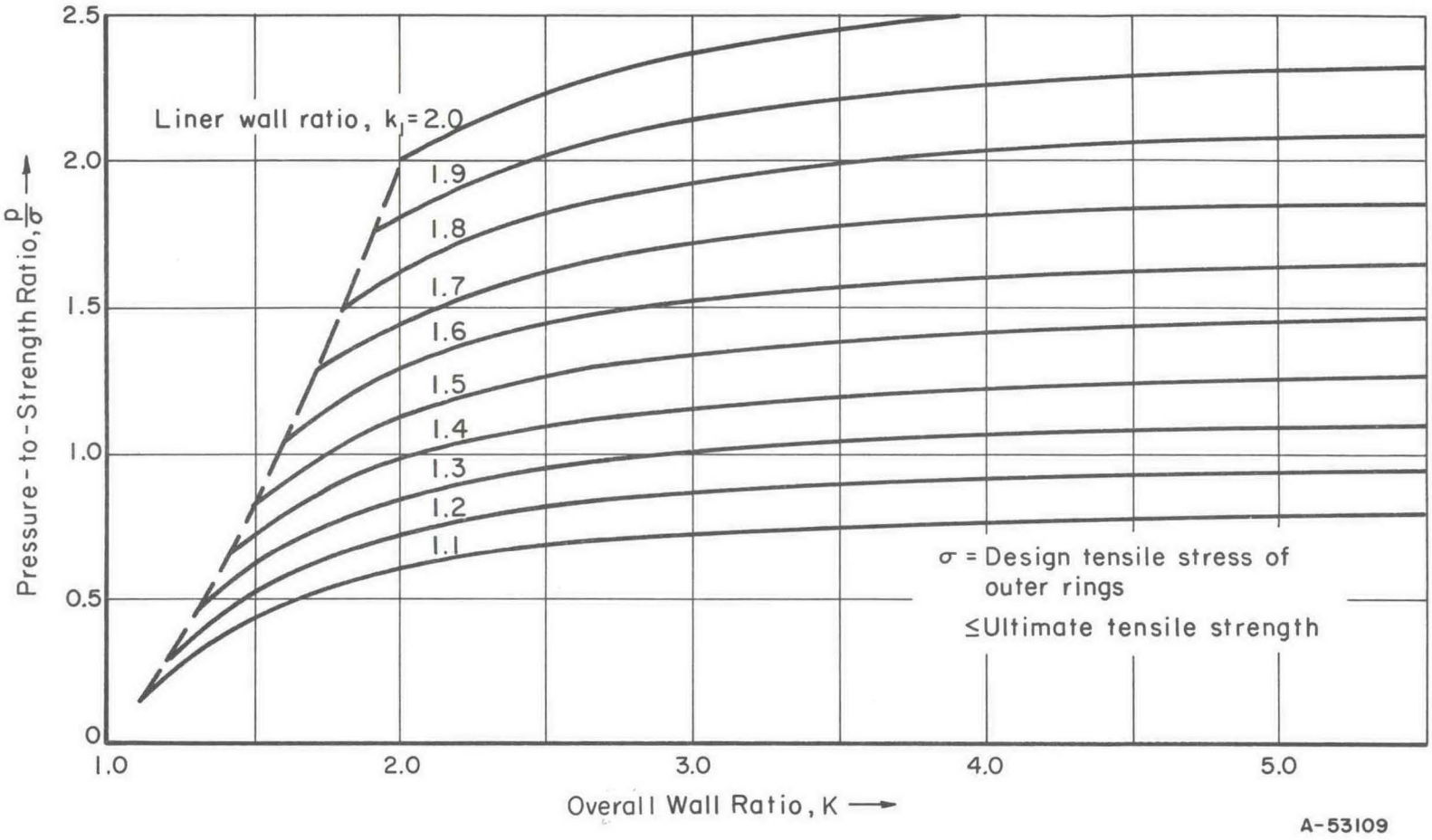

FIGURE 13. LIMIT TO MAXIMUM PRESSURE-TO-STRENGTH RATIO, p/σ, IN MULTI-RING CONTAINER WITH HIGH-STRENGTH LINER BASED ON SHEAR FATIGUE STRENGTH OF THE OUTER RINGS

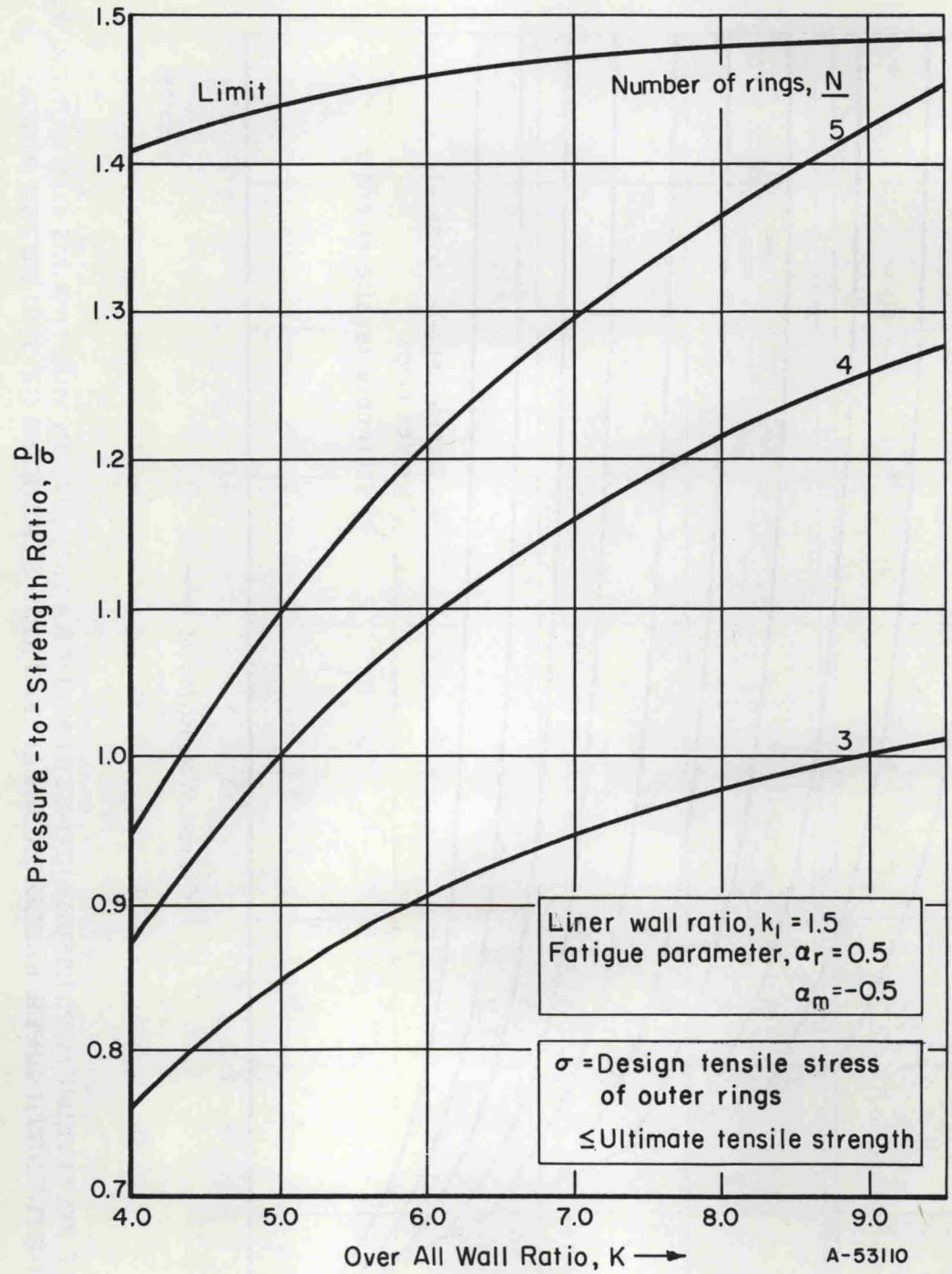

FIGURE 14. INFLUENCE OF NUMBER OF RINGS ON MAXIMUM PRESSURE-TO-STRENGTH RATIO, p/σ, IN MULTI-RING CONTAINER WITH HIGH-STRENGTH LINER

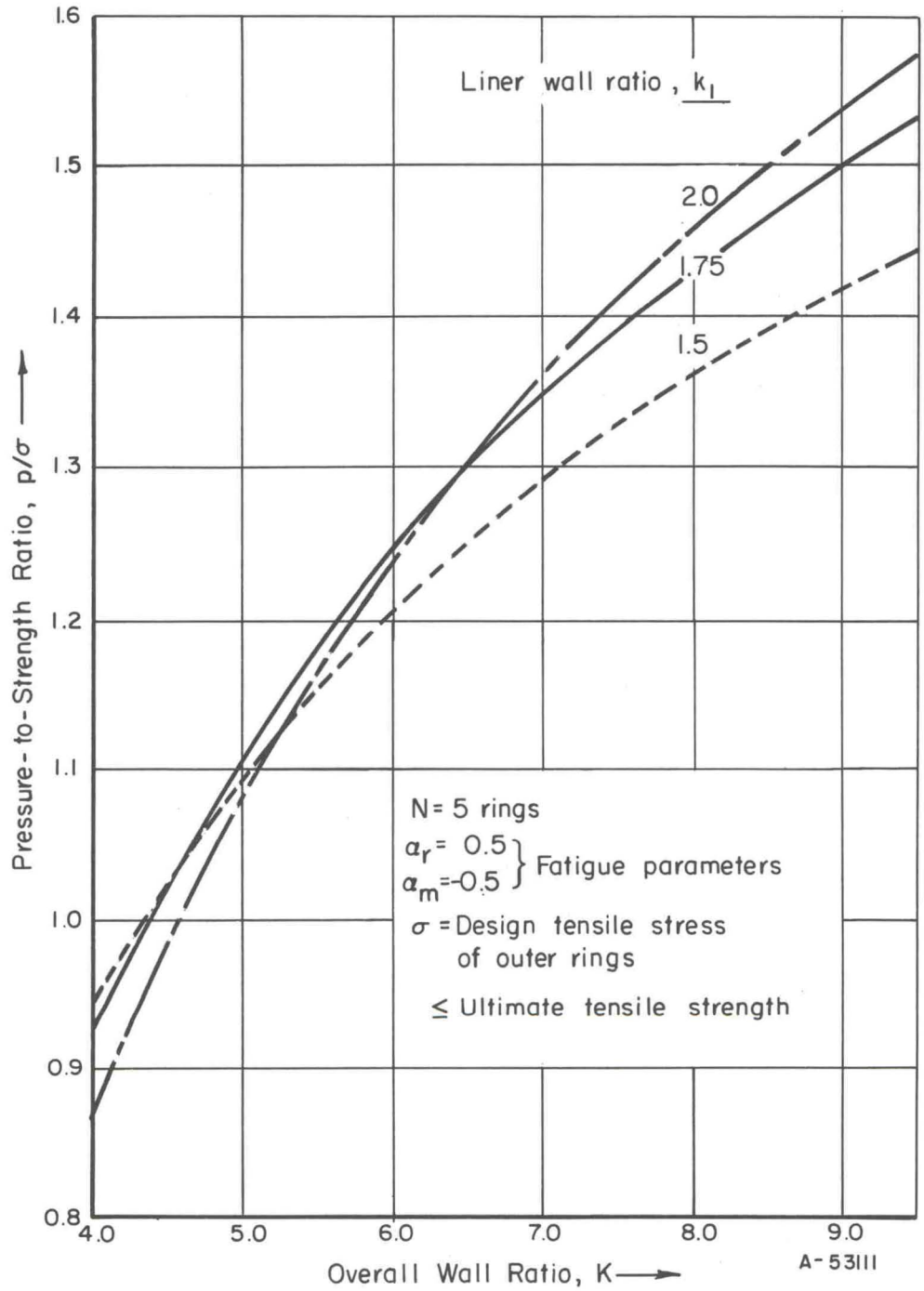

FIGURE 15. INFLUENCE OF LINER SIZE ON MAXIMUM PRESSURE-TO-STRENGTH RATIO, p/σ, IN MULTI-RING CONTAINER WITH HIGH-STRENGTH LINER

The interferences Δ_n required between the outer cylinders is again given by Equation (36) for $n \geqq 2$. The residual pressures q_n needed in calculating the Δ_n are found from Equation (35) for p_n given by Equations (49) and (41). In the calculation of the u_n from Equation (17a), the values of the moduli of elasticity, E_n at temperature should be used.

The container designed for use at temperature will have residual pressures q_n^* at room temperature different from the q_n necessary at temperature. The q_n^* are found as follows: the u_n^* are first expressed in terms of q_n^* from Equation (17a) using the values of E_n at room temperature, the Δ_n are expressed in terms of the u_n^* from Equations (52) and (36) for $\Delta T = 0$. This procedure gives the following system of equations in the q_n^*:

$$A_{11}q_1^* + A_{12}q_2^* = E_2 \frac{\Delta_1}{r_1}$$

$$A_{nn-1}q_{n-1}^* + A_{nn}q_n^* + A_{nn+1}q_{n+1}^* = E_n\frac{\Delta_n}{r_n}, \quad n = 2, 3, \ldots, N-1 \qquad (53a, b, \ldots)$$

where

$$A_{11} = \frac{k_2^2 + 1}{k_2^2 - 1} + \nu + \frac{E_2}{E_1}\left(\frac{k_1^2 + 1}{k_1^2 - 1} - \nu\right)$$

$$A_{12} = \frac{-2k_2^2}{k_2^2-1}$$

$$A_{nn-1} = \frac{-2}{k_n^2-1}$$

$$A_{nn} = \frac{k_n^2 + 1}{k_n^2 - 1} + \frac{k_{n+1}^2 + 1}{k_{n+1}^2 - 1} = 2\frac{k_n^2 + 1}{k_n^2 - 1}$$

$$A_{nn+1} = \frac{-2k_{n+1}^2}{k_{n+1}^2-1} = -2\frac{k_n^2}{k_n^2-1}$$

and where Δ_1 and the Δ_n, $n \geqq 2$ have been previously calculated for $\Delta T \neq 0$. There are N-1 linear equations (53a, b, ...) in N-1 unknowns q_n, $n = 1, 2, \ldots, N-1$ ($Q_N = 0$). These are easily solved by matrix solution on the computer.

Having calculated the residual pressures q_n^* at room temperature the residual stresses can be calculated from Equations (16a, b). These residual stresses can then be checked in order to assure that they are within tolerated bounds. Examples of such calculations are described later when specific designs are considered. Next, the ring-segment container is considered.

Ring-Segment Container

A ring-segment container has been shown in Figure 7(b). For this design, the equilibrium requirement, Equation (24), relates p_1 and p_2. Under shrink-fit it is assumed that the segments just barely contact each, i.e., the segments carry no hoop stress. (If the segments were in strong contact with each other then they would act like a complete ring, i.e., they would carry compressive hoop stress, and the distinction between a ring-segment container and a multi-ring container would be lost.) Thus, the same equilibrium requirement applies to the residual pressures q_1 and q_2. This requirement is

$$p = p_1/k_2, \qquad q = q_1/k_2 \tag{54a,b}$$

In order to determine the pressures p_1 and q_1 the following radial deformation equation is formulated:

$$u_2(r_2) - u_2(r_1) + \Delta_{12} + \alpha_2\Delta T\,(r_2 - r_1) = u_3(r_2) - u_1(r_1) + \alpha_3\Delta T r_2 - \alpha_1\Delta T r_1 \tag{55}$$

where

Δ_{12} = the manufactured interference defined as the amount $(r_2 - r_1)$ of the segments exceeds $(r_2 - r_1)$ of the cylinders

$u_m(r_m)$ = the radial deformation of component n at r_m due to pressure p_n or q_n at r_n and p_{n-1} or q_{n-1} at r_{n-1}

α_n = thermal coefficient of expansion of component n

ΔT = temperature change from room temperature.

If the elasticity solutions, Equations (17a) and (22a), for the u_n, and Equation (54a) for p_2 are substituted into Equation (55) and the resulting expression solved for p_1, then there results

$$p_1 = \frac{1}{g}\left\{\frac{2p}{k_1^2-1} + 2\frac{E_1}{E}\frac{k_2k_3^2p_3}{(k_3^2-1)} + \frac{E_1\Delta_{12}}{r_1} - \Delta T E_1\left[k_2(\alpha_3 - \alpha_2) + (\alpha_2 - \alpha_1)\right]\right\} \tag{56}$$

where

$$g = \frac{k_1^2+1}{k_1^2-1} + \frac{E_1}{E_2}\left[\frac{2(k_2-1)}{k_2+1} + \frac{M_1}{\beta_1}\left(f_3(r_1) - k_2 f_3(r_2)\right)\right] + \frac{E_1}{E_3}\left[\frac{k_3^2+1}{k_3^2-1} + \nu\right] - \nu \tag{57}$$

The E_n are the moduli of elasticity at temperature. The parameters M_1 and β_1 and the function $f_3(r)$ have been defined previously in reference to Equations (22a, b). The procedure for finding q_1 is the same as that for finding p_1 except that $p = 0$ and q_3 replaces p_3, i.e.,

$$q_1 = \frac{1}{g}\left\{ 2\,\frac{E_1}{E}\,\frac{k_2 k_3^{\,2} q_3}{(k_3^{\,2}-1)} + \frac{E_1 \Delta_{12}}{r_1} - \Delta T E_1 \left[k_2(\alpha_3-\alpha_2) + (\alpha_2-\alpha_1) \right] \right\} \tag{58}$$

A fatigue analysis of the high-strength liner is now conducted. The range in the hoop stress at the bore is:

$$(\sigma_\theta)_r = \frac{(\sigma_\theta)_{max} - (\sigma_\theta)_{min}}{2} = \frac{p}{2}\,\frac{(k_1^{\,2}+1)}{(k_1^{\,2}-1)} - \frac{(p_1-q_1)k_1^{\,2}}{k_1^{\,2}-1} \tag{59}$$

where Equation (16a) has been used. (p_1-q_1) is given by Equation (58), but an expression for (q_3-p_3) is needed before Equation (59) can be used to solve for p. The expression for (p_3-q_3) is obtained from Equation (35) with (p_2-q_2) replacing p and with $k_3^{\,2}k_4^{\,2}\ldots k_N^{\,2}$ replacing K^2 in Equation (34). There results

$$q_n = p_n - \frac{(p_2-q_2)\,(k_{n+1}^{\,2}\,k_{n+2}^{\,2}\ldots k_N^{\,2}-1)}{(k_3^{\,2}\,k_4^{\,2}\ldots k_N^{\,2}-1)}\,,\quad n \geqq 3 \tag{60}$$

Substituting for (q_3-p_3) from Equation (60) into (58), then substituting for (p_1-q_1) from Equation (58) into (59), equating $(\sigma_\theta)_r$ and $\alpha_r\sigma_1$ from Definition (13a), and solving for p/σ_1, one obtains

$$\frac{p}{\sigma_1} = \frac{2\alpha_r(k_1^{\,2}-1)^2(g-h)}{\left[(g-h)\,(k_1^{\,4}-1) - 4k_1^{\,2} \right]} \tag{61}$$

where

$$h = \frac{2E_1\,k_n^{\,2}\,(k_n^{\,2(N-3)}-1)}{E_3\,(k_n^{\,2(N-2)}-1)} \tag{62}$$

($k_3 = k_4 = \ldots = k_n$ for the outer cylinders as shown by Equation (48). Therefore, $k_3^{\,2}\,k_4^{\,2}\ldots k_N^{\,2} = k_n^{\,2(N-2)}$ in the expression for h.)

It is easily shown that (g-h) is independent of N, the number of components. Therefore, p/σ_1 given by Equation (61) is independent of N. However, p/σ_1 is dependent upon k_1 whereas for the multi-ring container it was not as previously shown by Equation (47). This dependence is also shown in Figure 16. From this figure it is evident that the ring-segment container cannot withstand as great a pressure as the multi-ring container if the over-all size is the same. This result is believed due to the fact that the segments do not offer any support to the liner – they are "floating" members between the liner and the third component, another ring. The effect is more pronounced as the segment size is increased. This is shown in Figure 17 where it is seen that the pressure decreases with increasing segment size.

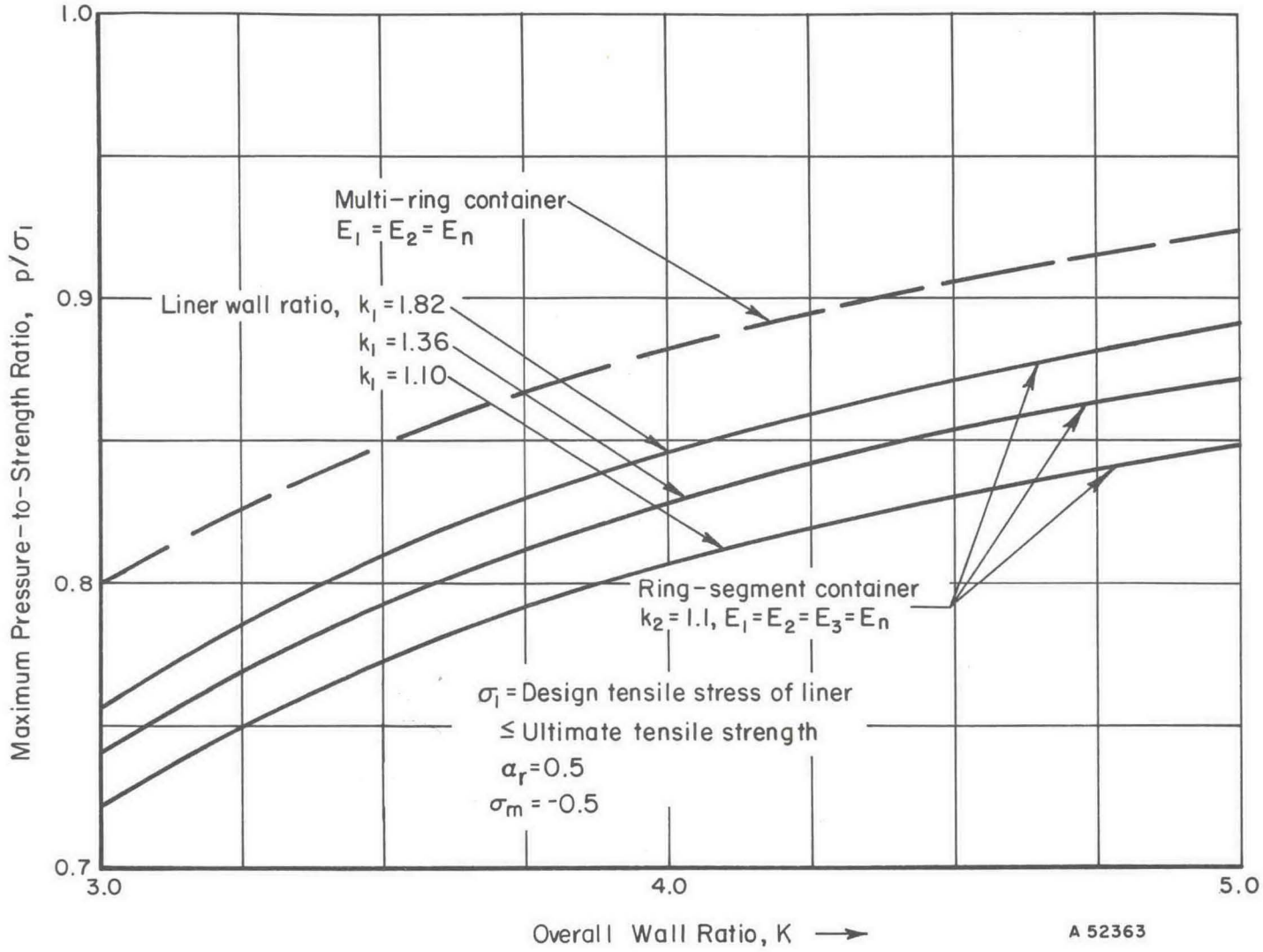

FIGURE 16. COMPARISON OF MULTI-RING CONTAINER WITH RING-SEGMENT CONTAINER FOR VARIOUS k_1

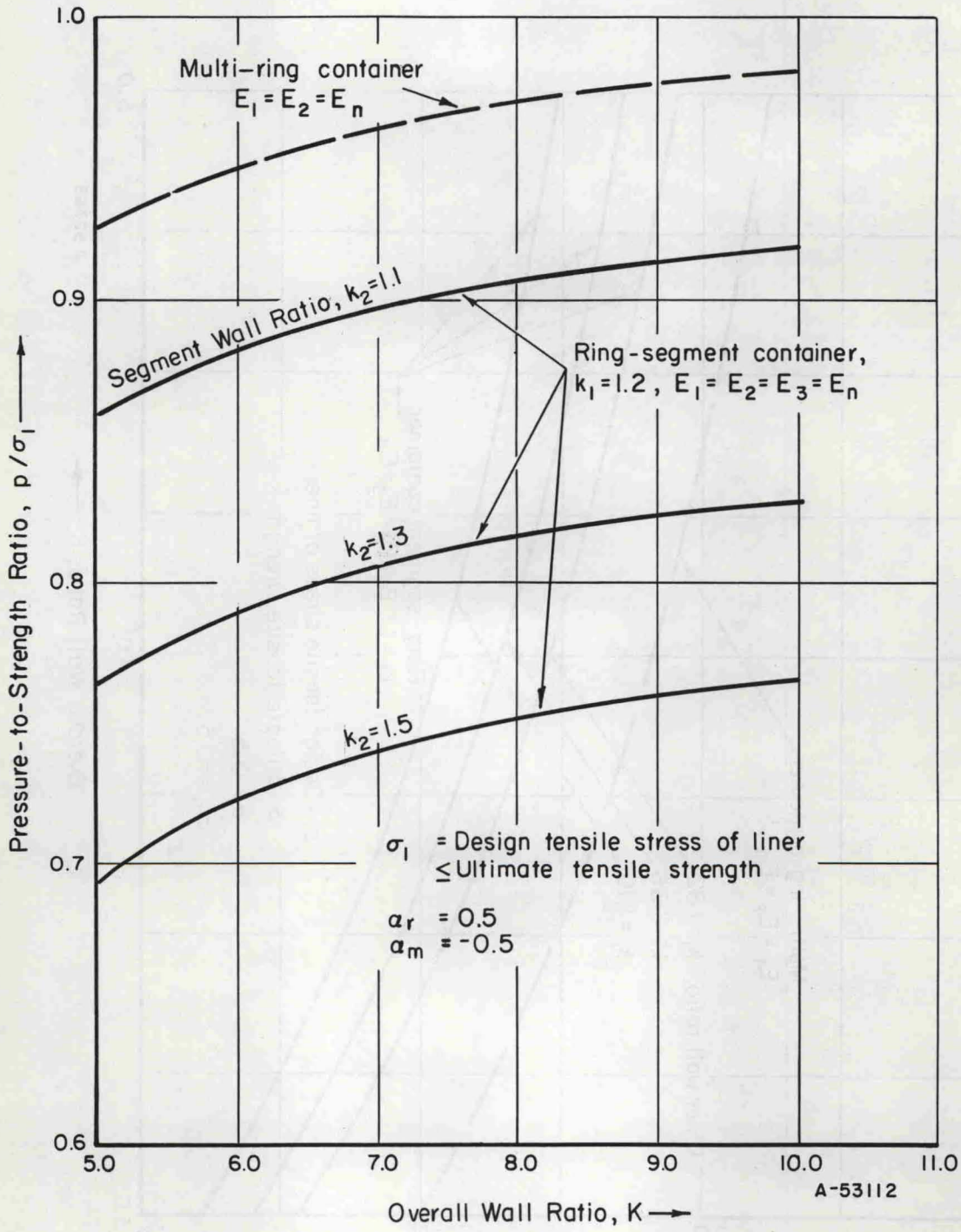

FIGURE 17. COMPARISON OF MULTI-RING CONTAINER WITH RING-SEGMENT CONTAINER FOR VARIOUS SEGMENT WALL RATIOS

The detrimental effect of insufficient segment support to the liner can be reduced by using a high modulus material, tungsten carbide, for the segment material. This is shown in Figure 18. However, the reduction is not sufficient enough to increase the pressure capability of the ring-segment container to that of the multi-ring container. This conclusion is based on results for various k_1 and k_2.

The fatigue analysis of the outer ductile cylinders is conducted in the same manner as it was done for the multi-ring container, except now the component numbers are $n = 3, 4, \ldots, N$. The result is

$$\frac{p}{\sigma} = \frac{\alpha_r (k_n^2 - 1)(N-2)}{k_n^2 \left[\frac{(\alpha_r - \alpha_m)}{2} \frac{(k_1^2+1)}{k_2 k_1^2} + \frac{(3\alpha_r + 2\alpha_m)}{k_2 (k_1^2 - 1)(g-h)} \right]} \tag{63}$$

This result is plotted in Figure 19 which shows the effect of increasing k_1 and comparison with the multi-ring container. Although p/σ can be increased by use of segments, the ring-segment container has the limitation of lower p/σ_1 as shown before in Figures 16 and 17.

The effect on p/σ of increasing the segment modulus was also investigated. However, the effects were found to be insignificant.

Ring-Fluid-Segment Container

The ring-fluid-segment container has been illustrated in Figure 7(c). This container is a combination of a ring-segment container for the inner part and a multi-ring container for the outer part. All of the equations derived for the multi-ring container can be used for the outer part. For the inner part, Equations (54a, b), (55), (56), (57), and (58) apply. The latter equation applies with $q_3 = 0$. Equation (59) is valid and can be used to find p/σ_1 for the liner. (Equation (60) is not needed since p_3 is given.) Solving for p/σ_1, one finds

$$\frac{p}{\sigma_1} = \frac{\alpha_r (k_1^2 - 1)}{\left[\frac{k_1^{2+1}}{2} - \frac{2}{g} \frac{k_1^2}{(k_1^2 - 1)} - 2 \frac{E_1}{E_3} \frac{p_3}{p} \frac{k_1^2 k_2 k_3^2}{g(k_3^2 - 1)} \right]} \tag{64}$$

This equation shows that an increase in p_3/p gives and increases in p/σ_1.

Let σ_3 be the ultimate tensile strength of component 3, the outer cylinder of the inner part of the ring-fluid-segment container. If fatigue relation, Equation (12), is used for this cylinder, then there results

$$\sigma_3 = \frac{k_3^2}{k_3^2 - 1} \left[\frac{5}{2} (p_2 - p_3) - \frac{1}{2} q_2 \right] \tag{65}$$

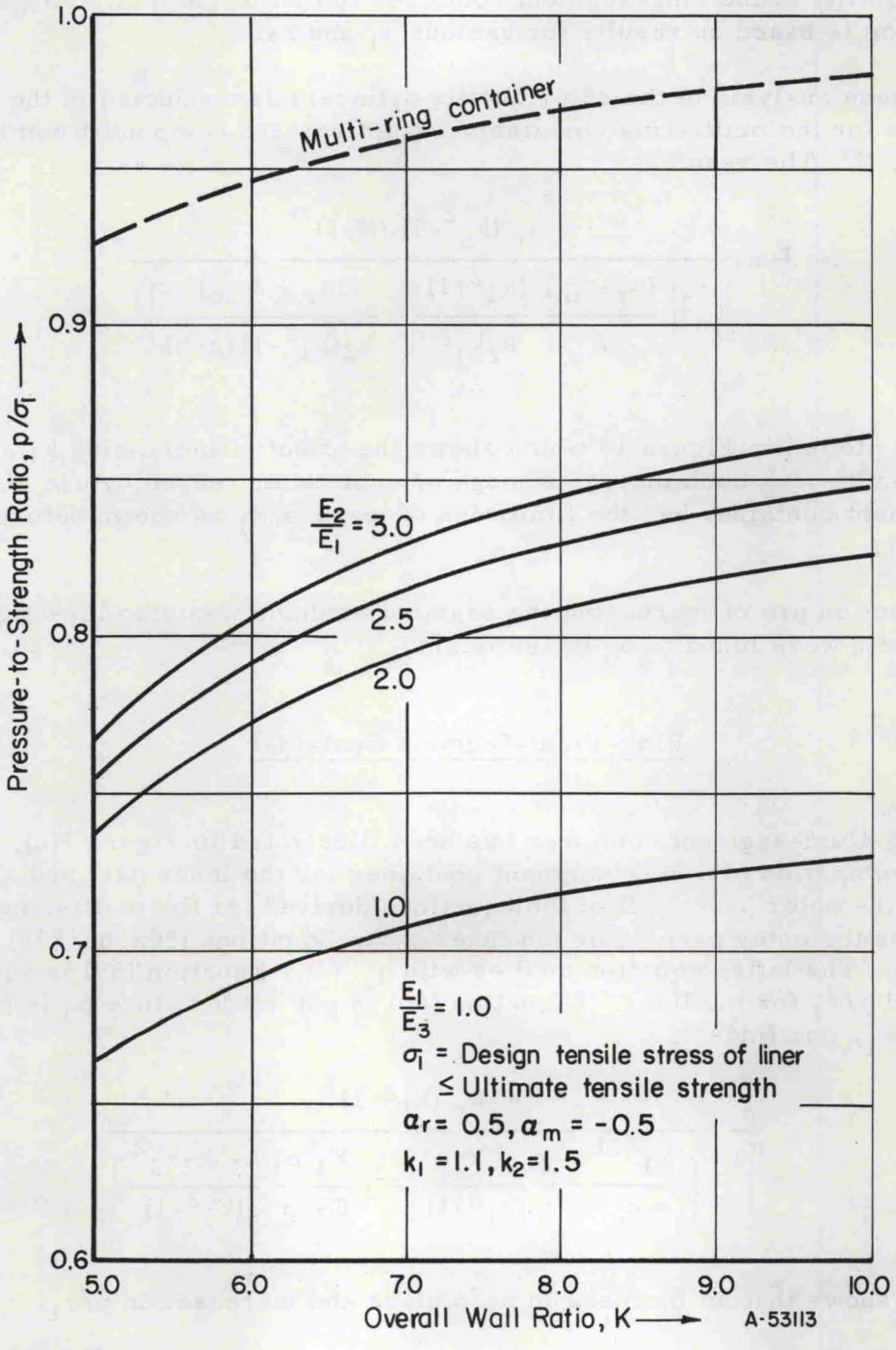

FIGURE 18. EFFECT OF ELASTIC MODULUS OF SEGMENTS ON PRESSURE-TO-STRENGTH RATIO, p/σ_1, FOR THE RING-SEGMENT CONTAINER

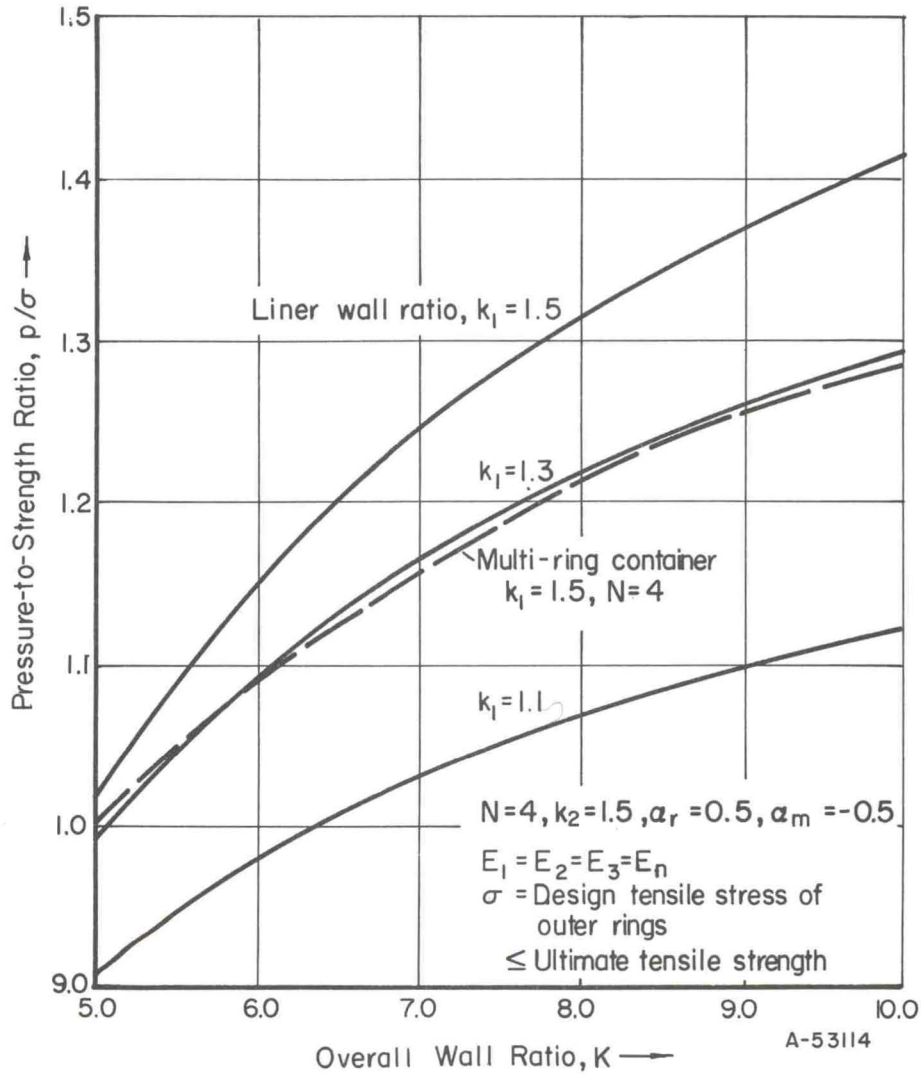

FIGURE 19. EFFECT OF LINER SIZE ON PRESSURE-TO-STRENGTH RATIO, p/σ, FOR RING-SEGMENT CONTAINER

The pressures p_2 and q_2 are related to p_1 and q_1 via Equations (54a, b). p_1 and q_1 are related by Equation (58) with $q_3 \equiv 0$. One other equation involving p_1 and q_1 is needed which is found from the Definition (13b) for the parameter α_m, i.e.,

$$\alpha_m \sigma_1 = \sigma_m = \frac{(\sigma_\theta)_{max} + (\sigma_\theta)_{min}}{2} = \frac{p}{2} \frac{k_1^2 + 1}{k_1^2 - 1} - \frac{(p_1 + q_1)}{k_1^2 - 1} k_1^2$$

at r_o.

Solving for p_1 and q_1, finding p_2 and q_2, substituting into Equation (65), and solving for p/σ_3, one obtains

$$\frac{p}{\sigma_3} = \frac{(k_3^2 - 1)}{k_3^2 \left\{ \frac{2}{k_2} \frac{q_1}{p} + \frac{5}{g(k_1^2 - 1) k_2} + \frac{5}{2} \frac{p_3}{p} \left[\frac{2E_1}{gE_2} \frac{k_3^2}{(k_3^2 - 1)} - 1 \right] \right\}} \qquad (66)$$

where

$$\frac{q_1}{p} = \frac{(\alpha_r - \alpha_m)}{2} \frac{(k_1^2 - 1)}{k_1^2} \frac{\sigma_1}{p} .$$

The pressure-to-strength ratios p/σ_1 and p/σ_3 are plotted in Figures 20 and 21 as a function of segment size k_2 and wall ratio K' for $k_1 = 1.1$, $p_3/p = 0.2$, $\alpha_r = 0.5$, and $\alpha_m = -0.5$. The pressure-to-strength ratios increase with K' or equivalently with k_3, since $K' = k_1 k_2 k_3$. The behavior shown for $k_1 = 1.1$ is the same as that found previously for the ring-segment container; i.e., p/σ_3 increases with increasing k_2, but p/σ_1 decreases. However, if k_1 is increased to 1.5 from 1.1, then p/σ_1 also increases with k_2 for large K' as shown in Figure 22. p/σ_3 continues to increase with k_2 as shown in Figure 23. Thus, both p/σ_1 and p/σ_3 increase with large K' for $k_2 = 2.0$ and $k_1 = 1.5$. For values of k_2 between 2.0 and 4.0, however, computer calculations show that p/σ_1 and p/σ_3 first continue to increase and then decrease.

The pressure-to-strength ratios can also be increased by increasing the support pressure p_3. This is shown in Figure 24. With the high ratios shown, it is theoretically possible to have bore pressures as high as 1,000,000 psi in ring-fluid-segment container. However, practicable limitations regarding excessive interference and size requirements, which are discussed later, considerably reduce the pressure capability of this design.

The interferences and residual pressures for outer and inner parts of the ring-fluid-segment container can be calculated using the analysis derived previously for the multi-ring container and the ring-segment container, respectively.

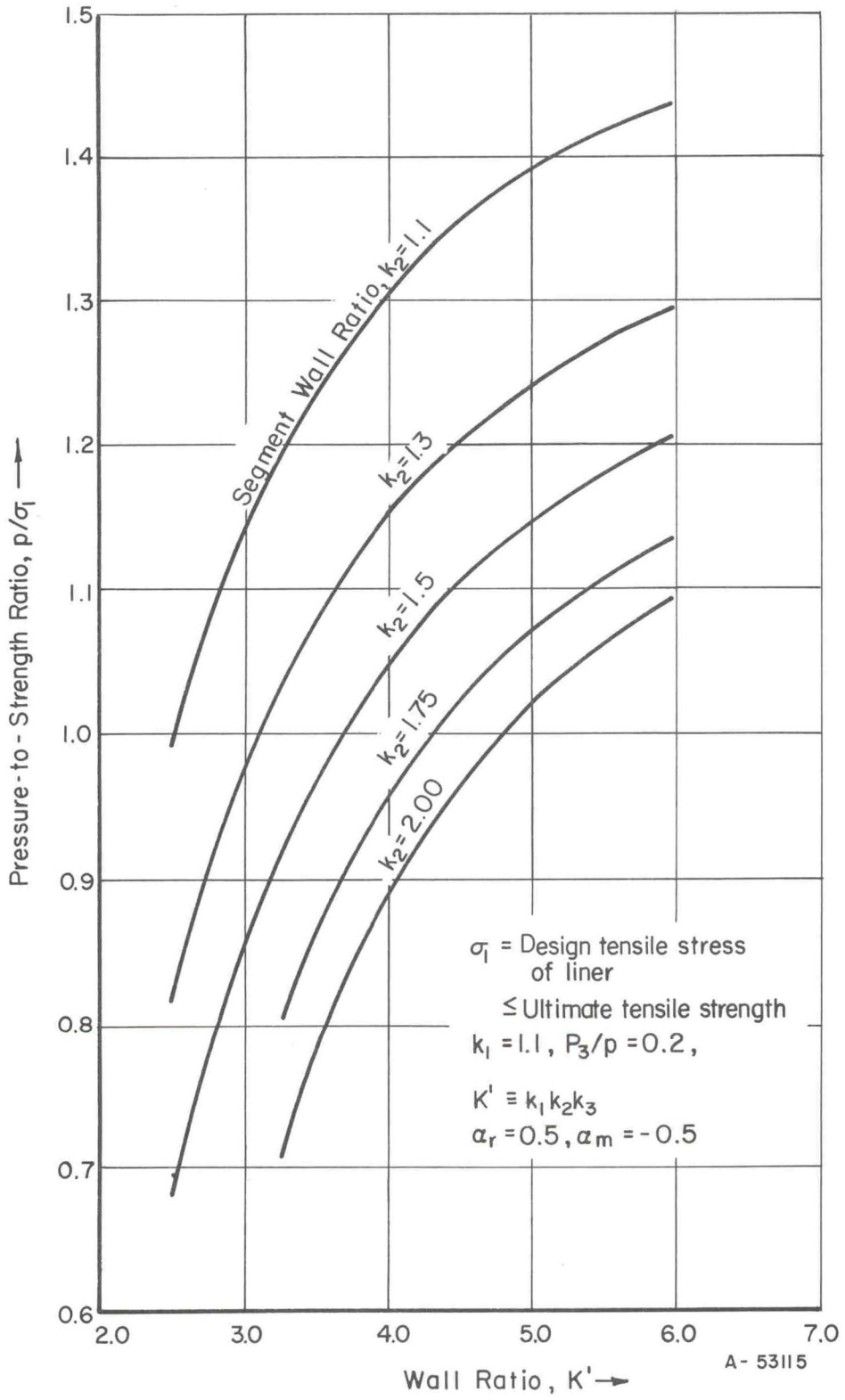

FIGURE 20. EFFECT OF SEGMENT SIZE ON THE PRESSURE-TO-STRENGTH RATIO, p/σ_1, FOR THE RING-FLUID-SEGMENT CONTAINER

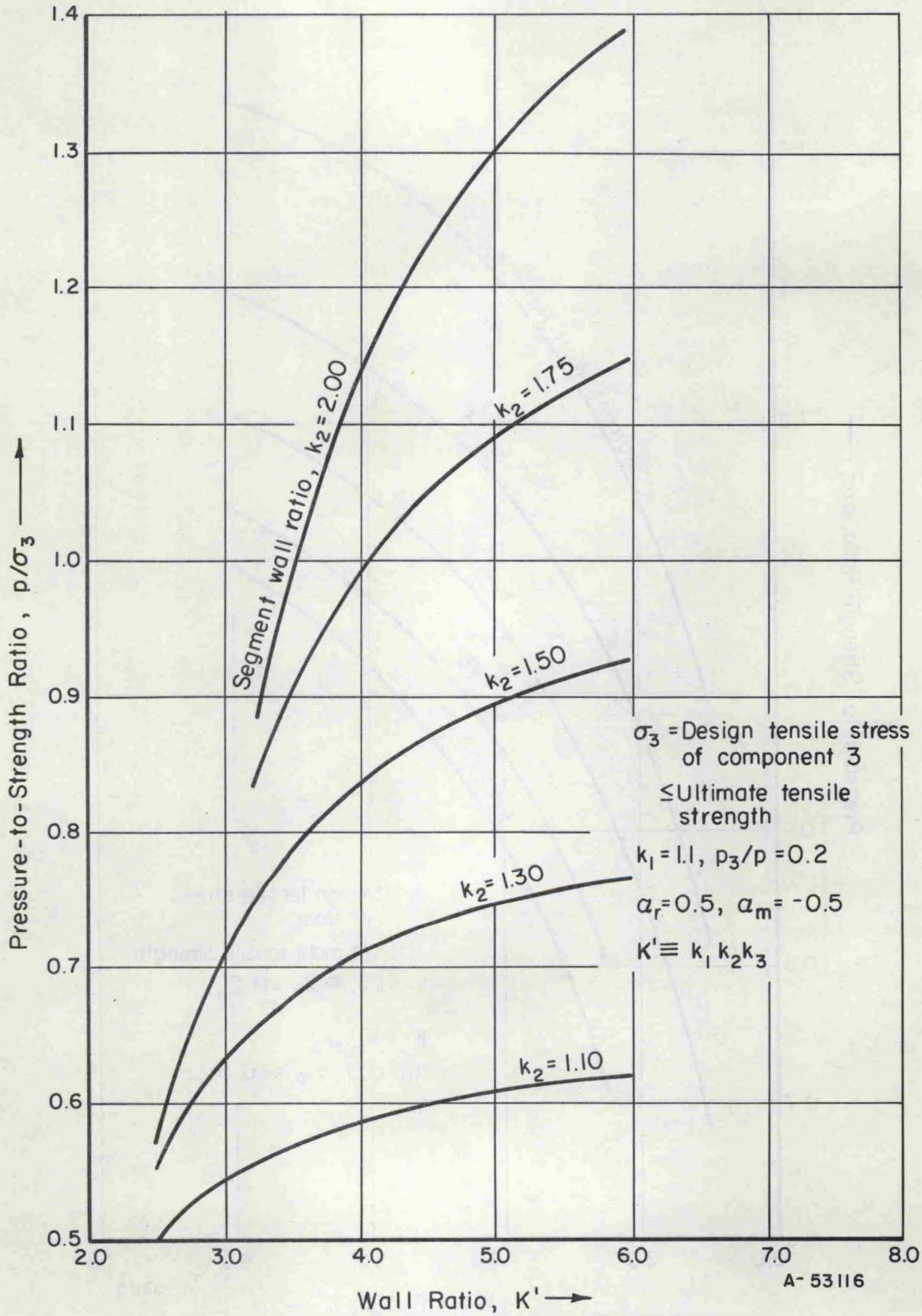

FIGURE 21. EFFECT OF SEGMENT SIZE ON THE PRESSURE-TO-STRENGTH RATIO, p/σ_3, FOR THE RING-FLUID-SEGMENT CONTAINER

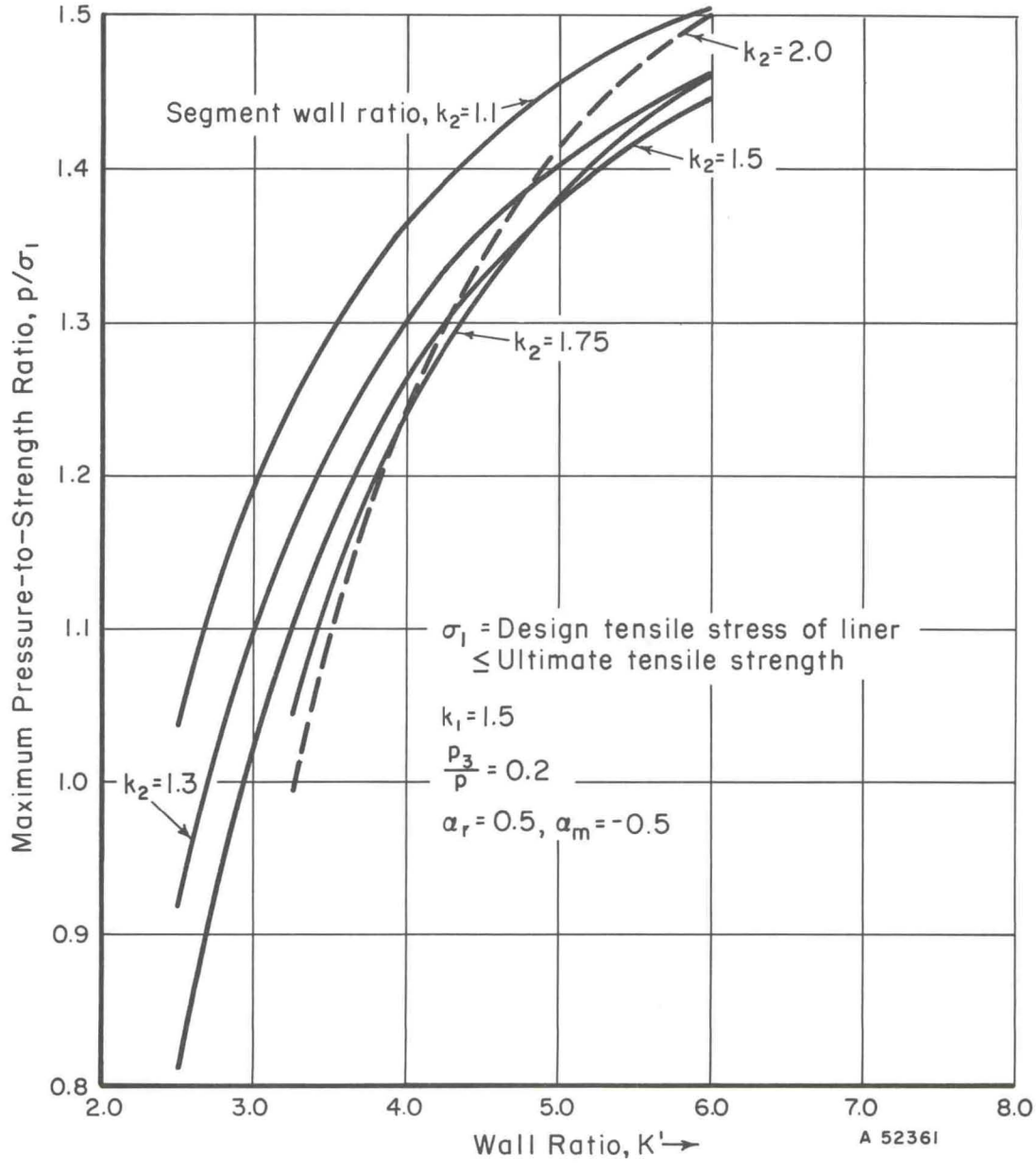

FIGURE 22. EFFECT OF SEGMENT SIZE ON THE PRESSURE-TO-STRENGTH RATIO ρ/σ_1 FOR THE RING-FLUID-SEGMENT CONTAINER

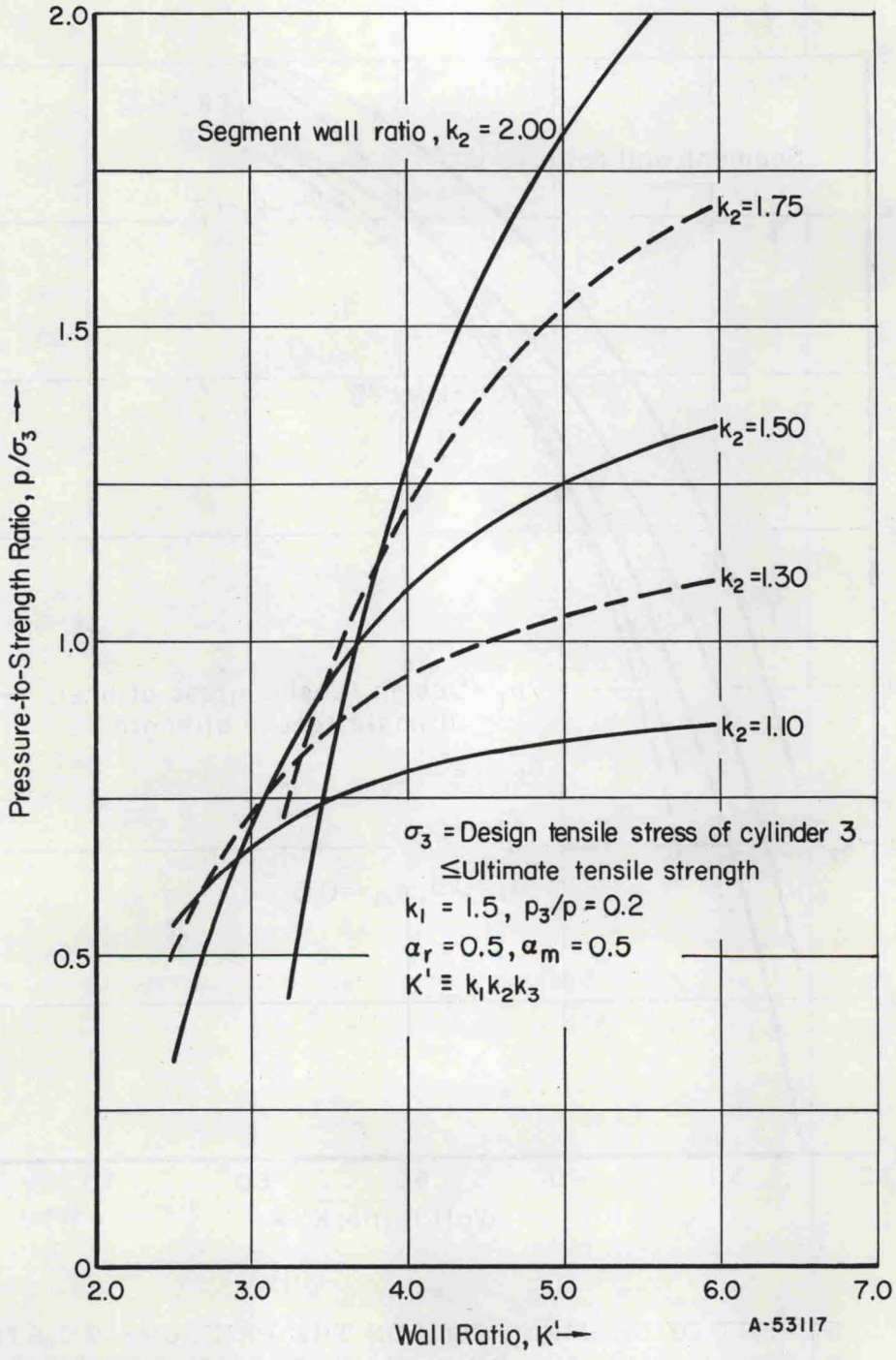

FIGURE 23. EFFECT OF SEGMENT SIZE ON THE PRESSURE-TO-STRENGTH RATIO, p/σ_3, FOR THE RING-FLUID-SEGMENT CONTAINER

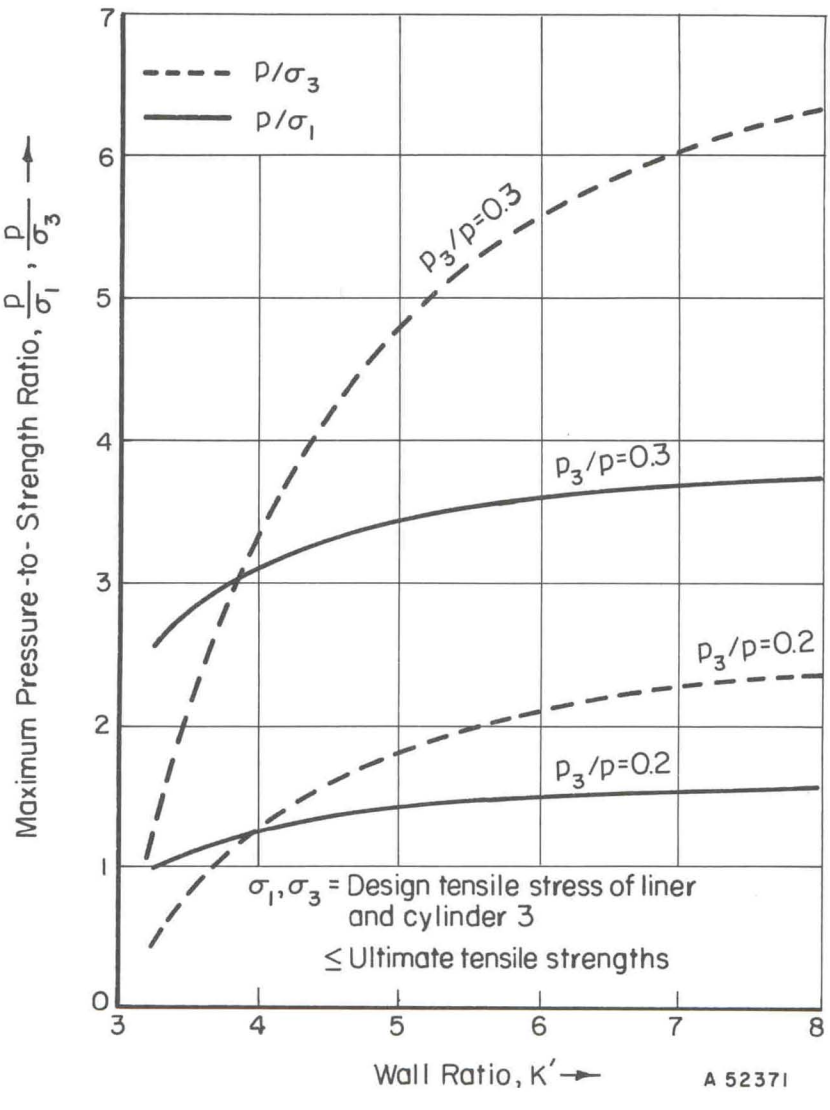

FIGURE 24. EFFECT OF SUPPORT PRESSURE p_3 ON BORE PRESSURE CAPABILITY FOR THE RING-FLUID-SEGMENT CONTAINER

$\alpha_r = 0.5$, $\alpha_m = -0.5$
$k_1 = 1.5$, $k_2 = 2.0$.

Pin-Segment Container

The analysis of the pin-segment container, shown in Figure 7(d), also assumes a high-strength liner. It is also assumed that any manufactured interference is taken up during assembly by slack between pins and holes. Therefore, the residual pressure q_1 between liner and segments is zero at room temperature and nonzero at temperature only if the coefficient of thermal expansion of the liner, α_1, is greater than that of the segments, α_2. In this analysis, it is assumed that $\alpha_1 \geqq \alpha_2$.

The following radial deformation equation must be satisfied:

$$u_1(r_1) + \alpha_1 \Delta T r_1 = u_1(r_1) + \alpha_2 \Delta T r_2 \tag{67}$$

where

$u_1(r_1)$ = the radial deformation of the liner at r_1 due to p at r_o and p_1 at r_1 when $p \neq 0$, and due to q_1 at r_1 when $p = 0$

$u_2(r_1)$ = the radial deformation of the segments at r_1 due to p_1 or q_1 at r_1 and the pin loading at r_2.

Substituting into Equation (67), Equations (17a) and (26a) for u_1 and u_2, and solving for p_1, one gets

$$p_1 = \frac{1}{g_2}\left[\frac{2p}{k_1^2-1} + E_1\Delta T\,(\alpha_1 - k_2\alpha_2)\right] \tag{68}$$

where

$$g_2 = \frac{E_1}{E_2}\left[\frac{k_2^2+1}{k_2^2-1} + \nu + \frac{M_2 f_3(r_1)}{\beta_1} + E_2\,\frac{G_2}{r_1} + g_{m4}(r_1)\right] + \frac{k_1^2+1}{k_1^2-1} - \nu \quad . \tag{69}$$

Similarly, q_1 is found if p is taken as zero; i.e.,

$$q_1 = \frac{E_1\Delta T\,(\alpha_1 - k_2\alpha_2)}{g_2} \quad . \tag{70}$$

Formulating the range in hoop stress $(\sigma_\theta)_r$ at the bore (Equation (59) and using the definition $\alpha_r\sigma_1 = (\sigma_\theta)_r$, we get the following expression for p/σ_1:

$$\frac{p}{\sigma_1} = \frac{2\alpha_r\,(k_1^2 - 1)^2\,g_2}{\left[g_2\,(k_1^4 - 1) - 4k_1^2\right]} \tag{71}$$

[Equation (71) is identical in form to Equation (61).]

The pressure-to-strength ratio p/σ_1 is plotted in Figure 25. Comparing this figure with Figure 12 for the multi-ring container with $\alpha_r = 0.5$, it is evident that both containers have the same limit $p/\sigma_1 \to 1$ for large wall ratios. However, $\alpha_r = 0.5$ is possible only if $\alpha_m \leqq 0$ as shown in Figure 9. Actually, $\alpha_m = +0.5$ is likely in the pin-segment container if $\alpha_r = 0.5$ because any interference is expected to be lost in taking up slack between pins and holes. In this case, then, $\alpha_r = 0.5$ would mean only one cycle life whereas $\alpha_r = 0.5$ means 10^4 to 10^5 cycles life in the multi-ring container. If this assembly problem could be eliminated by careful machining and selective fitting of pins, then theoretically with sufficient compressive prestress, the p/σ_1 ratio of the pin-segment container could be made to approach that of the multi-ring container.

Since no prestress has been assumed for the pin-segment container, $\alpha_r = \alpha_m = 0.35$ for 10^4 to 10^5 cycles as shown by Figure 9. For $\alpha_r = 0.35$, it is found that p/σ_1 is limited to 0.7 at best. Therefore, the maximum pressure in the pin-segment container is $p = 0.7\ (300,000) = 210,000$ psi for 10^4 to 10^5 cycles life.

The stresses in the segments have not yet been considered. High stresses develop around the pin holes. These too limit the pressure in the pin-segment container. Analysis of the stresses in the segments is described in Appendix A. For the purpose of estimating stresses in the segments the interface pressure p_1 is needed. Therefore, plots of p_1/p are provided in Figure 26. It is evident that the interface pressure p_1 is appreciably less than the bore pressure p_1 especially for large k_1 and small k_2.

The pins are analyzed in Appendix B. In order to carry the pressure loading p_1, it is found that the pin-to-segment-diameter ratio must be

$$\frac{d}{2r_1} = \frac{8}{3}\,\frac{t}{d}\,\frac{p_1}{\tau} \tag{72}$$

where

d = pin diameter

t = segment thickness

$2r_1$ = inside segment diameter

τ = maximum shear stress in pin.

Strip-Wound Container

An analysis was not conducted for the strip-wound container, because it is possible to estimate its relative strength based upon the results of the analysis of the multi-ring container. The strip-wound (wire-wrapped) cylinder uses basically the same principle as the multi-ring container. It has a cylindrical inner cylinder, the liner, under prestress, but the prestress in the liner is provided by wrapping strips or wire under tension onto the liner.

In order to estimate the pressure-to-strength ratio of the strip-wound vessel it is assumed that it behaves overall as a thick cylinder under internal pressure after the

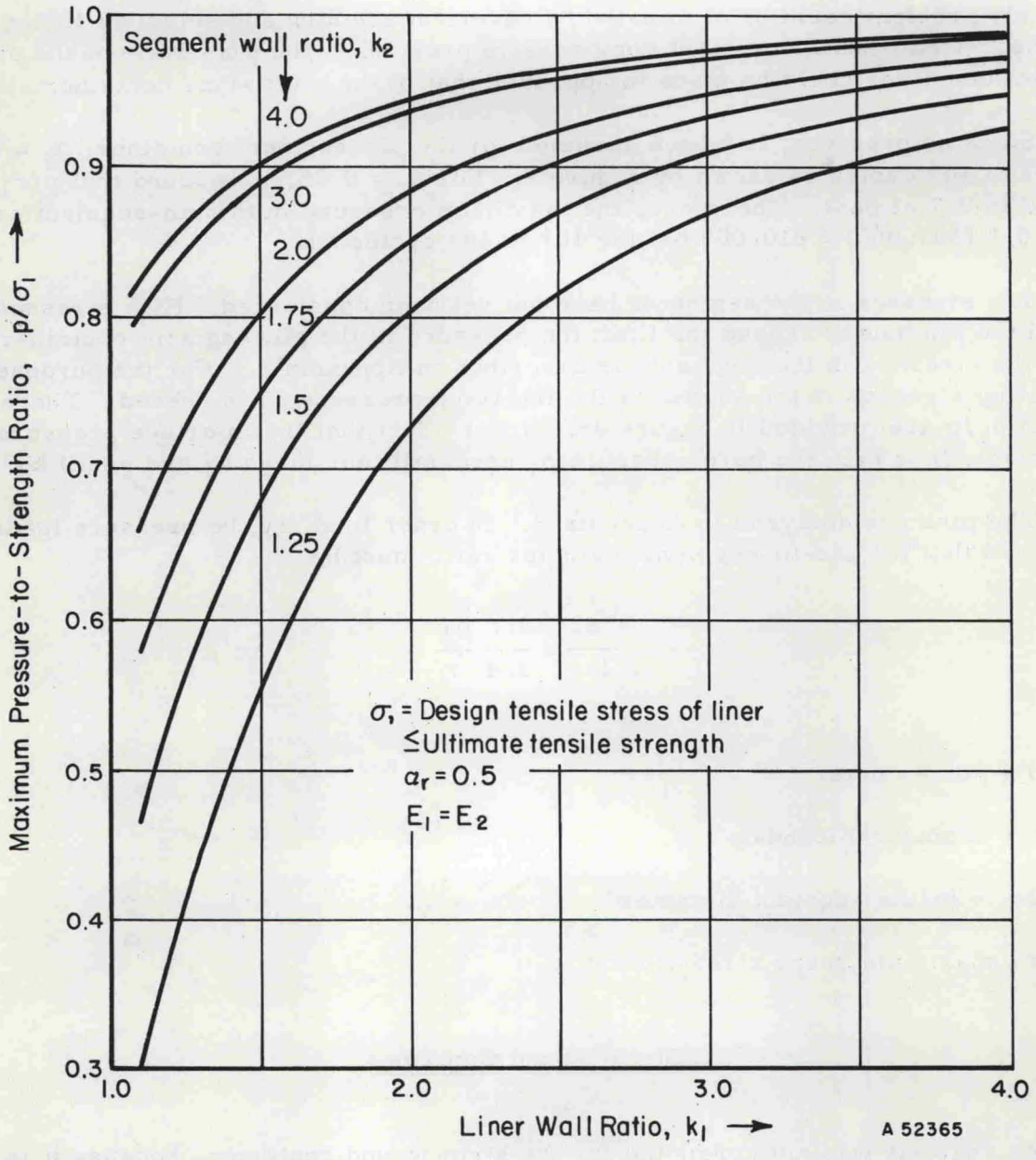

FIGURE 25. MAXIMUM PRESSURE-TO-STRENGTH RATIO, p/σ_1, FOR THE PIN-SEGMENT CONTAINER

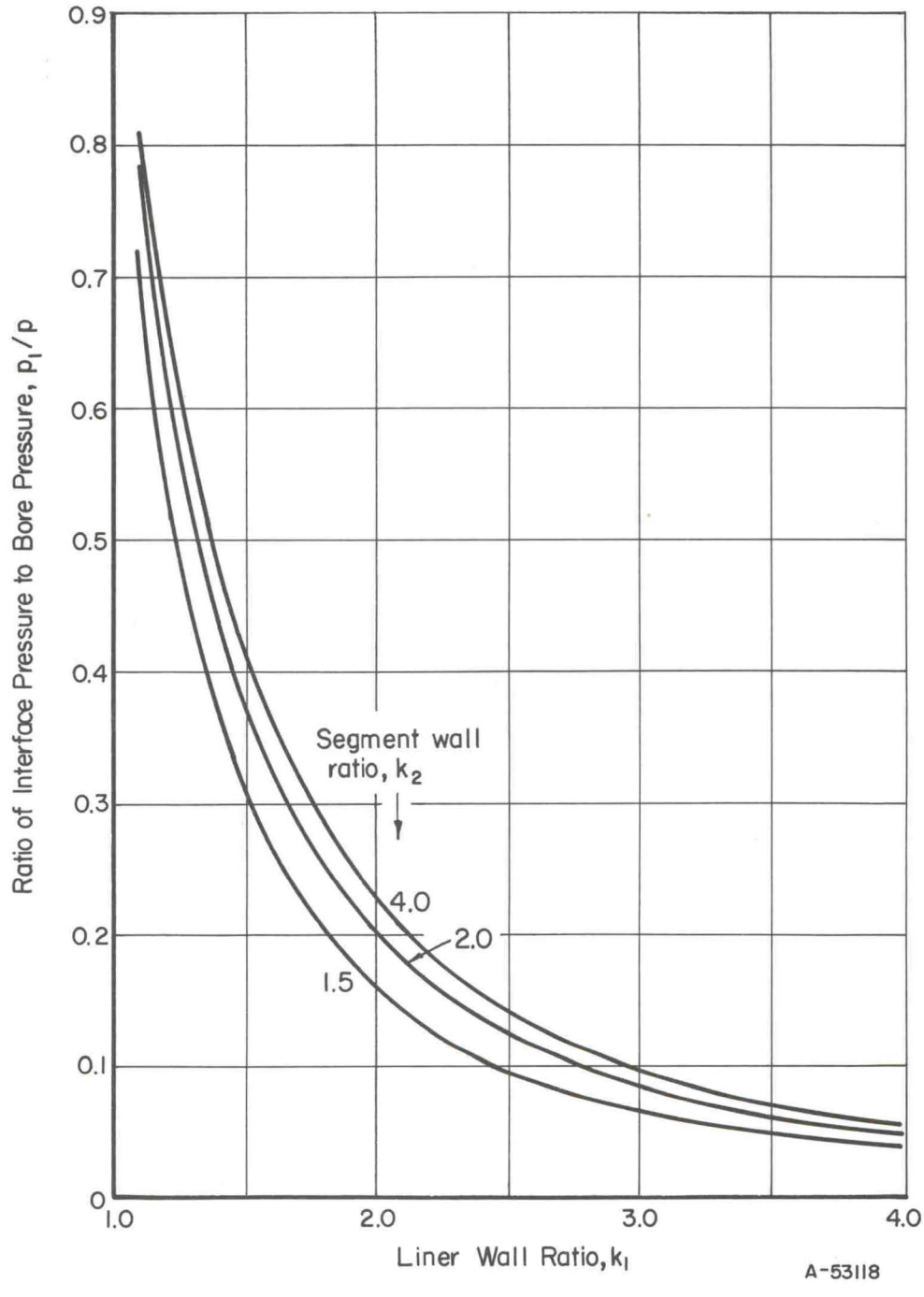

FIGURE 26. RATIO OF INTERFACE PRESSURE BETWEEN SEGMENTS AND LINER TO BORE PRESSURE FOR THE PIN-SEGMENT CONTAINER

strip has been wound on. Referring to Equation (47), we see that the pressure-to-strength ratio p/σ_1 depends only on the overall wall ratio K and α_r the stress-range parameter for the liner material. If K for the strip-wound vessel is taken as the ratio of the outside diameter of the last strip layer to the inner bore diameter, then Equation (47) can be used to estimate its pressure capability. Therefore, it may be concluded that the strip-wound container has a maximum pressure equal that of the multi-ring container. However, unknown local stress concentrations and contact conditions between strips may be detrimental in the strip-wound design. Because of these possible disadvantages and no better pressure capability than the multi-ring container, detailed analysis of the strip-wound vessel is not warranted. However, the strip-wound design does offer advantages in producibility of large diameter containers as pointed out later in the Design Requirements ... section of this report.

Controlled Fluid-Fill Multi-Ring Container

A controlled fluid-fill container, shown in Figure 27, has been proposed by Berman[20]. All the rings are assumed to be made of the same ductile material and a shear strength criterion applies. Like the ring-segment-fluid container this container also uses the fluid-pressure support principle. The advantage of this design is that under static applications the residual stress limitation (the limit curve in Figure 10) can be overcome by controlling the pressures p_n; i.e., the pressures p_n can be reduced to zero as the bore pressure, p, is reduced to zero. There are no shrink fits, so there are no residual stresses. Berman's analysis was based upon static strength. A similar analysis is now conducted based on fatigue strength.

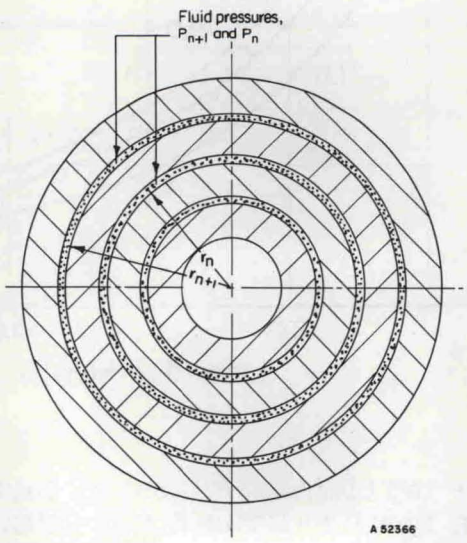

FIGURE 27. CONTROLLED FLUID-FILL CYLINDRICAL-LAYERED CONTAINER [REFERENCE (20)]

In order that each ring have the same shear stress under static pressure, Berman finds that the same relation, Equation (33) (first found by Manning[5]), applies for the controlled fluid-fill container that also applies for the multi-ring container designed for static shear strength. If this result is used in a shear fatigue analysis (assuming ductile materials), then Equation (33) can be interpreted as the maximum shear stress developed during a cycle of pressure, i.e.,

$$(S)_{max} = \frac{p}{N} \frac{K^{2/N}}{(K^{2/N}-1)} \tag{73}$$

If the pressures p_n are reduced to zero, then the minimum shear stress during a cycle of pressure is zero. Therefore, the semirange and mean shear stresses are equal,

$$S_m = S_r = \frac{pK^{2/N}}{2N(K^{2/N}-1)} \tag{74a, b}$$

where S_m and S_r are defined in Equations (8a, b).

If Equation (74a, b) are substituted into the fatigue relation, Equation (12), there results

$$\sigma = \frac{5p}{2N} \frac{K^{2/N}}{(K^{2/N}-1)} \tag{75}$$

It is surprising that this result, Equation (75), is the same as Equation (43) plotted in Figure 11, the result of the shrink-fit analysis, except now the limit Equation (45) no longer applies. Therefore, now p/σ can be made as large as desired simply by increasing N. The only problem is that the required N or K may be too large to be practical. For example, assume σ = 150,000 psi (ultimate strength of a ductile steel), N = 8 and K = 16. Calculating p we find that p = 240,000 psi. Thus, it is concluded that for fatigue applications under high pressure the controlled-fluid-fill multi-ring container becomes too large to be practical. Eight rings also means there are seven annuli under fluctuating pressures. (The magnitudes of these pressures are all different and are given by an equation similar to Equation (41).) Design of mechanical apparatus to supply and control all these pressures presents practical difficulties also.

DESIGN REQUIREMENTS AND LIMITATIONS FOR HIGH-PRESSURE CONTAINERS

As already indicated, the theoretically predicted maximum pressure capability for the four containers considered in detail in the present study are as follows for 10^4 to 10^5 cycles life:

Container	Maximum Pressure, p, psi
Multi-ring	300,000
Ring-segment	300,000
Ring-fluid-segment ($p_3/p = 0.3$)	~1,000,000
Pin-segment	210,000

These predictions are based on an ultimate tensile strength of 300,000 psi for the liner and 200,000 psi for the outer cylinders or components, and apply to any operating temperature provided these are the strengths at temperature.

For liners with ultimate tensile strengths much greater than 300,000 psi, the theoretical maximum pressure capability of the various designs may be improved appreciably. This is true if it can be assumed that the higher strength materials would exhibit the same fatigue behavior as that shown in Figure 9 for steels with ultimate tensile strength ranging from 250,000-310,000 psi at room temperature. (Tensile strengths of 410,000 psi have been reported for AISI M50 steel. If the previous assumption is correct, then a multi-ring or ring-segment container with an M50 liner would have a theoretical maximum pressure capability of 410,000 psi. However, these containers may require that some of ductile outer cylinders have ultimate tensile strengths greater than 200,000 psi.)

Possible Manufacturing and Assembling Limitations

It is important to note that the theoretical pressures given in the above tabulation may not be achievable for each design because of practicable design limitations. For example, the outside diameters required for designs having 6- and 15-inch bore diameters are as follows:

Container	Outside Diameter, inches	
	6-inch Bore Design	15-inch Bore Design
Multi-ring	51.0	127.5
Ring-segment	60.0	150.0
Ring-fluid-segment	229.5	573.5
Pin-segment	90.4	180.2

It may be impossible to obtain steel cylinders in such large sizes (10- to 50-foot diameters) with ultimate strengths of 200,000 psi, and it may be impossible to machine and transport these large cylinders. Also heat treatment of heavy sections may be a problem. This may not be the case for pin-segment container, however. In this instance, it may be possible to forge the large steel pins (18.2 inches and 45.4 inches in diameter respectively, based on a design shear stress of 50,000 psi in fatigue for the pins) and the segments (thick plates). This indicates an advantage of the pin-segment design for vessels with $p \leqq 210,000$ psi.

A pin-segment arrangement may also be used to advantage as a replacement for the outer cylinder in the other container designs. This would help overcome the difficulties associated with the large steel cylinders. A wire wrap or strip wrap could also be used to this advantage as a replacement to outer cylinders.

The limitations in some of the designs due to large-diameter outer cylinders may also be partially overcome by using the autofrettage process to provide some additional prestress at the liner bore. The process introduces compressive prestresses by plastic deformation of the bore. This approach could reduce the size and number of outer rings that otherwise would be needed to achieve the total prestress by shrink fitting alone. In fact, the autofrettage process could be used to improve the size efficiency of all the design concepts considered. However, if autofrettaging is employed, then high-strength steels with appreciable amounts of ductility should be selected for the liner because the process requires plastic deformation of the bore.

In addition to the potential problem of cylinder size, the theoretical pressures may not be possible to achieve because excessive interferences may be required for shrink-fit assembly. The maximum interferences required for the designs with the above theoretical pressures are as follows:

Container	Maximum Interference Required, inch/inch
Multi-ring	$\Delta_1/r_1 = 0.0036$
Ring-segment ($k_2 = 1.1$, $\frac{E_2}{E_1} = 3.0$)	$\Delta_{12}/r_1 = 0.0028$
Ring-fluid-segment ($k_2 = 2.0$)	$\Delta_{12}/r_1 = 0.0164$
Pin-segment	None, except for a small amount to take up slack during assembly

For the multi-ring container, the interference required between the liner and cylinder 2 as manufactured is $\Delta_1/r_1 = 0.0036$ in./in. This is a reasonable value and corresponds to a temperature difference of 400 to 500 F for assembly. However, the interference as manufactured is not always the same as the interference as assembled. Suppose that the multi-ring container is assembled ring by ring from the inside out. Each ring expands as it is shrunk on and the assembly interference progressively increases beyond the manufactured interference. Formulas for the assembly interference can also be derived. Derivations are given in Appendix B.

The interference required for the ring-fluid-segment container is $\Delta_{12}/r_1 = 0.0164$ in./in. This interference requirement is severe, if not impossible, especially when one considers assembling not only the liner and cylinder 3, but also a number of segments all at the same time. (Δ_{12} is the interference required between the liner, segments, and cylinder 3. Δ_{12} is also the assembly interference as well as the manufactured interference since the liner, cylinder 3, and the segments must be assembled simultaneously.) The large magnitude for Δ_{12} is primarily due to large radial elastic deformation of the segments under pressure. This is shown as follows: from Equation (22a) it is found that

$$\frac{E_2 (u_1 - u_2)}{r_1 p_1} = 0.69 \text{ for } k_2 = 2 \text{ and } p_2 = p_1/k_2 \quad ,$$

where u_1 and u_2 are the radial displacements of the segment and r_1 and r_2, respectively. From a computer calculation for the ring-fluid-segment container p_1 at pressure ($\sigma_r = -p_1$ at r_1), is found to be $p_1/\sigma_1 = 2.2$. Thus,

$$\frac{E_2 (u_1 - u_2)}{r_1 \sigma_1} = 2.2 (0.69) = 1.518 .$$

Hence, $\frac{u_1 - u_2}{r_1} = 0.0152$ in./in.

for $\sigma_1 = 300,000$ psi and $E_2 = 30 \times 10^6$ psi, and it is evident that large interference, $\Delta_{12} = 0.0164$ in./in., is required to overcome large deformation of the segments under pressure. This is a disadvantage for the containers having segments in their designs.

Another potential disadvantage of these designs is the possible problem of gouging the liner with the corners of the segments if the components are assembled by pressing. A further factor that must be considered in the design of segments is bending deformation. This is discussed in Appendix A.

The severe interference requirements imposed by the segments are reduced if the segment size (k_2) is reduced and if a higher modulus material is used for the segments. These effects are shown above for the ring-segment container which has a lower interference requirement; i.e., $\Delta_{12} = 0.0028$ in./in. However, selection of a high modulus material must be done with care, because tensile stresses do develop in the segments as shown in Appendix A and many high modulus materials have low tensile strengths.

Thus, it is seen that some theoretical container designs for high pressure may be impossible to fabricate because of the large outside diameters and interferences required. In order to obtain a more realistic evaluation of the various design concepts, predictions of pressure capability are made for more practicable design requirements, i.e., outside diameters limited to 72 inches and the interferences limited to 0.007 in./in. maximum. These predictions are as follows for 10^4-10^5 cycles life:

Container		Bore Diameter, inches	Outside Diameter, inches	Number of Components, N	Maximum Pressure, p, psi
Multi-ring	($k_1 = 2.0$)	6	51.0	5	300,000
	($k_1 = 1.5$)	15	72.0	7	275,000
Ring-segment ($k_2 = 1.1$, $E_2/E_1 = 3.0$)	($k_1 = 2.0$)	6	60.0	6	290,000
	($k_1 = 1.5$)	15	72.0	8	265,000
Ring-fluid-segment ($k_1 = 1.5$, $k_2 = 2.0$, $k_3 = 1.25$)	($p_3/p = 0.3$)	6	72.0	10	286,000
	($p_3/p = 0.2$)	15	72.0	5	118,000
Pin-segment ($k_1 = 1.3$, $k_2 = 2.0$)		6	72.0	3	195,000
		15	(a)	--	--

(a) OD $\leq$ 72.0 not possible for 10^4-10^5 cycles life and $\alpha_r = \alpha_m = 0.35$ if no prestress is provided.

It is evident that lower maximum pressures are now predicted, particularly for the 15-inch bore designs. The reduction in pressure capability is due only to the restriction in outside diameter for the multi-ring, ring-segment, and pin-segment containers. However, both the outside diameter and interference limitations reduce the predicted pressure for the ring-fluid segment container. The reduction for this container is severe and is caused by three effects. The first is excessive deformation of the segments for

$k_2 = 2.0$. The other effects are coupled; reducing the outside diameter while maintaining the design pressure increases the interference required, but limiting the interference causes a reduction in maximum pressure because the interference depends upon the pressure.

Residual Stress Limitations

A container designed for a specific cyclic pressure requires certain residual stresses (prestresses) at operating temperature. It is also important, however, to check the residual stresses at room temperature because of differences in thermal expansion.

Calculations of residual stresses are given here for the multi-ring container as an example. (Residual stresses and operating stresses are given for all containers in Appendix C where computer programs are also listed. The specific container design discussed here is the one considered in the foregoing section for a bore diameter of 6 inches. Calculations are performed for design applications at room temperature, 500 F, and 1000 F. The material data assumed are given in Table 11. The liner material is assumed to be 18 percent Ni maraging steel, and the outer cylinders are assumed to be made of modified H-11 steel. The differences in thermal expansion for these materials are likely to be the largest expected among the steels that may be used.

TABLE 11. ELEVATED-TEMPERATURE DATA FOR 18% Ni MARAGING STEEL AND H-11 STEEL[a]

	70 F	500 F	1000 F
	Modulus of Elasticity, psi		
18% Ni Maraging	26.5×10^6	23.0×10^6	18.7×10^6
H-11	30.0×10^6	27.4×10^6	22.8×10^6
	Coefficient of Thermal Expansion, in./in./F		
18% Ni Maraging	5.6×10^{-6}	5.6×10^{-6}	5.6×10^{-6}
H-11	7.12×10^{-6}	7.25×10^{-6}	7.37×10^{-6}

(a) Poisson's ratio taken as constant, $\nu = 0.3$ for both materials.

Results are given in Table 12. The range and mean stress parameters were $\alpha_r = 0.5$ and $\alpha_m = 0.5$, respectively. The results show that the excessive residual stresses at room temperature occur for the multi-ring container having a required prestress, $\sigma_\theta = -\sigma_1$ at 500 F and 1000 F; i.e., the residual stress $\sigma_\theta < -\sigma_1$ at room temperature, where σ_1 is the design stress and $\sigma_1 \leqq$ ultimate tensile strength. The reason for this is the larger interferences required for elevated-temperature application as shown in Table 12. Larger interferences are necessary for high-temperature applications because the outer rings expand more than the liner due to the differences in thermal expansions as shown in Table 7. On the other hand, reduction of the temperature from operating

temperature to room temperature causes the outer rings to tend to contract more than the liner. The liner resists the contraction and the residual interface pressures are increased, thereby increasing the magnitude of the residual hoop stress at the bore.

If the multi-ring container is to be used at 500 F and 1000 F with the material properties given in Table 11, then the prestress requirement, $\sigma_\theta = -\sigma_1$ at temperature ($\alpha_m = -0.5$) has to be relaxed. Accordingly, calculations of residual stresses and interferences are rerun for $\alpha_m = -0.3$ (prestress $\sigma_\theta = -0.8\ \sigma_1$ at temperature). These results are shown in Table 9. With $\alpha_m = -0.3$, excessive residual stresses at room temperature are avoided for the 500 F design. However, for operation at 1000 F, $\alpha_m > -0.3$ is necessary since $\sigma_\theta < -\sigma_1$ at room temperature for the 1000 F design with $\alpha_m = -0.3$.

Decreasing the interference fit (from those in Table 12 to those in Table 13), in order to avoid excessive residual stresses at room temperature, increases $(\sigma_\theta)_{max}$ from 0 to positive values. As pointed out in the latter part of the Fatigue Criteria section, zero to small $(\sigma_\theta)_{max}$ is expected to be beneficial in preventing the detrimental effect of fluid pressure from entering voids in the material. Therefore, if excessive residual stresses are to be avoided in containers designed for high temperatures, and if $(\sigma_\theta)_{max}$ is to be kept small, then the thermal coefficients of expansion of the component parts of the container should be more closely matched than those of Table 11. Preferably the coefficient of thermal expansion should be larger for the liner than for the outer cylinders; this would cause a reduction rather than an increase in residual stresses upon decreasing the temperature from operating temperature to room temperature.

Other Possible Material Limitations

It has been postulated that a maximum-tensile-stress fatigue criterion applies to the high-strength liner. Accordingly, fatigue data from uniaxial tension and rotating-beam bending tests were used to evaluate fatigue behavior of liners for high-pressure containers. However, the state of stress in an open-end hydrostatic extrusion container is biaxial and in a closed-end container a triaxial state of stress exists. (A triaxial state of stress may also occur in a shrink-fit open-end container where axial stresses may be produced by interface friction between shrink-fitted rings.) The effect of combined stresses on the fatigue strength of high-strength steels is unknown. It is pointed out, however, that the analyses performed in this study allow for arbitrary material behavior; i.e., the fatigue parameters α_r and α_m used in tha analysis are left arbitrary in the equations and could be determined from combined-stress fatigue experiments.

It has also been postulated that a compressive mean stress may benefit material fatigue strength under cyclic fluid pressure. However, biaxial and triaxial fatigue behavior under compressive mean stress is unknown. Even fatigue data in the uniaxial case are lacking for conditions of compressive mean stress.

Also unknown is the possible fracture of high-strength steels under large compressive stresses. Pugh and Green[21] and Crossland and Dearden[22] found for cast iron that the fracture strain and ductility (and the maximum shear stress at fracture) are increased by superimposing hydrostatic pressure. Bridgman[23] found similiar but less conclusive results for steel. These are favorable results for the effect of true hydrostatic pressure, but the possibility of similiar behavior when only one principal stress (the radial stress in a container) is highly compressive is unknown and should be

TABLE 12. LINER-BORE STRESSES AND INTERFERENCES FOR A 6-INCH BORE MULTI-RING CONTAINER WITH K = 8.5, N = 5, $k_1 = 2.0$, $k_n = 1.44$, $n \geq 2$, $\alpha_r = 0.5$, $\alpha_m = -0.5$[a]

	Stresses at Bore of Liner[b]								
	Residual Stresses at RT			Prestresses at Temperature			Operating Stress at Pressure and Temperature		
	σ_r/σ_1	σ_θ/σ_1	S/σ_1	σ_r/σ_1	σ_θ/σ_1	S/σ_1	σ_r/σ_1	σ_θ/σ_1	S/σ_1
RT Design	0	-1.000	-0.5000	0	-1.0000	-0.5000	-0.9727	0	0.4863
500 F Design	0	-1.1230	-0.5615	0	-1.0000	-0.5000	-0.9727	0	0.4863
1000 F Design	0	-1.2998	-0.6499	0	-1.0000	-0.5000	-0.9727	0	0.4863

	Dimensionless Interference Required as Manufactured[c]	
	Between Cylinders 1 and 2 for p = 300,000 psi[d], $E\Delta_1/r_{1p}$	Between Outer Cylinders n and n + 1 $E\Delta_n/r_{np}$
RT Design	0.358	0.343
500 F Design	0.454	0.343
1000 F Design	0.533	0.343

(a) The k_n, K, α_r, and α_m are defined by Equations (5), (6), and (13a, b), respectively. Material data are given in Table 11. The liner is 18% Ni steel and the outer cylinders are H-11 steel.

(b) σ_r is the radial stress, σ_θ the hoop stress, S the shear stress ($S = (\sigma_\theta - \sigma_r)/2$), and σ_1 is the design strength - less than or equal to the ultimate tensile strength of the liner.

(c) E is the modulus of elasticity of the outer cylinders. Δ_n is interference in inches between cylinders n and n + 1. r_n is the outer radius of cylinder n.

(d) $E\Delta_1/r_1p$, at elevated temperatures, depends on p. $\sigma_1 = 310,000$ psi is required, ($p = 0.9727\sigma_1$).

TABLE 13. LINER-BORE STRESSES AND INTERFERENCES FOR A 6-INCH BORE MULTI-RING CONTAINER WITH K = 8.5, N = 5, $k_1 = 2.0$, $k_n = 1.44$, $n \geq 2$, $\alpha_r = 0.5$, $\alpha_m = -0.3$[a]

	Stresses at Bore of Liner[b]								
	Residual Stresses at RT			Prestresses at Temperature			Operating Stress at Pressure and Temperature		
	σ_r/σ_1	σ_θ/σ_1	S/σ_1	σ_r/σ_1	σ_θ/σ_1	S/σ_1	σ_r/σ_1	σ_θ/σ_1	S/σ_1
RT Design	0	-0.8000	-0.4000	0	-0.8000	-0.4000	-0.9727	0.2000	0.5863
500 F Design	0	-0.9054	-0.4527	0	-0.8000	-0.4000	-0.9727	0.2000	0.5863
1000 F Design	0	-1.0505	-0.5253	0	-0.8000	-0.4000	-0.9727	0.2000	0.5863

	Dimensionless Interference Required as Manufactured[c]	
	Between Cylinders 1 and 2 for p = 300,000 psi[d], $E\Delta_1/r_1p$	Between Outer Cylinders n and n + 1 $E\Delta_n/r_np$
RT Design	0.217	0.304
500 F Design	0.309	0.304
1000 F Design	0.383	0.304

(a) The k_n, K, α_r, and α_m are defined by Equations (5), (6), and (13a, b), respectively. Material data are given in Table 11. The liner is 18% Ni Steel and the outer cylinders are H-11 steel.

(b) σ_r is the radial stress, σ_θ the hoop stress, S the shear stress ($S = (\sigma_\theta - \sigma_r)/2$), and σ_1 is the design strength - less than or equal to the ultimate tensile strength of the liner.

(c) E is the modulus of elasticity of the outer cylinder. Δ_n is interference in inches between cylinders n and n + 1. r_n is the outer radius of cylinder n.

(d) $E\Delta_1/r_{1p}$, at elevated temperatures, depends on p. $\sigma_1 = 310,000$ psi is required ($p = 0.9727\sigma_1$).

investigated. This is a particularly important factor because the difference between the hoop stress and the high compressive radial stress represents an extremely large shear stress.

The effect of a brittle-ductile transition in high-strength steels on the fatigue behavior near and above the transition temperature is another factor which may need to be considered.

RECOMMENDATIONS

Proposed Materials Study

The possible material limitations discussed in the preceding section suggests that a materials study be conducted. The biaxial and triaxial fatigue behavior of high-strength steels under compressive mean stress should be investigated. The objective of the study would be to establish a fatigue criterion for these materials under combined-stress states. The effect of large transverse compressive stresses of magnitudes one to three times the ultimate tensile strength, upon the flow and fracture characteristics of high-strength steels should also be studied. Moreover, a brittle-ductile transition in high-strength steels may influence fatigue behavior at elevated temperatures – an investigation of this factor may also be worthwhile.

Suggested High-Pressure Container

The results of the investigations on various containers have shown that fluid-pressure support is beneficial and that prestress is also beneficial in increasing the predicted fatigue strength under cyclic pressure loading. Use of high-strength steels for the liners of the containers was also found necessary. Although the controlled fluid-fill design, Figure 27, uses the fluid-support principle, the required size and complexity of the fluid-fill apparatus for fatigue application makes the design impracticable. Use of shrink-fits to provide compressive prestress can reduce the required size and the number of pressure annuli as the ring-fluid-segment design indicates. Although the latter design has the benefit of prestress from shrink-fitting it requires large interferences because of large deformations of the segments and large outer cylinders because the segments offer no hoop support.

A suggested design which appears to minimize the problems introduced by segments is shown in Figure 28. It is made up of two multi-ring units and a fluid-pressure support annulus. Three rings are shown in each part of Figure 28, but the number of rings can be varied to give the best design. For example, for containers having small bores, one ring is sufficient in the inner part. It is easily shown (using the tensile fatigue criterion for the inner ring) that a cyclic bore pressure of 450,000 psi is possible with one inner ring of wall ratio, $k_1 = 1.65$ and a support pressure p_1 of 250,000 psi. A multi-ring container for the outer part can be designed for 10^4 to 10^5 cycles at 250,000 psi as shown in this study.

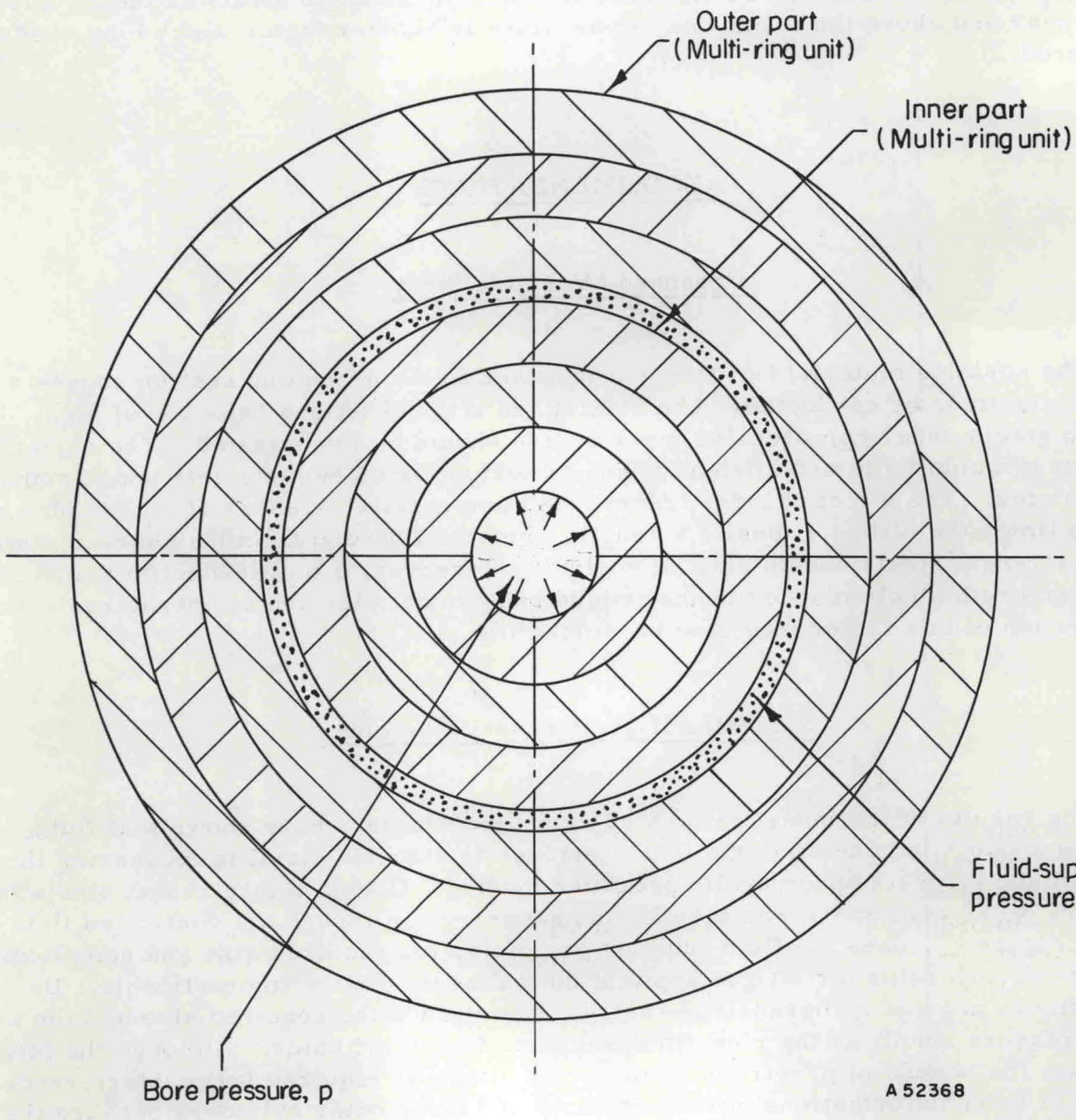

FIGURE 28. SUGGESTED FLUID-SUPPORT MULTI-RING CONTAINER FOR HIGH PRESSURE

The design involves the combined use of interference-fit multi-ring construction with fluid-pressure support.

Example calculation:

for the liner: $(\sigma_\theta)_{max} = p \dfrac{(k_1^2 + 1)}{(k_1^2 - 1)} - 2 \dfrac{p_1 k_1^2}{k_1^2 - 1}$ at the bore

$$= 450,000 \left(\frac{3.72}{1.72}\right) - 2\,(250,000) \left(\frac{2.72}{1.72}\right)$$

$$= 184,000 \text{ psi}$$

$$(\sigma_\theta)_{min} = 0$$

$$(\sigma_\theta)_r = (\sigma_\theta)_m = 92,000 \text{ psi}$$

$$\alpha_r = \alpha_m = \frac{92,000}{263,000} = 0.35 \text{ for } \sigma_1 = 263,000 \text{ psi.}$$

$\alpha_r = \alpha_m = 0.35$ gives 10^4-10^5 cycles life as shown in Figure 9. If $\sigma_u = 300,000$ psi is the ultimate strength of liner material, then the factor of safety is $\frac{300}{263} = 1.14$ on the liner.

The outer part can be designed with $p/\sigma_1 \rightarrow 1$ for $\alpha_r = 0.5$ as shown in Figure 12. If $\sigma_1 = 250,000$ psi and the ultimate strength of the inner cylinder of the outer part is 300,000 psi then the factor of safety is $\frac{300}{250} = 1.2$ on the outer part. Larger factors of safety are possible with the suggested design if lower support pressures and larger liners are used.

The outside diameter requirements may be reduced by using a multi-ring unit in the inner part rather than just one ring. In this case, it may be that the fluid-support pressure should not be reduced to zero with the bore pressure but reduced to some minimum value in order to provide some prestress in the outer cylinder of the inner part. Controlling the pressure in one annulus does not present as many difficulties as it does in the controlled fluid-fill container design where there are many annuli.

The suggested design can be analyzed using analyses similar to those used in this study. It is suggested that this be done.

REFERENCES

(1) Fiorentino, R. J., Sabroff, A. M., and Boulger, F. W., "Investigation of Hydrostatic Extrusion", Final Technical Documentary Report No. AFML-TD-64-372, Contract No. AF 33(600)-43328 (January, 1965).

(2) Fiorentino, R. J., Abramowitz, P. H., Sabroff, A. M., and Boulger, F. W., "Development of the Manufacturing Capabilities of the Hydrostatic Extrusion Process", Interim Engineering Progress Report No. IR-8-198 (III), Contract No. AF 33(615)-1390 (August 1965).

(3) Fiorentino, R. J., Gehrke, J. H., Abramowitz, P. H., Sabroff, A. M., and Boulger, F. W., "Development of the Manufacturing Capabilities of the Hydrostatic Extrusion Process", Interim Engineering Progress Report No. IR-8-198 (I), Contract No. AF 33(615)-1390 (February, 1965).

(4) Manning, W.R.D., "High Pressure Engineering", University of Nottingham, Bulleid Memorial Lectures, Vol II, Lecture II, Chapter 4 (1963).

(5) Manning, W.R.D., "The Design of Compound Cylinders for High Pressure Service", Engineering, pp 349-352 (May 2, 1947).

(6) Manning, W.R.D., "Residual Contact Stresses in Built-Up Cylinders", Engineering, p 464 (Dec. 8, 1950).

(7) Poulter, T. C., "High Pressure Apparatus", U. S. Patent No. 2,554,499 (May 9, 1951), Code No. P67.35, Annotated Bibliography on High Pressure Technology, ASME, Butterworths (May, 1964).

(8) Ballhausen, C., German Patent No. 1,142,341, January 17, 1963.

(9) Gerard, G., and Brayman J., "Hydrostatic Press for an Elongated Object", Barogenics, Inc., U. S. Patent No. 3,091,804, June 4, 1963.

(10) Fuchs, F. J., Jr., "Production Metal Forming With Hydrostatic Pressures", Western Electric Company, ASME Publication No. 65-PROD-17 (June 1965).

(11) Zeitlin, Alexander, Brayman, J., and Boggio, F. George, "Isostatic and Hydrostatic Equipment for Industrial Applications of Very High Pressure", ASME Paper No. 64-WA/PT-14.

(12) Manson, S. S. and Hirschberg, M. H., "Fatigue Behavior in Strain Cycling in the Low and Intermediate Cycle Range", 10th Sagamore Army Materials Research Conference, Sagamore, New York (August 13-16, 1963).

(13) Morrison, J.L.M., Crossland, B., and Parry, J.C.S., "The Strength of Thick Cylinders Subjected to Repeated Internal Pressure", J. of Engineering for Industry, Trans. ASME, Series B, Vol 82, pp 143-153 (1960).

(14) Aerospace Structural Materials Handbook, Vol I, Table 3.051.

(15) Gilewicz, E. P., Fragetta, W. A., Mehra, V., and Krohn, R., "Research on the Binary Iron-Nickel Alloys With 20-25% Ni", ASD-TDR-62-996, Fig. 107 (June, 1964).

(16) Lunn, J. A., Sampson, H. B., Federico, A. M., and Macaulay, J. R., "Nickel Maraging Steels, Preliminary Investigation of 250 and 300 Bar", North American Aviation Report No. NA63H-202, pp 22-27 (March 15, 1963).

(17) Booth, E. T., Brodrick, R. F., Friesecke, B. P., and Schofield, B. H., "Fatigue and Dynamic Creep of High Strength Steels", ASD-TDR-62-480 (August, 1962).

(18) O'Connor, H. C. and Morrison, J. L. M., "The Effect of Mean Stress on the Push-Pull Fatigue Properties of an Alloy Steel", Int. Conf. on the Fatigue of Metals, Inst. of Mech. Engineers, London (September, 1956).

(19) Timoshenko, S. and Goodier, J. N., "Theory of Elasticity", 2nd Edition, McGraw-Hill, pp 58-59, 66-67 (1951).

(20) Berman, I., "Design and Analysis of Commercial Pressure Vessels to 500,000 psi", ASME Paper No. 65-WA/PT-1, to be published in Trans. ASME, J. Basic Engineering.

(21) Pugh, H. Ll. D., and Green, D., "The Effect of Hydrostatic Pressure on the Plastic Flow and Fracture of Metals", Proc. Instn. Mech. Engrs., Vol. 179, Pt. 1, No. 12, 1964-65, pp 415-437.

(22) Crossland, B., and Dearden, W. H., "The Plastic Flow and Fracture of a "Brittle" Material (Gray Cast Iron) With Particular Reference to the Effect of Fluid Pressure", Proc. Instn. Mech. Engrs. Vol. 182, 1958 p. 805.

(23) Bridgman, P. W., "Studies in Large Plastic Flow and Fracture", 1952 (McGraw-Hill, New York).

APPENDIX A

ELASTICITY SOLUTION FOR A RING SEGMENT

APPENDIX A

ELASTICITY SOLUTION FOR A RING SEGMENT

A ring segment is shown in Figure 29. Its geometry is defined by the radii r_1 and r_2 and the angle α. The loading of the segment is a pressure p_1 at r_1 and p_2 at r_2. For equilibrium, p_2 is related to p_1 by Equation (24) in the text; i.e.,

$$p_2 = \frac{p_1}{k_2} \tag{A.1}$$

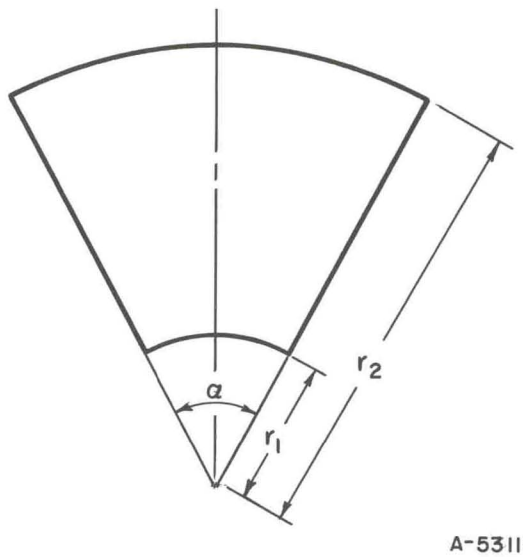

FIGURE 29. GEOMETRY OF RING SEGMENT

The solution for the stresses within the segment is found by superposition of two solutions: The Lamé solution for a cylinder, Equations (16a-c) and (17a, b) in the text, plus a bending solution, Equations (48) and (53) in Reference (19). The bending solution removes the moment from the sides of the segment that exists in the Lamé solution. The latter equations for the bending solution are written as

$$(\sigma_r)_b = \frac{4M_1 p_1}{\beta_1} f_1(r), \quad (\sigma_\theta)_b = \frac{4M_1 p_1}{\beta_1} f_2(r), \quad (\tau_{r\theta})_b = 0 \tag{A.2a-c}$$

and

$$\left(\frac{u}{r}\right)_b = \frac{M_1 p_1}{E_2 \beta_1} f_3(r) + \frac{G_1 p_1}{r} \cos\theta$$

$$\left(\frac{v}{r}\right)_b = \frac{8M_1 p_1}{E_2 \beta_1} (k_2^2 - 1)\theta - \frac{G_1 p_1}{r} \sin\theta \qquad \text{(A. 3a-c)}$$

where $f_1(r)$, $f_2(r)$, and $f_3(r)$ are defined by Equations (23a-c) in the text and where

$$\beta_1 \equiv (k_2^2 - 1)^2 - 4k_2^2 (\log k_2)^2 \qquad \text{(A. 4)}$$

The moment $M = M_1 p_1 r_1^2$ is found by integrating the negative of the Lamé hoop stress $(\sigma_\theta)_c$ for a cylinder given by Equation (16b) in the text over the side of the segment; i. e.,

$$M = -\int_{r_1}^{r_2} (\sigma_\theta)_c \, r \, dr \ ,$$

hence,

$$M_1 = \frac{-1}{p_1 r_1^2} \int_{r_1}^{r_2} \left\{ \frac{(p_1 - p_2 k_2^2)}{k_2^2 - 1} - \frac{(p_2 - p_1) k_2^2}{k_2^2 - 1} \left(\frac{r_1}{r}\right)^2 \right\} r \, dr$$

$$M_1 = -\frac{1}{2}\left(1 - \frac{p_2}{p_1} k_2^2\right) + \left(\frac{p_2}{p_1} - 1\right) \frac{k_2^2}{k_2^2 - 1} \log k_2 \qquad \text{(A. 5)}$$

G_1 is found by taking a reference point for the radial deflection u. If the point $r_0 = \frac{r_1 + r_2}{2}$, $\theta = 0$ is fixed,

then

$$G_1 = -\frac{M_1 r_0}{E_2 \beta_1} \left\{ -4(1+\nu) k_2^2 \left(\frac{r_1}{r_0}\right)^2 \log k_2 + 4(1-\nu) \left[k_2^2 \log\left(\frac{r_0}{r_1}\right) - \log \frac{r_0}{r_1} \right] - 4(k_2^2 - 1) \right\} \qquad \text{(A. 6)}$$

The equations for the total stresses and displacements in ring segments were programmed on the computer and some calculations carried out. Example results are given in Table 14 for $k_2 = 2.0$ and $\alpha = 60$ degrees. It is noted that a small residual stress σ_θ remains on the side of the segments. To be more accurate, i. e., to achieve sides entirely free of stress, the residual σ_θ could be removed using a "dipole" solution in addition to the bending solution. However, the self-equilibrating residual stress that would be removed has a local edge effect according to the principle of St. Venant. Therefore, the σ_θ stresses in Table 14 are believed to be indicative of the actual magnitude of hoop stresses in segments at the center.

TABLE 14. STRESSES AND DEFLECTIONS IN A RING SEGMENT, $k_2 = 2.0$, $\alpha = 60°$, $\nu = 0.3$

r/r_1	σ_r/p_1	σ_θ/p_1	$\frac{Eu}{rp_1}$ at $\theta = 0°$	$\frac{Ev}{rp_1}$ at $\theta = 30°$
1.0	-1.0000	0.0394	0.6324	-0.1301
1.1	-0.9068	0.0123	0.4877	-0.0853
1.2	-0.8310	-0.0033	0.3747	-0.0480
1.3	-0.7676	-0.0112	0.2846	-0.0164
1.4	-0.7137	-0.0137	0.2117	0.0107
1.5	-0.6670	-0.0126	0.1519	0.0341
1.6	-0.6260	-0.0089	0.1022	0.0547
1.7	-0.5896	-0.0033	0.0606	0.0728
1.8	-0.5568	0.0035	0.0254	0.0890
1.9	-0.5271	0.0113	-0.0046	0.1034
2.0	-0.5000	0.0197	-0.0303	0.1163

Appreciable bending, displacement v, is also noted. The bending increases with segment size and angle α as shown in Table 15. This bending would tend to cause the segments to dig into the liner as shown in Figure 30(a). Therefore, it is recommended that segments be designed with radii larger than the radii of mating cylinders in order to compensate for the change in radii due to bending. This is illustrated in Figure 30(b).

Note that the deflection u in Table 14 can have an arbitrary translational component; i.e., the segment is free to move radially a constant amount. In calculating interferences, the difference in deflection $u(r_1) - u(r_2)$ at $\theta = 0°$ is used and the constant amount drops out.

ELASTICITY SOLUTION FOR A PIN SEGMENT

A pin segment is shown in Figure 31. Its geometry is defined by the radii r_1 and r_2 and the angle α. r_2 is taken to the inside of the pin holes as indicated. The loading of the pin segment is more complicated than that of the ring segment as shown in Figure 32. A constant pressure p_1 is assumed to act at the inside. A variable pressure is assumed to act at the outside, i.e.,

$$\sigma_r = -p_1, \text{ at } r_1$$

$$\sigma_r = -p_2 (1 + \cos m\theta), \text{ at } r_2 \qquad \text{(A. 7a, b)}$$

In addition, a shear acts at r_2:

$$\tau_{r\theta} = -\tau \sin m\theta, \text{ at } r_2 \qquad \text{(A. 7c)}$$

TABLE 15. DEFLECTIONS IN RING SEGMENTS, $\nu = 0.3$

(a) $\alpha = 60°$

k_2	$\frac{Eu}{rp_1}$ at $\theta = 0°$, $r = r_1$	$\frac{Eu}{rp_1}$ at $\theta = 0°$, $r = r_2$	$\frac{Ev}{rp_1}$ at $\theta = \alpha$, $r = r_1$	$\frac{Ev}{rp_1}$ at $\theta = \alpha$, $r = r_2$
1.1	0.3463	0.2291	-0.0008	0.0447
1.2	0.3899	0.1730	-0.0221	0.0612
1.3	0.4287	0.1494	-0.0408	0.0652
1.4	0.4642	0.1153	-0.0576	0.0743
1.5	0.4970	0.0611	-0.0726	0.0931
2.0	0.6324	-0.0303	-0.1301	0.1163
3.0	0.8251	-0.0905	-0.2013	0.1243

(b) $k_2 = 2.0$

α	$\frac{Eu}{rp_1}$ at $\theta = 0°$, $r = r_1$	$\frac{Eu}{rp_1}$ at $\theta = 0°$, $r = r_2$	$\frac{Ev}{rp_1}$ at $\theta = \alpha/2$, $r = r_1$	$\frac{Ev}{rp_1}$ at $\theta = \alpha/2$, $r = r_2$
45°	0.6324	-0.0303	-0.1052	0.0835
60°	0.6324	-0.0303	-0.1301	0.1163
90°	0.6324	-0.0303	-0.1529	0.1957

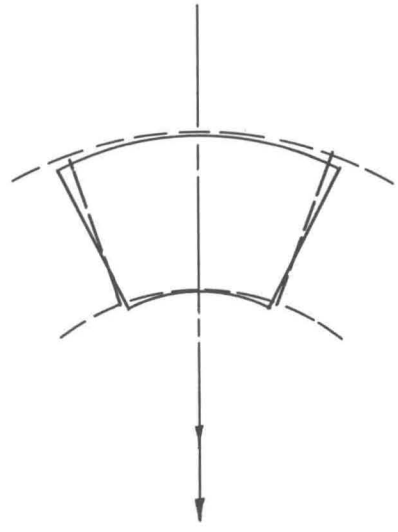

a. Segment Radii Initially Same As Radii of Mating Cylinders.

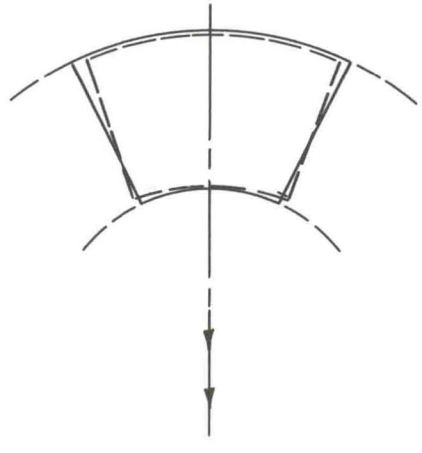

b. Segment Radii Initially Larger Than Radii of Mating Cylinders.

FIGURE 30. BENDING DEFORMATION OF RING SEGMENTS

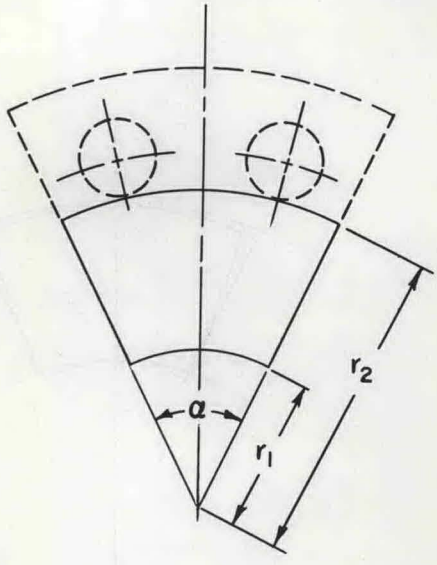

FIGURE 31. GEOMETRY OF PIN SEGMENT

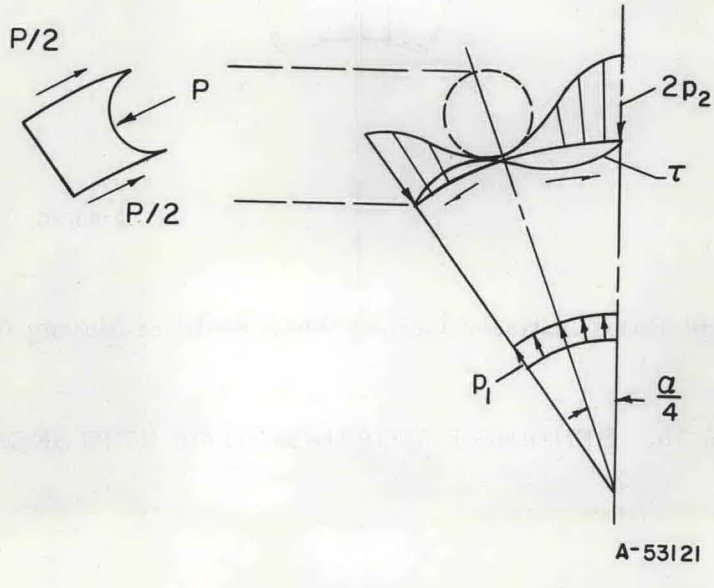

FIGURE 32. LOADING OF PIN SEGMENT

where

$$m = 4\pi/\alpha \tag{A. 8}$$

If N_s is the number of segments then $m = 2N_s$.

The shear force $\tau_{r\theta}$ must balance the pin force P shown in Figures 32 and 33. From Figure 32, it is seen for equilibrium of P, that it is required

$$t \int_{\alpha/4}^{\alpha/2} \tau_{r\theta} \cos\left(\theta - \frac{\alpha}{4}\right) r_2 d\theta = P/2$$

where t is the segment thickness. Substitution of (A. 7c) into this integral and integration gives

$$\tau = \frac{(m^2 - 1)\, P}{2mtr_2\,(1 + \cos \pi/m)} \tag{A. 9}$$

where P must be in equilibrium with p_1 as shown in Figure 33, i.e.,

$$P = p_1 r_1 t \ . \tag{A. 10}$$

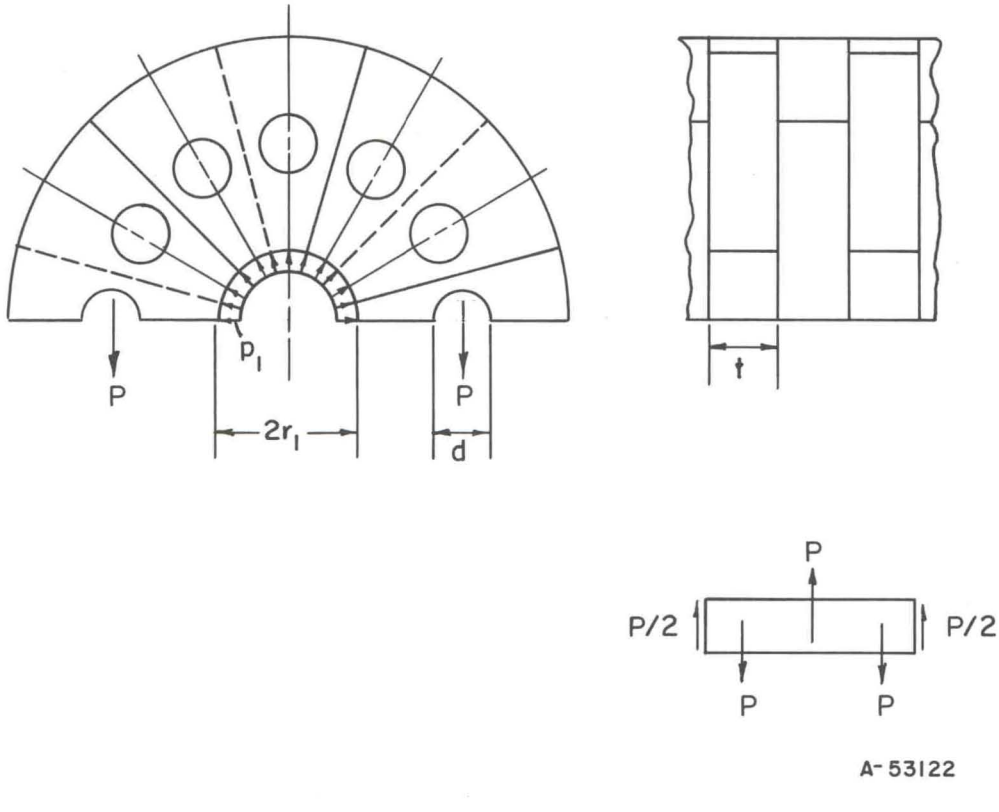

FIGURE 33. LOADING OF PINS

For radial equilibrium of the loadings shown in Figure 32, p_2 can be found by integration, i.e.,

$$2\int_0^{\alpha/2} [\tau_{r\theta}\sin\theta - \sigma_r \cos\theta]\, r_2 d\theta \Big|_{r_2} = 2p_1 r_1 \sin\frac{\alpha}{2} .$$

Substitution for $\tau_{r\theta}$ and σ_r from (A. 7b, c) and integration gives

$$p_2 = \frac{1}{(m^2-2)} \left[(m^2-1)\frac{p_1}{k_2} - m\tau\right] . \qquad \text{(A. 11)}$$

The stresses in a pin segment are found by superposition of three solutions: the Lamé solution for constant pressures p_1 and p_2 at the r_1 and r_2 respectively, a sinusoidal solution for the variable σ_r loading $-p_2 \cos m\theta$ at r_2, and a bending solution to remove the hoop stress of the first two solutions from the sides of the segments. The Lamé solution is given by Equations (16a-c) and (17a, b) in the text. The sinusoidal solution, taken from the cos $m\theta$ part of Equation (81) in Timoshenko and Goodier[19], is

$$\sigma_r = \Big[m(1-m)\, a_m \rho^{m-2} + (2-m)(1+m)\, b_m \rho^m - m(m+1)\, c_m \rho^{m-2} + (2+m)(1-m)\, d_m \rho^{-m}\Big] \cos m\theta$$

$$\sigma_\theta = \Big[m(m-1)\, a_m \rho^{m-2} + (m+2)(m+1)\, b_m \rho^m + m(m+1)\, c_m \rho^{-m-2} + (m-2)(m-1)\, d_m \rho^{-m}\Big] \cos m\theta \qquad \text{(A. 12a-c)}$$

$$\tau_{r\theta} = m\Big[(m-1)\, a_m \rho^{m-2} + (m+1)\, b_m \rho^m - (m+1)\, c_m \rho^{-m-2} + (-m+1)\, d_m \rho^{-m}\Big] \sin m\theta$$

where

$$\rho \equiv r/r_2 . \qquad \text{(A. 13)}$$

From the boundary conditions $\sigma_r = 0$, $\tau_{r\theta} = 0$ at r_1 and $\sigma_r = -p_2 \cos m\theta$, $\tau_{r\theta} = -\tau \sin m\theta$ at r_2 for the sinusoidal solution, the constants a_m, b_m, c_m, and d_m are found to be

$$a_m = \left(\frac{-p_2}{2} + \frac{\tau}{2}\right)\left[\frac{m^2 + (1-m^2)\, k_2^2 - k_2^{2m+2}}{\beta_2 (m-1)}\right] + \left(\frac{-p_2}{2} - \frac{\tau}{2}\right)\frac{k_2^2 (1 - k_2^{2m})}{\beta_2}$$

$$b_m = \left(\frac{-p_2}{2} + \frac{\tau}{2}\right) \frac{mk_2^2}{\beta_2} (k_2^2 - 1)$$
$$-\left(\frac{-p_2}{2} - \frac{\tau}{2}\right) \frac{m(k_2^2 - k_2^{2m+2})}{(m+1)\beta_2}$$

$$c_m = -\left(\frac{-p_2}{2} + \frac{\tau}{2}\right) \frac{k_2^2 (1 - k_2^{-2m})}{\beta_2}$$
$$+\left(\frac{-p_2}{2} - \frac{\tau}{2}\right)\left[\frac{(1 - m^2) k_2^2 - k_2^{-2m+2} + m^2}{\beta_2 (m+1)}\right]$$

$$d_m = \left(\frac{-p_2}{2} + \frac{\tau}{2}\right) \frac{mk_2^2 (k_2^2 - k_2^{-2m})}{\beta_2 (m-1)}$$
$$+\left(\frac{-p_2}{2} - \frac{\tau}{2}\right) \frac{m}{\beta_2} k_2^2 (k_2^2 - 1)$$

(A. 14a-d)

where

$$\beta_2 \equiv m\left[-m^2 k_2^4 + 2(m^2 - 1) k_2^2 + k_2^{2-2m} + k_2^{2m+2} - m^2\right] \quad \text{(A. 15)}$$

The bending solution is found in a similar manner to the method used previously for the ring segment. The resulting total stresses and displacements for the pin segment are given in Equations (25a-c) and (26a, b) in the text. The functions $g_{m1}(r)$, $g_{m2}(r)$, and $g_{m3}(r)$ in Equations (25a-c) are recognized as the coefficients of cos $m\theta$ and sin $m\theta$ in Equations (A. 12a-c). $g_{m4}(r)$ and $g_{m5}(r)$ in Equations (26a, b) are defined as:

$$g_{m4} \equiv -m(1+\nu) a_m \rho^{m-2} + \left[2(1-\nu) - m(1+\nu)\right] b_m \rho^m$$
$$+m(1+\nu) c_m \rho^{-m-2} + \left[2(1-\nu) + m(1+\nu)\right] d_m \rho^{-m}$$

$$g_{m5} \equiv m(1+\nu) a_m \rho^{m-2} + m\left[\frac{m+4}{m} + \nu\right] b_m \rho^m$$
$$+m(1+\nu) c_m \rho^{-m-2} + m\left[\frac{m-4}{m} + \nu\right] d_m \rho^{-m}$$

(A. 16a-b)

and G_2 is defined as

$$G_2 \equiv \frac{r_o}{E}\left\{ m(1+\nu) a_m \left(\frac{r_o}{r_2}\right)^{m-2} - \left[2(1-\nu) - m(1+\nu)\right] g_m \left(\frac{r_o}{r_2}\right)^m \right.$$
$$\left. -m(1+\nu) c_m \left(\frac{r_o}{r_2}\right)^{m-2} - \left[2(1-\nu) + m(1+\nu)\right] d_m \left(\frac{r_o}{r_2}\right)^{-m} \right\}$$

(A. 16c)

where

$$r_o = \frac{r_1 + r_2}{2} .$$

The bending moment is $M_2 p_1 r_1^2$ where

$$M_2 = \frac{1}{k_2^2 - 1}\left[\frac{k_2^2 - 1}{2} + k_2^2 \log k_2\right] + p_2\left[\frac{k_2^2}{2} + \frac{k_2^2 \log k_2}{k_2^2 - 1}\right]$$

$$+ \frac{1}{p_1}\left\{ - (m - 1)\, a_m\, k_2^{-m+2}\left[k_2^m - 1\right] - (m + 1)\, b_m\, k_2^{-m}\left[k_2^{m+2} - 1\right]\right.$$

$$\left. + (m + 1)\, c_m\, k_2^{m+2}\left[k_2^{-m} - 1\right] - (m - 1)\, d_m\, k_2^m\left[k_2^{-m+2} - 1\right]\right\} \qquad \text{(A. 17)}$$

β_1 was defined previously by Equation (A. 4).

The equations for stresses and deflections in pin segments were programmed on the computer and some calculations were carried out. Table 16 gives some results for $k_2 = 4.0$ and $\alpha = 60°$. At $\theta = \alpha/4 = 15°$ and $r/r_1 = 4$, edge of pin hole, it is noted that $\sigma_\theta / p_1 = 2.01$. This indicates the stress concentration effect of the hole. At $\theta = \alpha/2 = 30°$ appreciable σ_θ stress remains. The edge of the segment should be free of stress. Therefore, the results must be considered approximate. However, the residual σ_θ stress on the edge is self equilibrating and its removal would be expected to cause only a local effect near the edge according to the St. Venant principle.

Bending of the pin segment again is evident as shown by the v displacement. The variation of displacements and of the maximum σ_θ stress at the hole with segment geometry are shown in Table 17. Larger u displacements and smaller hoop stresses are found for larger k_2 and α. The bending displacement v increases with α but decreases with k_2.

The bending of pin segments would cause the inside corners to dig into the liner just as in the ring segments [Figure 30(a)]. Therefore, an inside diameter of the segments larger than the outside diameter of the liner would again be recommended to counteract the bending effect.

SOLUTION FOR SHEAR STRESSES IN PINS

The pins of the pin-segment container are subject to shear and bending as shown in Figure 33. The shear stress is larger than the bending stress and will be used as the critical stress in the pins. The maximum shear stress in a circular pin is given by

$$\tau_{max} = \frac{4}{3A}\,(P/2)$$

TABLE 16. STRESSES AND DEFLECTIONS IN A PIN SEGMENT, $k_2 = 4.0$, $\alpha = 60°$, $\nu = 0.3$

RESULTS AT THETA = 0.00 DEGREES

R/R1	SIGMA R/P1	SIGMA THETA/P1	TAU RTHETA/P1	EU/RP1	EV/RP1
1.000	-1.0000	-0.2009	0.0000	1.1739	0.0000
1.250	-0.8356	-0.1524	0.0000	0.7673	0.0000
1.500	-0.7174	-0.0967	0.0000	0.5167	0.0000
1.750	-0.6256	-0.0415	0.0000	0.3502	0.0000
2.000	-0.5522	0.0122	0.0000	0.2335	0.0000
2.250	-0.4948	0.0657	0.0000	0.1482	0.0000
2.500	-0.4555	0.1221	0.0000	0.0833	0.0000
2.750	-0.4409	0.1841	0.0000	0.0310	0.0000
3.000	-0.4598	0.2472	0.0000	-0.0143	0.0000
3.250	-0.5169	0.2840	0.0000	-0.0567	0.0000
3.500	-0.5954	0.2088	0.0000	-0.0980	0.0000
3.750	-0.6186	-0.1929	-0.0000	-0.1336	0.0000
4.000	-0.3755	-1.3937	-0.0000	-0.1456	0.0000

RESULTS AT THETA = 15.00 DEGREES

R/R1	SIGMA R/P1	SIGMA THETA/P1	TAU RTHETA/P1	EU/RP1	EV/RP1
1.000	-1.0000	-0.2009	0.0000	1.1048	-0.2753
1.250	-0.8355	-0.1525	0.0000	0.7120	-0.1703
1.500	-0.7169	-0.0972	0.0000	0.4707	-0.1003
1.750	-0.6236	-0.0433	0.0000	0.3109	-0.0503
2.000	-0.5449	0.0058	0.0000	0.1998	-0.0128
2.250	-0.4731	0.0478	0.0000	0.1202	0.0164
2.500	-0.3997	0.0797	0.0000	0.0625	0.0397
2.750	-0.3145	0.0998	0.0000	0.0218	0.0588
3.000	-0.2058	0.1129	0.0000	-0.0046	0.0747
3.250	-0.0670	0.1471	0.0000	-0.0178	0.0882
3.500	0.0863	0.2888	0.0000	-0.0202	0.0997
3.750	0.1788	0.7530	-0.0000	-0.0188	0.1097
4.000	-0.0000	2.0126	-0.0000	-0.0339	0.1185

TABLE 16. (Continued)

RESULTS AT THETA = 22.50 DEGREES

R/R1	SIGMA R/P1	SIGMA THETA/P1	TAU RTHETA/P1	EU/RP1	EV/RP1
1.000	-1.0000	-0.2009	-0.0000	1.0195	-0.4018
1.250	-0.8356	-0.1524	-0.0000	0.6437	-0.2465
1.500	-0.7171	-0.0970	-0.0002	0.4138	-0.1430
1.750	-0.6246	-0.0424	-0.0010	0.2620	-0.0691
2.000	-0.5486	0.0090	-0.0034	0.1567	-0.0139
2.250	-0.4839	0.0567	-0.0099	0.0809	0.0285
2.500	-0.4276	0.1009	-0.0245	0.0249	0.0613
2.750	-0.3777	0.1419	-0.0527	-0.0172	0.0866
3.000	-0.3328	0.1800	-0.0971	-0.0494	0.1057
3.250	-0.2920	0.2156	-0.1467	-0.0742	0.1219
3.500	-0.2545	0.2488	-0.1504	-0.0933	0.1436
3.750	-0.2199	0.2800	0.0371	-0.1082	0.1915
4.000	-0.1877	0.3094	0.7577	-0.1197	0.3124

RESULTS AT THETA = 30.00 DEGREES

R/R1	SIGMA R/P1	SIGMA THETA/P1	TAU RTHETA/P1	EU/RP1	EV/RP1
1.000	-1.0000	-0.2009	-0.0000	0.9021	-0.5149
1.250	-0.8356	-0.1524	-0.0000	0.5498	-0.3120
1.500	-0.7174	-0.0967	-0.0000	0.3355	-0.1768
1.750	-0.6256	-0.0415	-0.0000	0.1948	-0.0801
2.000	-0.5522	0.0122	-0.0000	0.0976	-0.0077
2.250	-0.4948	0.0657	-0.0000	0.0274	0.0487
2.500	-0.4555	0.1221	-0.0000	-0.0255	0.0938
2.750	-0.4409	0.1841	-0.0000	-0.0678	0.1307
3.000	-0.4598	0.2472	-0.0000	-0.1049	0.1614
3.250	-0.5169	0.2840	-0.0000	-0.1404	0.1874
3.500	-0.5954	0.2088	-0.0000	-0.1757	0.2097
3.750	-0.6186	-0.1929	0.0000	-0.2061	0.2290
4.000	-0.3755	-1.3937	0.0000	-0.2135	0.2459

TABLE 17. DISPLACEMENTS AND MAXIMUM HOOP STRESSES IN PIN SEGMENTS, $\nu = 0.3$

k_2	σ_θ/p_1 at $\theta = \alpha/4$, $r = r_2$	$\frac{Eu}{rp_1}$ at $\theta = 0$		$\frac{Ev}{rp_1}$ at $\theta = \alpha/2$	
		$r = r_1$	$r = r_2$	$r = r_1$	$r = r_2$
		(a) $\alpha = 60°$			
2.0	4.3266	1.0074	-0.0151	-0.6387	0.5367
3.0	2.7247	1.0681	-0.1303	-0.5313	0.3202
4.0	2.0126	1.1739	-0.1456	-0.5149	0.2459
5.0	1.6019	1.2865	-0.1397	-0.4068	0.2554
		(b) $k_2 = 3.0$			
α					
45°	3.3815	1.0516	-0.1281	-0.4082	0.2336
60°	2.7247	1.0681	-0.1303	-0.5313	0.3202
90°	2.0820	1.1137	-0.1305	-0.7382	0.5195

where A is the area of the pin and P/2 is the shear force shown in Figure 33. For $A = \frac{\pi d^2}{4}$ (d is pin diameter) and P given by Equation (A. 10), the maximum shear stress becomes

$$\tau_{max} = \frac{16}{3} \frac{p_1 r_1 t}{\pi d^2} \qquad \text{(A. 18)}$$

This equation is the basis of Equation (72) in the text.

APPENDIX B

DERIVATIONS OF FORMULAS FOR ASSEMBLY INTERFERENCES

APPENDIX B

DERIVATIONS OF FORMULAS FOR ASSEMBLY INTERFERENCES

The interferences Δ_n calculated in the text are the interferences required on the component parts as manufactured. However, the manufactured interference is not equal to the interference as assembled. The multi-ring container is taken as an example. It is assumed the rings are shrink-fit assembled one-by-one from the inside. The outer rings expand as they are shrunk on and the assembly interference for the next ring to be fitted is increased beyond the manufactured interference. The assembly interference between cylinders n and n + 1 is denoted by δ_n. It has dimensions of inches.

For assembly of cylinder n + 1 onto the other cylinders, δ_n is expressed as

$$\frac{\delta_n}{r_n} = \frac{\Delta_n}{r_n} + \frac{u'_n(r_n)}{r_n} \qquad \text{(B. 1)}$$

where

$u'_n(r_n)$ = radial displacement at r_n of cylinder n due to residual pressure q'_{n-1} at r_{n-1}.

q'_{n-1} = residual pressure at r_{n-1} due to assembly of cylinder n of wall ratio k_n onto a compound cylinder of wall ratio $k_1 k_2 \cdots k_{n-1}$ with an interference δ_{n-1}.

q'_{n-1} is calculated as follows:

$$\frac{\delta_{n-1}}{r_{n-1}} = \frac{u_n(r_{n-1}) - u_{n-1}(r_{n-1})}{r_{n-1}}$$

Substitution for u_n and u_{n-1} from Equation (17a) gives

$$\frac{\delta_{n-1}}{r_{n-1}} = \frac{1}{E_n(k_n^2-1)}\left[(1-v)\, q'_{n-1} + (1+v)\, q'_{n-1}\, k_n^2\right]$$

$$- \frac{1}{E_{n-1}(k_{n-1}^2\, k_{n-2}^2 \cdots k_1^2 - 1)}\left[-(1-v)\, q'_{n-1}\, k_{n-1}^2\, k_{n-2}^2 \cdots k_1^2 - (1+v)\, q'_{n-1}\right]$$

$$= \frac{q'_{n-1}}{E}\left[\frac{k_n^2+1}{k_n^2-1} + \frac{k_{n-1}^2\, k_{n-2}^2 \cdots k_1^2 + 1}{k_{n-1}^2\, k_{n-2}^2 \cdots k_1^2 - 1}\right]$$

where $E_n = E_{n-1} = E$ is assumed.

$$\text{Hence, } q'_{n-1} = E\left(\frac{\delta_{n-1}}{r_{n-1}}\right)\frac{\left(k_n^2-1\right)\left(k_{n-1}^2\, k_{n-2}^2 \cdots k_1^2-1\right)}{2\left(k_n^2\, k_{n-1}^2\, k_{n-2}^2 \cdots k_1^2 - 1\right)} \tag{B. 2}$$

Since

$$\frac{u'_n(r_n)}{r_n} = \frac{2\,q'_{n-1}}{E\left(k_n^2-1\right)} \tag{B. 3}$$

Substitution of (B. 2) and (B. 3) into (B. 1) gives

$$\frac{\delta_n}{r_n} = \frac{\Delta_n}{r_n} + \frac{\delta_{n-1}}{r_{n-1}}\frac{\left(k_{n-1}^2\, k_{n-2}^2 \cdots k_1^2 - 1\right)}{\left(k_n^2\, k_{n-1}^2\, k_{n-2}^2 \cdots k_1^2 - 1\right)} \tag{B. 4}$$

Now the $\frac{\delta_n}{r_n}$ can be calculated in sequence; i.e.,

$$\frac{\delta_1}{r_1} = \frac{\Delta_1}{r_1}$$

$$\frac{\delta_2}{r_2} = \frac{\Delta_2}{r_2} + \frac{\delta_1}{r_1}\frac{\left(k_1^2 - 1\right)}{\left(k_1^2\, k_2^2 - 1\right)} \quad \text{, etc.}$$

Equation (B. 4) applies if the rings are assembled from the inside out. If the rings are assembled one by one from the outside in, then the assembly interference for assembly of cylinder n-1 into the other cylinders is

$$\frac{\delta_n}{r_n} = \frac{\Delta_n}{r_n} + \frac{\delta_{n+1}}{r_{n+1}}\frac{\left(k_n^2 + 1\right)}{2}\frac{\left(k_{n+1}^2\, k_{n+2}^2 \cdots k_N^2 - 1\right)}{\left(k_n^2\, k_{n+1}^2 \cdots k_N^2 - 1\right)} \tag{B. 5}$$

Equation (B. 5) was found by an analogous procedure to that used in deriving (B. 4).

The method used to determine assembly interferences δ_n for the multi-ring container can also be used to determine assembly interferences for the other container designs. It is important to determine assembly interferences because they are larger than the manufactured interferences and excessive interference requirements may make a design impracticable.

APPENDIX C

COMPUTER PROGRAMS

APPENDIX C

COMPUTER PROGRAMS

The analyses described in the text were programmed in the FORTRAN IV alogarithmic language for calculation on Battelle's CDC 3400 computer. The following is a list of programs which includes a brief description of each:

PROGRAM COMPST1 – Analysis of compound (multi-ring) cylinder based upon static shear strength. Calculation of pressure-to-strength ratio p/2S in Figure 10 in the text.

PROGRAM COMPFG1 – Analysis of compound cylinder based upon shear fatigue strength. Calculation of pressure-to-strength ratio p/σ shown in Figure 11.

PROGRAM SEGMENT1 – Analysis of ring segment under radial pressures. Some results given in Appendix A.

PROGRAM SEGM2N – Analysis of pin segment under radial pressures and shear. Some results given in Appendix A.

PROGRAM COMPHS1 – Analysis of compound cylinder with high-strength liner. Calculations of pressure-to-strength ratios p/σ_1 and p/σ shown in Figures 12, 13, 14, and 15.

PROGRAM COMPHS2 – Analysis of compound cylinder with high-strength liner. Calculation of shrink-fit interferences, operating stresses, and prestresses.

PROGRAM PLTR1 – Analysis of Poulter (ring-segment) cylinder with high-strength liner. Calculation of pressure-to-strength ratios p/σ_1 and p/σ shown in Figures 16, 17, 18, and 19.

PROGRAM PLTR2 – Analysis of Poulter cylinder or pressure support cylinder (inner part of ring-fluid-segment container). Calculation of interferences, operating stresses, and prestress.

PROGRAM PSCYL1 – Analysis of pressure support cylinder (inner part of ring-fluid-segment container). Calculation of pressure-to-strength ratios p/σ_1 and p/σ_3 shown in Figures 20, 21, 22, 23, and 24.

PROGRAM PGSPNCYL – Analysis of segmented shear-pin (pin-segment) cylinder with high-strength liner. Calculation of pressure-to-strength ratio p/σ_1 and p_1/p shown in Figures 25 and 26.

Distribution List
(Contract No. AF 33(615)-1390)

AFML (MATB) (6 copies)
Attention Mr. G. A. Gegel
Wright-Patterson AFB, Ohio 45433

AFML (MAMP)
Attention Mr. K. Kojola
Wright-Patterson AFB, Ohio 45433

AFML (MAMP)
Attention Mr. V. DePierre
Wright-Patterson AFB, Ohio 45433

AFML (MAAM)
Attention Library
Wright-Patterson AFB, Ohio 45433

FTD
Attention TD-E2b
Wright-Patterson AFB, Ohio 45433

Defense Documentation Center (DDC) (30)
Cameron Station
5010 Duke Street
Alexandria, Virginia 22134

Air Force Systems Command
Attention SCR-2, Mr. Kniffen
Andrews Air Force Base
Washington 25, D. C.

Chief, Bureau of Naval Weapons
Department of the Navy
Washington 25, D. C.

Bureau of Naval Weapons
RRMA (Mr. T. Kearns)
Washington 25, D. C.

Commanding Officer
Attention Mr. S. V. Arnold,
Associate Director
Watertown Arsenal Laboratories
Watertown 72, Massachusetts

U. S. Atomic Energy Commission
Technical Information Services Extension
Attention Mr. Hugh Voress
P. O. Box 62
Oak Ridge, Tennessee

National Academy of Science
National Research Council
Div. of Eng. & Industrial Resources
Attention Mr. E. V. Bennett
Washington 25, D. C.

National Aeronautics & Space
Administration
Lewis Research Center
Attention Mr. George Mandel,
Chief, Library
21000 Brookpark Road
Cleveland 25, Ohio

Los Alamos Scientific Laboratory
Attention Dr. John E. Hockett
Los Alamos, New Mexico

Mr. William Bruckart (Aerojet-General,
Azusa, California)
1285 N. San Gabriel
Apartment 19
Azusa, California

U. S. Army Watervliet Arsenal
Attention Mr. T. E. Davidson
SWEWV-RDR
Watervliet, New York

Aerojet General Corporation
P. O. Box 296
Azusa, California

Aerojet General Corporation
Solid Rocket Department
P. O. Box 1947
Sacramento, California

Advanced Technology Laboratories
Division of American Standard
Attention Mr. W. C. Wolff,
Contracts Manager
369 Whisman Road
Mountain View, California

Allegheny Ludlum Steel Corporation
Research Center
Attention Mr. E. G. Flynn,
Supervising Metallurgist,
Extruded Products
Brackenridge, Pennsylvania

Aluminum Company of America
ALCOA Building
Attention Mr. R. W. Andrews
Pittsburgh, Pennsylvania

Aluminum Company of America
Attention Mr. Frederick C. Pyne
1200 Ring Building
Washington, D. C.

Mr. Hubert J. Altwicker
Lebanon, Ohio

Fansteel Metallurgical Corporation
Attention Mr. R. W. Yancey, Manager,
Special Development Projects
Number One Tantalum Place
North Chicago, Illinois 60064

Air Reduction Company
Central Research Department
Central Research Laboratories
Attention Mr. J. K. Hamilton
Murray Hill, New Jersey

Babcock & Wilcox Company
Attention Mr. James Barrett
Beaver Falls, Pennsylvania

Baldwin-Lima-Hamilton Corporation
Industrial Equipment Division
Attention Mr. B. Shalomith
Philadelphia, Pennsylvania 19142

AFML (MANF/Mr. J. H. Ross)
Wright-Patterson AFB, Ohio 45433

Mechanical Technology, Inc.
Attention Mr. Marshall Peterson
968 Albany Shaker Road
Latham, New York

Case Institute of Technology
Metallurgy Department
Attention Mr. H. Ll. D. Pugh
Cleveland 6, Ohio

Defense Metals Information Center
Battelle Memorial Institute
505 King Avenue
Columbus, Ohio 43201

The Boeing Company
Attention Mr. Vince A. Dornes,
Mgr., Manufacturing Development
Section
P. O. Box 3107
Seattle, Washington

Barogenics, Incorporated
Attention Mr. A. Zeitlin
50 MacQuesten Parkway South
Mount Vernon, New York 10550

The Brush Beryllium Company
Attention Mr. John Estess
17876 St. Clair Avenue
Cleveland, Ohio 44110

The Brush Beryllium Company
Attention Mr. R. G. O'Rourke
17876 St. Clair Avenue
Cleveland, Ohio 44110

Jet Propulsion Laboratory
California Inst. of Technology
Attention Mr. I. W. Newlan
4800 Oak Grove Drive
Pasadena 3, California

Canton Drop Forging & Mfg. Co.
Attention Mr. Chandis Brauchler
2100 Wilett Avenue
Canton, Ohio

Convair, A Division of General
Dynamics Corporation
Attention Mr. E. W. Fedderson,
Director, Mfg. Development
P. O. Box 1950
San Diego 12, California

Crucible Steel Company of America
Attention Dr. Walter Finley,
Director of Research
P. O. Box 88
Pittsburgh 30, Pennsylvania

Curtiss-Wright Corporation
Metals Processing Division
Attention Mr. Reese Williams
760 Northland Avenue
Buffalo 15, New York

Curtiss-Wright Corporation
Wright-Aeronautical Division
Attention Mr. R. J. Moran,
Manager, Manufacturing Engineering
Wood-Ridge, New Jersey

Douglas Aircraft Company, Inc.
Attention Mr. C. B. Perry, C-345,
Plant Engineering Supervisor
3855 Lakewood Boulevard
Long Beach 8, California

Douglas Aircraft Company, Inc.
Attention Mr. L. J. Devlin,
Materials Research & Process
Santa Monica, California

Dow Chemical Company
Metallurgical Laboratory
Attention Dr. T. E. Leontis,
Assistant to the Director
Midland, Michigan

E. I. du Pont de Nemours & Co.,
Incorporated
Pigments Department
Attention Dr. W. E. Lusby
Technical Manager, Metals Products
Wilmington 98, Delaware

E. I. du Pont de Nemours & Co.,
Incorporated
DuPont Metals Center
Attention Dr. L. J. Klinger
Baltimore, Maryland

Chance Vought Corporation
Vought Aeronautics Division
Attention Mr. G. A. Starr
P. O. Box 5907
Dallas, Texas

Alpha Metals, Inc.
Attention Mr. R. H. Hilsinger
56 Water Street
Jersey City, New Jersey 07304

E. I. du Pont de Nemours & Company,
Incorporated
Engineering Research Laboratory
Attention Mr. Donald Warren
Wilmington 98, Delaware

Erie Foundry Company
Attention Mr. J. E. Wilson,
General Sales Manager
Erie 6, Pennsylvania

Electrohydraulics, Incorporated
Attention Mr. Richard H. Wesley
3000 Classor-Boger Road
Fort Worth 11, Texas

Fansteel Metallurgical Corporation
Attention Mr. A. B. Michael,
Director, Metallurgical Research
2200 Sheridan Road
North Chicago, Illinois

Feller Engineering Company
Attention Mr. R. C. Zeile
Empire Building
Pittsburgh, Pennsylvania

General Electric Company
Aircraft Gas Turbine Division
Attention Mr. G. J. Wile,
Engineering Manager, Metallurgical Engineering Operations
Large Jet Engine Department,
Building 501
Cincinnati 15, Ohio

Grumman Aircraft Engineering Corp.
Manufacturing Engineering
Attention Mr. W. H. Hoffman,
Vice President
Plant 2
Bethpage, Long Island, New York

High Pressure Data Center
P. O. Box 60, University Station
Brigham Young University
Provo, Utah 84601

IIT Research Institute
Metals Research Department
Attention Dr. W. Rostoker
10 West 35th Street
Chicago, Illinois 60616

General Electric Company
F. P. D. Technical Information Center
Building 100
Cincinnati 15, Ohio

General Astrometal Corporation
Attention Mr. L. Smiley
320 Yonkers Avenue
Yonkers, New York

General Cable Corporation
Research Laboratory
Attention Mr. J. Szilard,
Director of Research
Bayonne, New Jersey

General Dynamics/Fort Worth
Attention P. R. de Tonnaneour,
Chief Librarian
P. O. Box 748
Fort Worth, Texas 76101

R. K. May
Chief of Applied Manufacturing
Research & Process Development
General Dynamics/Fort Worth
Fort Worth, Texas 76101

General Dynamics Corporation
Attention H. Richard Thornton
P. O. Box 748
Fort Worth, Texas 76101

General Dynamics
Attention Mr. F. H. Crane
P. O. Box 748
Fort Worth, Texas 76101

General Electric Company
Attention Library, LMC Department
1331 Chardon Road
Cleveland 17, Ohio

H. M. Harper Company
Attention Mr. K. G. Hookanson,
General Manager, Metals Division
Lehigh Avenue and Oakton Street
Morton Grove, Illinois

Harvey Aluminum, Inc.
Attention Mr. G. A. Moudry,
Technical Director
19200 South Western Avenue
Torrance, California

Haynes Stellite Company
Division of Union Carbide Corp.
Attention Mr. G. A. Fritzlen,
Manager, Technology
Kokomo, Indiana

Hunter Douglas Corporation
Div. of Bridgeport Brass Corp.
3016 Kansas Avenue
Riverside, California

Hunter Douglas Research Company
Attention Mr. Neal Gammell
887 East Second Street
Pomona, California 91769

Jones & Laughlin Steel Corporation
Attention Mr. Robert S. Orr,
Commercial Research Librarian
3 Gateway Center
Pittsburgh 30, Pennsylvania

Kaiser Aluminum & Chem. Corporation
1625 "I" Street, N. W.
Washington 25, D. C.

Lockheed Aircraft Corporation
Attention Mr. Green
Manufacturing Methods Division
Burbank, California

La Salle Steel Company
Attention Mr. Elliot Nachtman
P. O. Box 6800-A
Chicago 80, Illinois

Lewis Research Center
Attention Capt. J. O. Tinius
AFSC/STLO
21000 Brookpark Road
Cleveland, Ohio

The Ladish Company
Metallurgical Department
Attention Mr. J. Yoblin
Cudahy, Wisconsin

Magnethermic Corporation
Attention Mr. J. A. Logan
Youngstown, Ohio

The Martin Company
Attention Mr. L. Laux, Chief,
Manufacturing Research & Development
Baltimore 3, Maryland

The Martin Company
Denver Division
Attention Mr. R. F. Breyer,
Materials Engineering
Mail No. L-8, P. O. Box 179
Denver 1, Colorado

Marquardt Aircraft Company
16555 Saticoy Street
P. O. Box 2013 South Annex
Van Nuys, California

McDonnell Aircraft Corporation
Lambert - St. Louis Municipal Airport
Attention Mr. H. Siegel
P. O. Box 516
St. Louis 3, Missouri

North American Aviation, Inc.
Attention Mr. Walter Rhineschild
International Airport
Los Angeles 45, California

Nuclear Metals, Inc.
Attention Mr. Klein, Vice President
Concord, Massachusetts

National Forge Company
Attention Mr. James R. Beckser,
Project Engineer
Press Form Products
Irvine, Warren County, Pennsylvania

Oregon Metallurgical Corporation
Attention Mr. F. H. Vandenburgh,
Vice President & Sales Manager
P. O. Box 484
Albany, Oregon

Kennecott Copper Corporation
Ledgemont Laboratory
Attention Mr. Stanley H. Gelles
128 Spring Street
Lexington 73, Massachusetts

Republic Aviation Corporation
Attention Mr. A. Kastelowitz,
Director of Manufacturing Research
Farmingdale, Long Island, New York

Republic Steel Corporation
Republic Research Center
6801 Brecksville Road
Cleveland 31, Ohio

Reynolds Metals Company
503 World Center Building
Washington 6, D. C.
Attention Mr. Stuart Smith

Rohr Aircraft Corporation
Attention Mr. F. E. Zinnerman,
Manager, Manufacturing Research
P. O. Box 878
Chula Vista, California

Ryan Aeronautical Company
Attention Mr. L. J. Hull, Chief
Metallurgist
Materials & Process Laboratory
Lindberg Field
San Diego 12, California

Reading Tube Corporation
Attention Mr. Griffith Williams, Jr.
P. O. Box 126
Reading, Pennsylvania 19603

Western Electric Company
Engineering Research Center
Attention Mr. Frank J. Fuchs, Jr.
Princeton, New Jersey

Sandia Corporation
Livermore Laboratory
Attention Mr. M. W. Mote, Jr.
P. O. Box 969
Livermore, California

Solar Aircraft Company
A Division of International
Harvester Company
Attention Librarian
2200 Pacific Avenue
San Diego 12, California

Thompson-Ramo-Wooldridge, Inc.
Staff Research & Development
Chemical & Metallurgical Department
Attention Mr. A. S. Nemy
23555 Euclid Avenue
Cleveland 17, Ohio

Texas Instruments Corporation
Metals & Controls
Attention Mr. J. Buchinski
34 Forest Street
Attleboro, Massachusetts 02703

United States Steel Corporation
Products Development Division
525 William Penn Place
Pittsburgh, Pennsylvania

Universal Cyclops Steel Corporation
Refractomet Division
Attention Mr. C. P. Mueller,
General Manager
Bridgeville, Pennsylvania

University of California
Los Alamos Scientific Laboratory
P. O. Box 1663
Los Alamos, New Mexico

United Aircraft Corporation
Research Laboratories
Attention Mr. H. Peter Barie
East Hartford, Connecticut

Director, USAEL
Hq. USAECOM
Attention AMSEL RD-PEE (Mr. Divita)
Ft. Monmouth, New Jersey 07703

Wah Chang Corporation
Attention Mr. K. C. Li, Jr.
233 Broadway
New York, New York

Wolverine Tube
Division of Calumet & Hecla, Inc.
Attention Mr. D. F. Grimm, Manager
Special Metals, Research &
Development Division
17200 Southfield Road
Allen Park, Michigan

Jeffrey Manufacturing Company
Columbus 16, Ohio

Wyman-Gordon Company
Attention Mr. Arnold Rustay,
Technical Director
Grafton Plant
Worcester Street
North Grafton, Massachusetts

Westinghouse Electric Corporation
Attention Mr. F. L. Orrell,
Section Manager, Development
Contracts
P. O. Box 128
Blairsville, Pennsylvania

Watervliet Arsenal
Process Engineering Section
Benet Laboratories
Attention Mr. Leonard Liuzzi
Watervliet, New York

Lombard Corporation
Attention Mr. Daniel A. Katko
Vice President
639 Wick Avenue
P. O. Box 177
Youngstown 1, Ohio

SEPIE
Wright-Patterson AFB, Ohio

SEPIR
Wright-Patterson AFB, Ohio

Clevite Corporation
Attention Mr. Gail F. Davies
540 East 105th Street
Cleveland 8, Ohio

Sun Oil Company
Attention Mr. E. M. Kohn
Marcus Hook, Pennsylvania

General Electric Company
Attention Mr. W. C. Gutjahr
118 W. First Street
Dayton, Ohio 45402

Pressure Technology Corporation of
America
Attention Dr. A. Bobrowsky
453 Amboy Avenue
Woodbridge, New Jersey

National Aeronautics & Space
Administration
Lewis Research Center
Attention Mr. C. P. Blankenship
M.S. 105-1
21000 Brookpark Road
Cleveland, Ohio 44135

Ravens-Metal Products, Inc.
Attention Mr. Lloyd A. Cook
P. O. Box 1385
Parkersburg, West Virginia

Voi-Shan Manufacturing Company
Technical Sales Department
Attention Mrs. Virginia Kuidroff
8463 Higuera Street
Culver City, California

Reynolds Metals Company
Attention Mr. J. Harry Jackson,
General Director
Metals Research Division
Richmond, Virginia

Allis-Chalmers
Attention Dr. Laird C. Towle
Research Physicist
Box 512
Milwaukee, Wisconsin 53201

GCA Viron Division
Attention Mr. W. H. Schaumberg,
Manager
Instrumentation and Communication
7585 Viron Road, N.E.
Minneapolis, Minnesota 55432

Dr. R. K. Pitler
Technical Director
Special Metals Corporation
New Hartford, New York 13413

Titanium Metals Corporation of America
Attention Mr. W. M. Parris
Senior Research Engineer
P. O. Box 2128
Henderson, Nevada 89015

GM Defense Research Laboratories
Box T
Santa Barbara, California
Attention Dr. Arfon H. Jones
Materials and Structures Laboratory

Western Electric Company
Attention Mr. Fred Radakovich,
Senior Staff Engineer
Dept. 7224, Hawthorne Station
Chicago, Illinois 60623